University of Natural Resources and Life Sciences, Vienna
Department of Water, Atmosphere and Environment
Institute of Hydraulics and Rural Water Management

Master Thesis

Spatial and Temporal Impacts of Stone Bunds on Soil Physical Properties

A Case Study in the Northern Ethiopian Highlands

to obtain the academic degree of

Diplomingenieur

submitted by

Bakk. techn. Schürz, Christoph

Vienna, March 2014

Supervisor: Ao.Univ.Prof. Dipl.-Ing. Dr.nat.techn. Klik, Andreas

Co-Supervisor: Dipl.-Geow. Dr.nat.techn. Schwen, Andreas

Acknowledgements

To reach the point of knowledge where I am now is not only my own credit, but far more results of constant support from people that surround me. Here, I want to thank them.

First, I want to express my sincere gratitude to my supervisor Andreas Klik who made this possible. He gave me not only the support and freedom to gain knowledge in an interesting research field, but also gave me the possibility to work in an environment that impressed me beyond scientific work. I also want to thank my Co-supervisor Andreas Schwen and Stefan Strohmeier for their constant support during the field work in Ethiopia, when communication was not always easy and also for the great input they gave me during the analysis of the data and writing of this work.

As this work took place in the greater context of a project there were many cooperation partners that gave great support during the field work. Here, I want to mention ICARDA, ARARI, GARC, as well as the ADA who sponsored this project. Of those organizations I especially want to thank Feras Ziadat and Wondimu Bayu for their great support and input during the work in Ethiopia. For his help in organizing and sorting out issues in the field I want to thank Baye Ayalew. Without his help the simplest things would not have been possible.

A special thank goes also to Claire, Ingrid and Florian, my colleagues who shared all the experiences during our time in Ethiopia with me. Working together with you, but also experiencing a whole new environment together with you was vital support for me.

An inquisitive mind must be stimulated by the right environment. Therefore, I express my greatest gratitude to my parents that always gave me all encouragement and freedom I needed to reach my goals and always believed in what I was doing. Last but not least, I want to thank my friends that support but also challenge me day by day and make life interesting.

Abstract

Central issue of rain fed agriculture systems in the Ethiopian highlands is to store rain water in the soil during the rainy season. The aim is to maximize plant available water and to reduce surface runoff and soil erosion. Stone bunds are a common practice for soil and water conservation (SWC), influencing the translation processes of surface runoff. However, changes in surface hydrology affect the temporal and spatial properties of soil physical parameters.

The objective of this work is to find a relationship between the spatial distribution of soil properties and the location of the stone bunds, but also to monitor the temporal behavior of those soil parameters, to better understand the impact of stone bunds on soil water movement. The research area is located in the Gumara-Maksegnit watershed in Northern Ethiopia. There, two representative transects were selected: One transect crosses three fields with SWC measures applied perpendicular to them on a length of approximately 71 m. The second transect crosses the same hill slope in an area without conservation structures at a length of 55 m. During the rainy season in 2012 soil physical properties were monitored in specific spatial and temporal intervals. The measurements included bulk density, soil texture, and volumetric water content. Tension infiltration experiments were performed to determine saturated hydraulic conductivity for areas near stone bunds and the center of the fields on one hand, but also to derive soil water characteristics for the certain positions at the hill slope. Slope steepness and stone cover along the transects were assessed, using survey and photogrammetric analysis.

The analyses that were used in this approach were able to reveal spatial and temporal characteristics of the assessed soil properties under the influence of stone bunds. For near surface volumetric water content a clear periodic behavior along the stone bunds was found, with significantly higher values in the vicinity of the stone bunds. Additionally, an earlier increase in water content over the rainy season was found for the transect with SWC. The bulk density showed significantly lower values in the zones where accumulation of sediment material takes place. Saturated hydraulic conductivity but also soil water characteristics show temporal changes but also spatial differences that are most likely induced by differences in soil structure. The strongest spatial relationship was found for inclination and near surface soil water content.

Table of Contents

List of Figures

List of Tables

1 Introduction

Land degradation is a central issue in the Ethiopian highlands. The highlands are most suitable for agriculture in Ethiopia and therefore, support a major part of human population and livestock (Hurni, 1988). Increasing population and limited arable land raised the pressure on competing resources, such as forests and grazing land. These factors and political decisions, for instance the nationalization of land in 1974 have led to vast deforestation that reduced the forested areas from 34 % to less than 3 % of the total area in the last decades (Friis, 1992; Taddese, 2001). As steeper slopes are used for crop production, surface runoff and soil erosion are major threats to the agricultural used areas, depleting the soils and decreasing the crop production (Nyssen et al., 2000). Additionally, strong climatic variability makes agricultural production even more insecure. Droughts and subsequently famine were the consequence, for example in 1973 and 1984 (Taddese, 2001). In the same time period programs for soil conservation and afforestation were initiated by the Ethiopian government in cooperation with international agencies and intensive research in these fields is still ongoing (Herweg and Ludi, 1999; Hurni, 1988).

The present master thesis was prepared in the scope of the project “Unlocking the potential of rain-fed agriculture in Ethiopia for improved rural livelihood”. The aim of the project is to investigate strategies to reduce soil degradation and increase the productivity of rain-fed agriculture in the Gumara-Maksegnit watershed in the Ethiopian highlands. The project was realized in an international cooperation between the International Center for Agricultural Research in the Dry Areas (ICARDA), Amhara Regional Agricultural Research Institute (ARARI), and the University of Natural Resources and Life Sciences, Vienna (BOKU) funded by the Austrian Development Agency (ADA). The main focus of the research activities of BOKU University was laid on the upland processes of soil erosion as well as on the sediment discharge out of the catchment.

The work presented in this thesis investigated the impact of stone as soil and water conservation measures on various soil properties. Transect measurements of several soil parameters comparing a plot with stone bunds to the case of no conservation measures were performed in the Gumara-Maksegnit watershed throughout the rainy season of 2012. Subsequent analysis of the data shows spatial and temporal behavior of the parameters, but also differences between the case of soil and water conservation and without. The results of this work might contribute to a better understanding of the behavior of various soil properties under the influence of stone bunds for the specific loamy soils of the region.

2 Objectives

Prior to the field work hypothesis were defined, derived from knowledge that can be seen as common sense about the impact of stone bunds. The hypotheses are as follows:

- Stone bunds work as a barrier for eroded sediment material. Therefore, eroded soil accumulates behind the stone bunds.
- Different soil fractions behave different concerning erosion processes. Therefore, material that accumulates behind the stone bunds is different in texture, structure, and bulk density compared to soil that is not eroded.
- As soil texture, structure, and bulk density differ on a spatial basis also soil water retention and infiltration differ.
- Stone bunds work also as a barrier for surface runoff and therefore lead to higher soil water contents in the vicinity of the stone bunds compared to areas without and farther away from the stone bunds.
- As some of the parameters are influenced by the same processes, similarities in their spatial patterns must be present.

According to the stated hypotheses the objectives for this work were formulated:

- Characterize the spatial and temporal behavior of the assessed soil parameters considering the influence of the stone bunds as soil and water conservation measure.
- Analyze similarities in the spatial behavior of different soil parameters for different time steps.
- Assess the differences in the temporal and spatial behavior of the soil parameters influenced by stone bunds compared to the case where no soil and water conservation measures were applied.

3 Theoretical Background

3.1 Land degradation

There are many definitions for the term land degradation available in literature. Here are mentioned two examples:

United Nations Environmental Programme (UNEP):

“Land degradation is a long-term loss of ecosystem function and services, caused by disturbances from which the system cannot recover unaided.” (Dent et al., 2007)

Food and Agriculture Organization of the United Nations (FAO):

“Land degradation: is the reduction in the capacity of the land to provide ecosystem goods and services and assure its functions over a period of time for the beneficiaries of these.” (FAO, 2013)

3.1.1 Land degradation on a global basis and Africa

Over the last decades a drastic change in the land use was taking place. The major driving forces are the strong increase in the human population, their higher demands in resources and the subsequent intensification of production, but also political issues and climate change. The greatest changes in the recent decades were shown by conversion from forests to cropland, woodland or grassland. Unsustainable land use induces land degradation. On a global basis a large proportion of the land surface and at least one third of the world’s population (predominantly in poor regions) is affected by the effects of land degradation (Dent et al., 2007, p. 84 ff.; Jones et al., 2012, p. 3 ff.). UNEP (2007) defines chemical contamination, soil erosion, nutrient depletion, water scarcity, and salinity as the major causes of land degradation leading to a deterioration of human livelihood.

Some of the processes induced by such unsustainable land use are irreversible, such as severe gullying or advanced salinization. Other processes such as sheet soil erosion can be decelerated and prevented or even reversed, for example adding nutrients to nutrient-depleted soils (Scherr and Yadav, 1996, p. 3). Eventually, poor land use practices lead to a reduced productivity, which leads subsequently to socio-economic problems, such as insecure food production, migration and damages to the ecosystems (FAO, 2013).

A recent approach to assess the land degradation on a global basis was established by Bai et al. (2008). They defined losses in the net primary productivity as a parameter for land degradation. The parameter is based on biomass production and rain-use efficiency derived from remote sensing data. The parameter describes only the developments in the recent decades and does not consider areas that are now in poor conditions because of historical developments. However, Figure 3.1 shows that the areas affected most by land degradation are still the countries of sub-Saharan Africa and Indo-China.

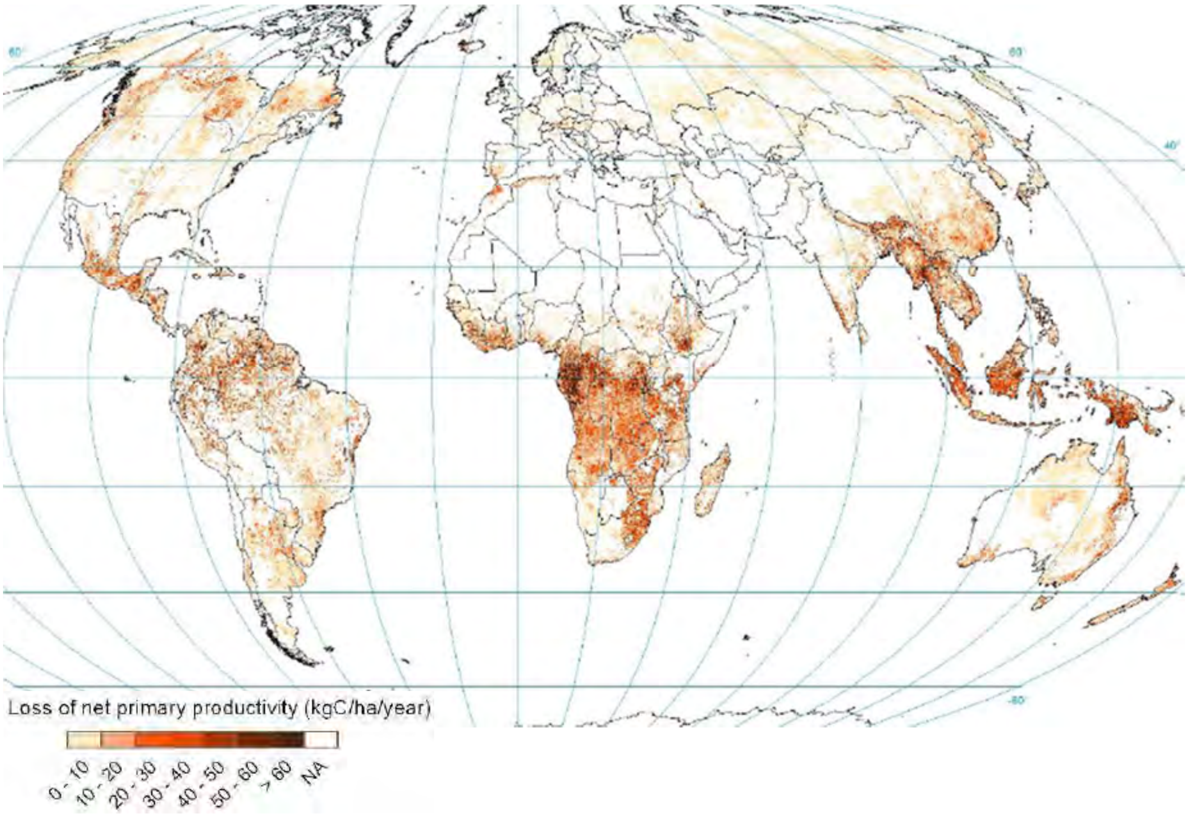

Figure 3.1: Losses of the net primary productivity as an indicator for land degradation for the time period of 1981-2003 (Bai et al., 2008).

On continental scale more than 16 % of the African land area is affected by land degradation induced by human activities. The most severe causes for land degradation in Africa are overgrazing, agricultural mismanagement, and deforestation (Jones et al., 2013, p. 149). Figure 3.2 shows the main types of soil degradation that occur on the African continent. Erosion by water is the dominant form of degradation, but also other forms are strongly present that affect whole countries such as wind erosion and nutrient depletion (Jones et al., 2013, p. 149). According to this map almost all of Ethiopia is primarily affected by water erosion.

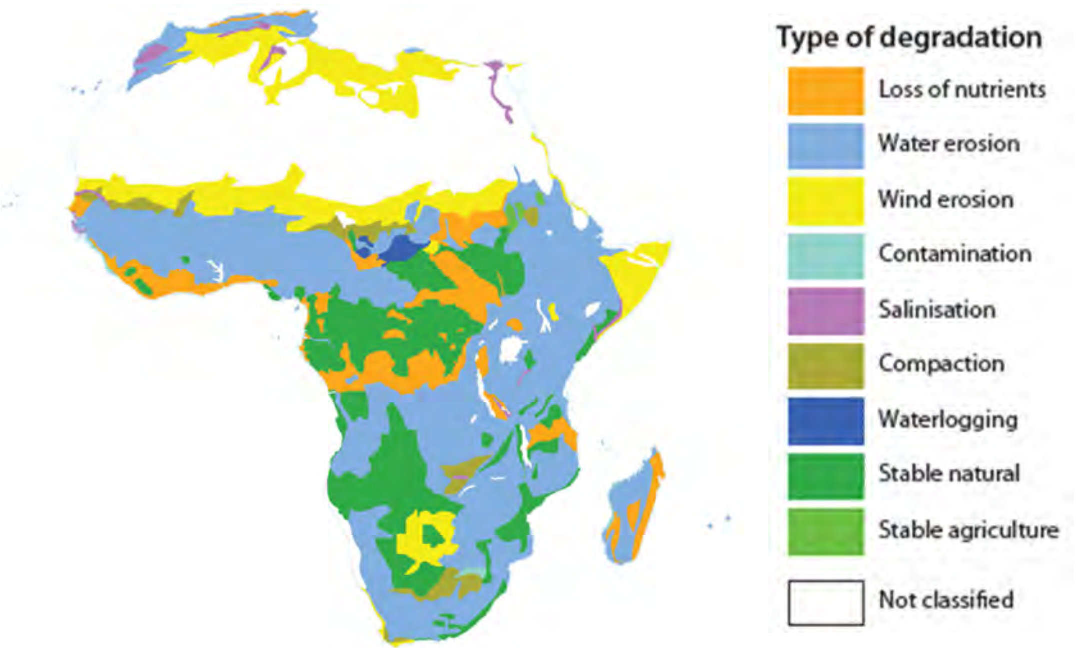

Figure 3.2: Types of soil degradation on the African continent (Jones et al., 2013)

3.1.2 Land degradation in Ethiopia

The majority of the Ethiopian population lives in the rural area. About 80 to 85 % of the people work in the agricultural sector, which is small structured. Subsistence farming is dominant and plant production is almost entirely rainfed (Mengistu, 2006, p. 5). High climatic variability makes therefore the whole agricultural sector vulnerable. As the highlands in the northern part of Ethiopia are most suitable for rainfed agriculture this area supports a large extent of smallholder farmers and livestock (Hurni, 1988). A strong increase in the population (the population in Ethiopia has tripled over the last 40 years (DESA, UN, 2013)) over the past decades and political decisions such as the nationalization of land in 1974 created a strong pressure on the limited land resources. Vast deforestation and transformation to crop land and grazing land were the reason, reducing the forested areas from 34 % to less than 3 % of the total area (Taddese, 2001). Water erosion is the most dominant cause of land degradation in the Ethiopian highlands. Clearing the forested areas and cultivating steeper slopes made the effects of soil erosion by water more severe (Hurni, 1988; Taddese, 2001). As rainfall increases with altitude and crop production is most intensive in the agro-climatic Dega zone (2300-3200 m a.s.l.) the largest soil erosion rates are expected there (Hurni, 1988). In a study from 1987 Hurni estimated the annual soil erosion rates for different land use in Ethiopia, with average rates of 42 t ha^{-1} yr^{-1} and 5 t ha^{-1} yr^{-1} for cropland and grazing land respectively. Erosion rates for the highlands showed even higher values. The erosion exceeds the formation process by a factor of 4 to 10 on cropland and 0.8 to 2.3 on grassland (Hurni, 1988).

3.2 Erosion by water

Soil erosion is the disruption of soil by the impact of exogenesic factors such as water or wind (Zachar, 1982, p. 16) involving the processes of detachment, transport and deposition of soil particles. It is a process taking place naturally on a geologic time scale. However, anthropogenic influences, such as changes in the land use and intensive use of this resource accelerate the erosion process significantly (Blanco and Lal, 2008, p. 3; Van-Camp et al., 2004). This means, that the process of soil erosion is inevitable. Eroding the fertile topsoil usually leaves back less fertile soil layers underneath, therefore affecting the soil productivity. This process must be minimized to a tolerable level, to sustain soil productivity on a long term basis (Blanco and Lal, 2008, p. 3). The tolerance was initially defined as a balance of erosion and formation of soil. However, formation of soil can vary on a large scale (Roose, 1996). Various literatures define threshold values of tolerable soil erosion, that does not affect soil productivity. Blanco and Lal (2008) for example mention a tolerance level for soil and water conservation planning in the USA with a value of 11 t ha^{-1} yr^{-1}. However, many literatures define too large threshold values and any soil loss that exceeds 1 t ha^{-1} yr^{-1} must be considered as not sustainable on a long term basis (Ecologic Institute and SERI, 2010; Van-Camp et al., 2004).

On a global basis as well as in Ethiopia, *erosion by water* is, among the different types of land degradation the most severe (Jones et al., 2013; Oldeman, 1992). In general water erosion is the gradual destruction and abrasion of soil induced by rain, fluvial or non-fluvial water (Blanco and Lal, 2008, p. 21; Zachar, 1982, p. 27). From the initial impact of a raindrop, over the formation of surface runoff, to the concentration of runoff, water erosion takes place involving different processes but also different scales in space and magnitude of impact. As consequence, various classifications of precipitation driven water erosion are available in literature (Zachar, 1982, p. 47). Below a common classification is shown.

Splash erosion is caused by the impact of raindrops on the soil surface. When hitting the soil the raindrops release their kinetic energy in form of splash. The impact splashes the soil and forms small craters. The kinetic energy of a raindrop is a function of its velocity and size (Blanco and Lal, 2008, p. 21).

Sheet or interrill erosion is more or less uniform erosion on the soil surface of a slope (Zachar, 1982, p. 49). After the initial phase where splash erosion is dominant, runoff develops quickly and transports detached and naturally weathered soil particles. The erosion rate due to sheet flow is strongly dependent on the rainfall intensity, the interrill erodibility of the soil, and the slope (Blanco and Lal, 2008, p. 23). Further important factors for interrill erosion are the crusting of the soil that strongly influences the infiltration of water and therefore defines the amount of surface runoff, but also the micro-topography of a slope (Van-Camp et al., 2004). Sheet erosion evens the soil surface and increases uniformity of the sheet erosion. However, accumulation of runoff water occurs that can initiate *rill erosion* (Zachar, 1982, p. 49, see Figure 3.3). The results of sheet erosion often become visible as lighter colored areas of soil on a slope, as top soil with higher organic matter content was eroded and lighter colored subsoil is exposed (FAO, 1965, p. 23)

Rill erosion occurs when the flow is more concentrated. Small rills and channels form where the flow is intense enough to erode particles directly (Van-Camp et al., 2004). As more and more particles get eroded by the flow, the rills enlarge. However, rills can easily be reversed by tillage. Under intensive rainfall events rill erosion can cause large soil loss (Blanco and Lal, 2008, p. 23).

Gully erosion is irreversible by usual land preparation techniques, as channels erode too deep into the soil. Gully development often follows sheet and rill erosion where runoff on a slope is sufficient in volume and velocity, but also where concentrated flow occurs long enough to develop deep channels. Anthropogenic initiation is often the case on tracks for people and livestock (FAO, 1965, p. 26)

Figure 3.3: Sedimented soil on a field in northern Ethiopia. Small scaled preferential flow paths are visible that can develop small rills (photo: C.Schürz)

Figure 3.4: Retrograde gully development on a field in northern Ethiopia. Accumulated flow incises soil and forms a gully (photo: C.Schürz)

3.3 Soil and water conservation measures

Soil and water conservation (SWC) can be defined as measures to maintain or enhance the productivity of soil that is at risk of degradation or already degraded (Van Lynden et al., 2002). The measures taken can be defined according to their approach. Proper land and soil management can be applied as a preventive measure, whereas mitigation measures have to be taken to defeat currently occurring soil erosion. When the degradation is severe and reversion is impossible at a certain time scale, rehabilitation measures need to be taken (Van-Camp et al., 2004). An important factor is to take measures that are feasible within the financial and human capacities. Furthermore, awareness has to be raised for the environmental and economic benefits of any measure, and most important is that the chosen measures are accepted among the users, to ensure sustainable management (Hudson, 1987, p. 26; Van-Camp et al., 2004).

Soil and water conservation measures basically can be divided into two groups:

Biological conservation covers measures such as conservation tillage practices, conservation farming practices, or cropping practices to improve water use efficiency. Conservation tillage practices include reduced tillage, no-till, mulch tillage, or stubble mulch farming. These practices however, are better applicable in mechanized high production with good rainfall and less for subsistence farming. Conservation farming practices include for example strip cropping to reduce erosion, rotation to improve fertility with legumes for example, or fallowing to build up soil moisture before sowing. Improved water use efficiency can be achieved by using specific drought resistant crop varieties (Hudson, 1987, p. 25 ff.).

Mechanical conservation measures include different forms of terraces, furrow systems, ridging, or bunds. The mechanical measures are designed according to one or more objectives they might follow. Objectives can be for example modification of the slope, influencing the surface runoff or to enable cultivation of steep slopes. Types of terraces are versatile, such as level terraces for irrigation, graded terraces to control runoff, or methods to absorb most of the rain, for instance the traditional methods fanya juu in Africa or murundum in South America. The principle of ridging is to make ridges and furrows and additionally dam the furrows with small ties, to increase the surface storage. However, this method is sensitive to overtopping water (Hudson, 1987, p. 38 ff.).

3.3.1 Stone bunds

Stone bunds are 20 to 40 cm high embankments of stones built in shallow trenches along contour lines using large and medium sized (40 to 5 cm) rock fragments from neighboring fields for construction (Morgan, 2005, p. 212; Nyssen et al., 2007). Their construction requires less soil movement compared to bench terraces and are therefore more applicable to small farmers. However, if stone bunds are constructed with irregularities and deviate from the contour lines, ponding behind the bunds may occur (Hudson, 1987, p. 66). Immediately after construction stone bunds reduce the slope length for surface runoff and provide retention space for runoff and sediments. On a medium and long term basis sediments accumulate and fill up the retention space. This leads to a reduction in slope steepness and subsequently the formation of bench terraces (Bosshart, 1997).

According to the effectiveness of this measure various studies show different results for effects such as retention of soil and water or increase in crop yield. Nyssen et al. (2007) for example found an average sediment accumulation rate of 58 t ha^{-1} yr^{-1}, an increase in mean crop yield of 0.58 to 0.65 t ha^{-1} yr^{-1} and enhanced moisture storage in deep soil horizons induced by stone bunds constructed in the Tigray highlands for the year 2002. Studies from Hengsdijk et al. (2005) and Herweg and Ludi (1999) on the other hand showed only limited effects on soil conservation and crop yield respectively.

Also according to the acceptance of the measure different opinions are stated. Where Nyssen et al. (2007) says that the majority of the farmers interviewed are in favor of building stone bunds on their land and see the benefits of the measure, Hengsdijk et al. (2005) found only a low rate of adoption due to the poor performance of the measure.

Figure 3.5: Stone bunds in the Gumara-Maksegnit watershed in the northern Ethiopian highlands (photo: C.Schürz)

4 Materials and Methods

This work consists of two major parts, a field work and a statistical analysis of the data. The fieldwork was performed in Ethiopia in the rainy season of 2012 involving the repeated measurement of various soil parameters along a hill slope. Subsequently, the collected data was analyzed for spatial and temporal characteristics.

The data collection included definition of the study site and its hill topography, measurements of precipitation and elevation, and the determination of various soil characteristics, such as volumetric water content, bulk density, near saturated hydraulic conductivity, characteristics of water retention, soil texture, and stone cover.

The statistical analyses included simple descriptive statistics to compare various data sets for differences in variability and mean, but also analyses to find periodic behavior and similarities in the spatial domain applying autocorrelation, spectral and cross-semivariogram analysis to the data.

4.1 Study area

The study area is described by location, climate and soil characteristics with specific outline of the study site and experimental set up.

4.1.1 Location and Topography

The Gumara-Maksegnit watershed is located in the North West Amhara region in Ethiopia about 45 km southwest of the city Gonder (see Figure 4.1). The watershed is a sub-catchment in the greater Lake T'ana basin that drains into the Gumara River, which subsequently drains into the Lake T'ana. The catchment covers an area of approximately 54 km^2 with an altitude that ranges from 1933 to 2852 m a.s.l. The topography is highly variable (GARC, 2010).

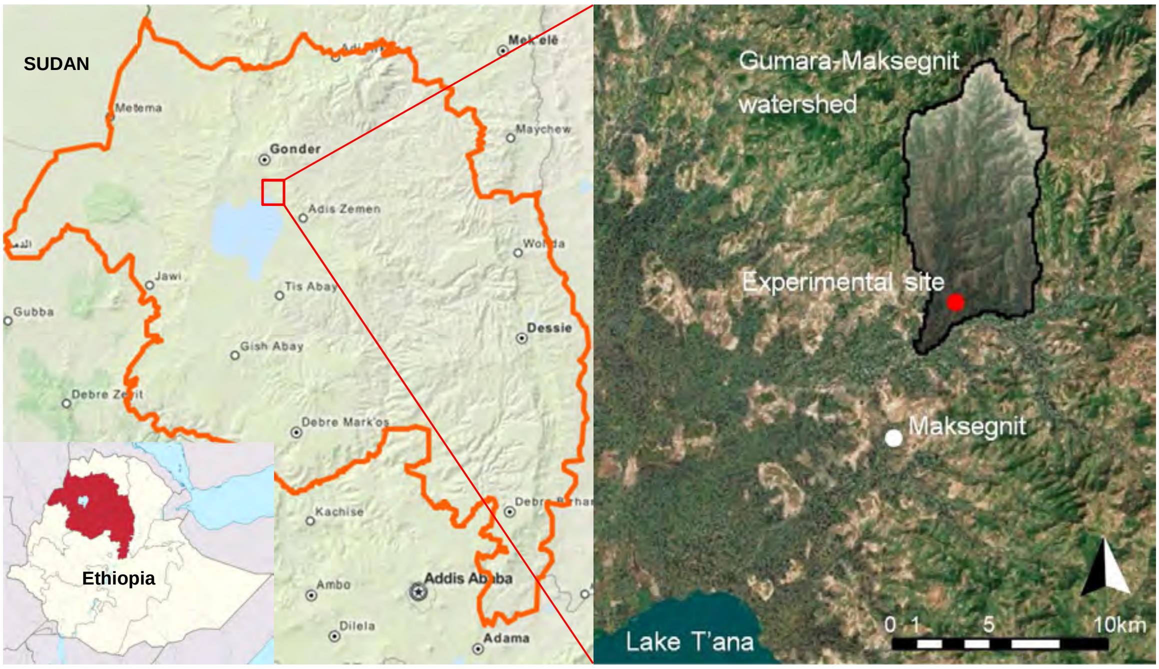

Figure 4.1: Overview of location of the study area left. The Amhara region is highlighted in red. The red box shows the location of the map section right. The map detail shows the location of the Gumara-Maksegnit watershed. The location of the experimental site is indicated by a red dot (Based on OpenStreetMap-RasRoach and TUBS via Wikimedia Commons).

Within the scope of the ongoing research in the watershed, two sub-catchments were defined that are subject to the analysis of the effectiveness of soil and water conservation measures on a long term basis. Both, the Ayaye and the adjacent Aba-K'aloye sub-catchment are located in the lower part of the watershed. The altitudes range from approximately 2012 to 2036 m a. s. l. The major parts of both sub-catchments show an average slope. To find effects on soil erosion and the sediment discharge SWC measures were applied in the Ayaye sub-catchment involving graded stone bunds to reduce sheet erosion and gabions to stabilize gullies. The Aba-K'aloye watershed remained untreated to compare the effects with the status quo. In this work the effect of the stone bunds on the soil physical parameters was the major interest. Therefore the experimental site was located in the Ayaye sub-catchment.

4.1.2 Climate and Agro-ecology

In Ethiopia three major seasons exist that are vernacularly called Kiremt, Bega, and Belg. Kiremt is the main rainy season which lasts from June to September. It contributes the major part to the annual rainfall. The driving influence in this season is the intertropical convergence zone that migrates northwards in this time period. It causes a persistent low that produces large amounts of precipitation. The season Bega follows the main rainy season and lasts from October to February. Dry air masses that are transported by northwestern winds from the Sahara dominate this season. The northern part of Ethiopia is generally dry in this season. The Belg (“small rain”) season lasts from March until May. It is mainly influenced by winds from the Gulf from Aden and the Indian Ocean and brings precipitation mainly to the south of Ethiopia but also leads to some rainfall in the Ethiopian highlands (Seleshi and Zanke, 2004; Dereje Ayalew, 2012).

The Ethiopian highlands, where the study area is located are highly variable in altitude and topography. These two characteristics are strongly correlated to climatic parameters such as temperature and precipitation (Goebel and Odenyo, 1984; Hurni, 1998). Hurni (1998) explains in his work the traditionally used terms of the altitude dependent climatic zones that are well known among Ethiopian land owners. As these zones are described by ranges of temperature and precipitation they consequently explain dominant agricultural land use in the different altitude zones. The zone with the highest altitudes above 3200 m a.s.l. is the Wurch zone. It is characterized as cold and moist. As frost is possible in such altitudes alpine grassland is predominant. The Wurch zone is followed by the Dega zone at altitudes between 2300 and 3200 m a.s.l. It is a cool and humid zone and the predominant crop is barley. The most dominant agricultural zone is the Weyna Dega zone located at altitudes between 1500 and 2400 m a.s.l. Moderate temperatures and sufficient rainfall allow the cropping of all major rainfed crops, such as teff and maize. At lower altitudes between 500 and 1500 m a.s.l. the Kolla zone follows. This zone is defined by warm temperatures and low precipitation that limits the growth of many crops. The dominant crop is sorghum. At altitudes below 500 m a.s.l. the Berha zone is located that is characterized by high temperatures and dry conditions (Dejene, 2003; Hurni, 1998).

The climatic conditions for the Gumara-Maksegnit watershed are characterized in Figure 4.2. The graph shows average minimum and maximum temperature monthly temperature, but also average monthly sums of the precipitation. The average values were determined from data measured at the meteorological station in Maksegnit (see Figure 4.1) over a 20 year time period between 1987 and 2007 for the precipitation and 10 years from 1997 to 2007 for the temperature (GARC, 2010).

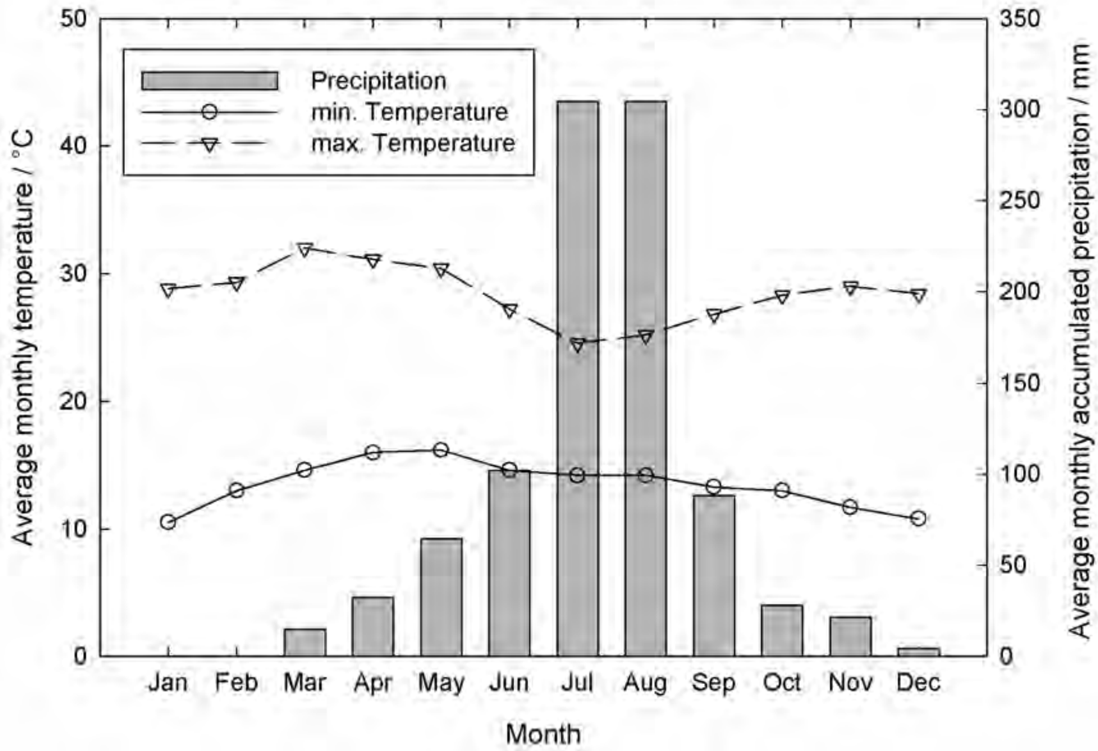

Figure 4.2: Climate graph for the study area. Average minimum and maximum monthly temperature are shown by solid line with circles and dashed line with triangles respectively. The grey bars indicate the average monthly sums of precipitation. The values are averages of measurements taken at the station Maksegnit in the time period from 1987 until 2007 (after GARC 2010).

More than 80 % of the annual rainfall falls in the Kerimt (main rainy) season with the largest amounts in July and August. In the Bega season and especially in January and February almost no rainfall is produced. In the small rainy season, the Belg season, some other 15 % of the annual rainfall occur. The annual rainfall within the 20 year time series shows an average of 1052 mm, but varies between 641 and 1678 mm (GARC, 2010). The minimum and maximum temperatures show the highest values in the Belg season with maxima of 16.1 and 32.0 °C respectively. The lowest minimum and maximum temperatures occur during the period with the most intensive rainfall with values of 10.6 and 25.3 °C respectively (GARC, 2010).

Due to the described climatic conditions of the study area one cropping season is possible starting at the beginning of the main rainy season. As the study area is located in the Weyna Dega agro-ecologic zone a large variety of rainfed crops were present, such as barley, wheat and teff, but also chick pea and sorghum.

4.1.3 Soils and Land use

The soils of the Lake T'ana basin are soils that are or have been strongly influenced by water, but also soils that are characteristic for mountainous areas (see Figure 4.3). The dominant reference soil groups around Lake T'ana are Nitisols, Luvisols, Leptosols, and Vertisols. Lake T'ana is located in a basin of clay rich Nitisols and Luvisols. Vertisols are heavy clay soils that show strong swelling and shrinking effects. As they are influenced by water they are located in valley floors. In the higher areas Leptosols are found. Leptosols are very shallow soils on a hard rock layer with high stone content (Jones et al., 2013, p. 50, p. 103).

Figure 4.4 shows a soil classification map of the Gumara-Maksegnit watershed that is the result of an intensive survey performed by the GARC. The texture ranges from sandy loam to clay. The sandy soils are mainly found in the upper positions and the steeper areas of the watershed, whereas the clay soils are mainly found close to the outlet of the watershed, where the slope is much smaller (GARC, 2010). As the experimental site is located in the lower area of the watershed higher clay contents were present as well as high stone cover of the topsoil.

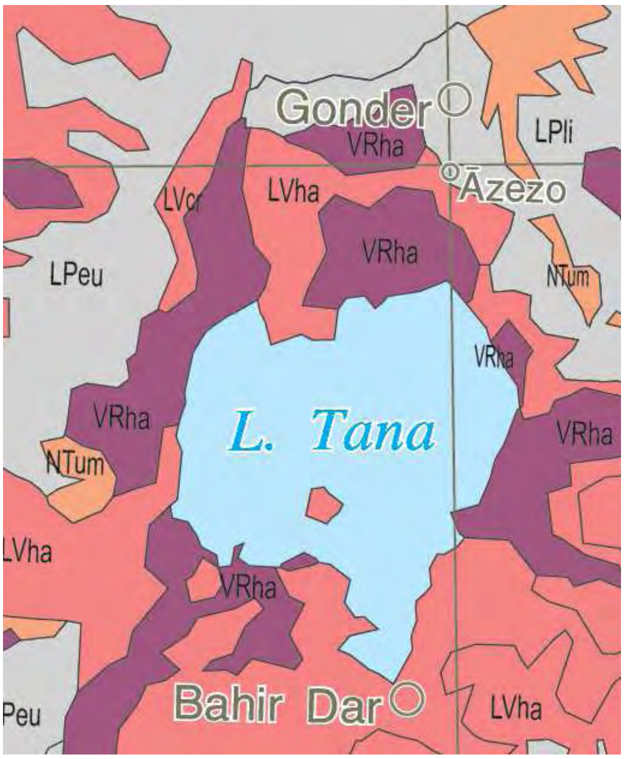

Figure 4.3: Soils of the Lake T'ana basin. The abbreviations NT, LV, VR, and LP stand for the reference soil groups Nitisol, Luvisol, Vertisol, and Leptosol respectively (based on Jones et al., 2013).

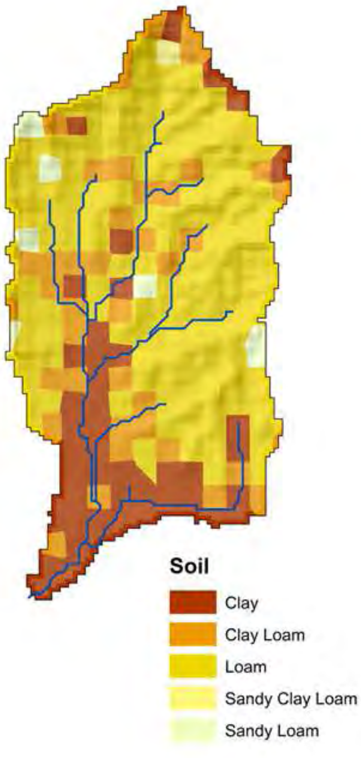

Figure 4.4: Soil classification map of the Gumara-Maksegnit watershed as result of a survey performed by GARC (Addis et al., 2013).

The dominant land use in the watershed is agriculture with more than 75 % of the areas cultivated; 23 % of the areas are forests and 2 % pasture land (Addis et al., 2013). Figure 4.5 shows the distribution of the land use in the watershed. Forest areas are predominant in the upper mountainous part of the watershed. Whereas the lower parts of the watershed are cultivated areas.

Figure 4.5: Land use map of the Gumara-Maksegnit watershed (Addis et al., 2013).

4.2 Experimental site

The experimental site was located in the Ayaye sub-catchment of the Gumara-Maksegnit watershed where SWC measures where applied. There, a hill slope was selected where several fields with stone bunds, but also an area without SWC measures were present. The two areas were similar in their slope, soil type but also in the planted crop. On both areas sorghum was planted in the season 2012. These facts were important prerequisites for the comparability of stone bunds to the case of no SWC measures regarding the measured parameters.

Along the chosen hill slope two transects were defined. One transect crossed three fields with stone bunds as SWC measures applied, perpendicular to the stone bunds. The transect had a length of approximately 71 meters. For comparison, the second transect involved the area where no SWC measures were applied on a length of approximately 55 meters.

Figure 4.6 represents a schematic plan of the experimental site. The arrows indicate the two transects and their directions down the hill slope. The performed measurements and their measurement intervals are represented by the black dots and gray triangles. The measurements and samplings along both transects included the assessment of the stone cover of the topsoil, the measurement of the near surface volumetric water content, taking disturbed and undisturbed soil samples, and performing tension infiltration measurements.

As the used methods of measurement and sampling were different in their expenditure of time, the measurements were performed in different spatial intervals but also different time frequency. Methods that required only little time in the field, such as measurement of the volumetric water content or taking undisturbed samples were performed in a dense sampling interval along both transects. Along the transect with SWC ten measurements were taken per field in between two stone bunds. For the areas around the stone bunds a denser interval of 1 meter was chosen. The additional measurements were distributed equally over the central parts of the fields with intervals between 2.9 and 4.5 meters (depending on the total length of each field). In total this resulted in 30 measurements along the transect with SWC per set of measurements. The measurements along the transect without SWC were performed with a constant interval of 2.5 or 5 meters which results in 11 or 21 measurements per data set.

The tension infiltration measurements were time consuming in their execution. Therefore the measurement interval was chosen very coarse with only one measurement in the upper, the center and the lower position of each field. In total 9 measurements were taken per set of tension infiltration measurements. The execution of tension infiltration measurements along the transect without SWC was omitted at all. As the soil texture was an important input parameter for the analysis of the tension infiltration measurements the disturbed soil samples were taken in the same temporal and spatial patterns.

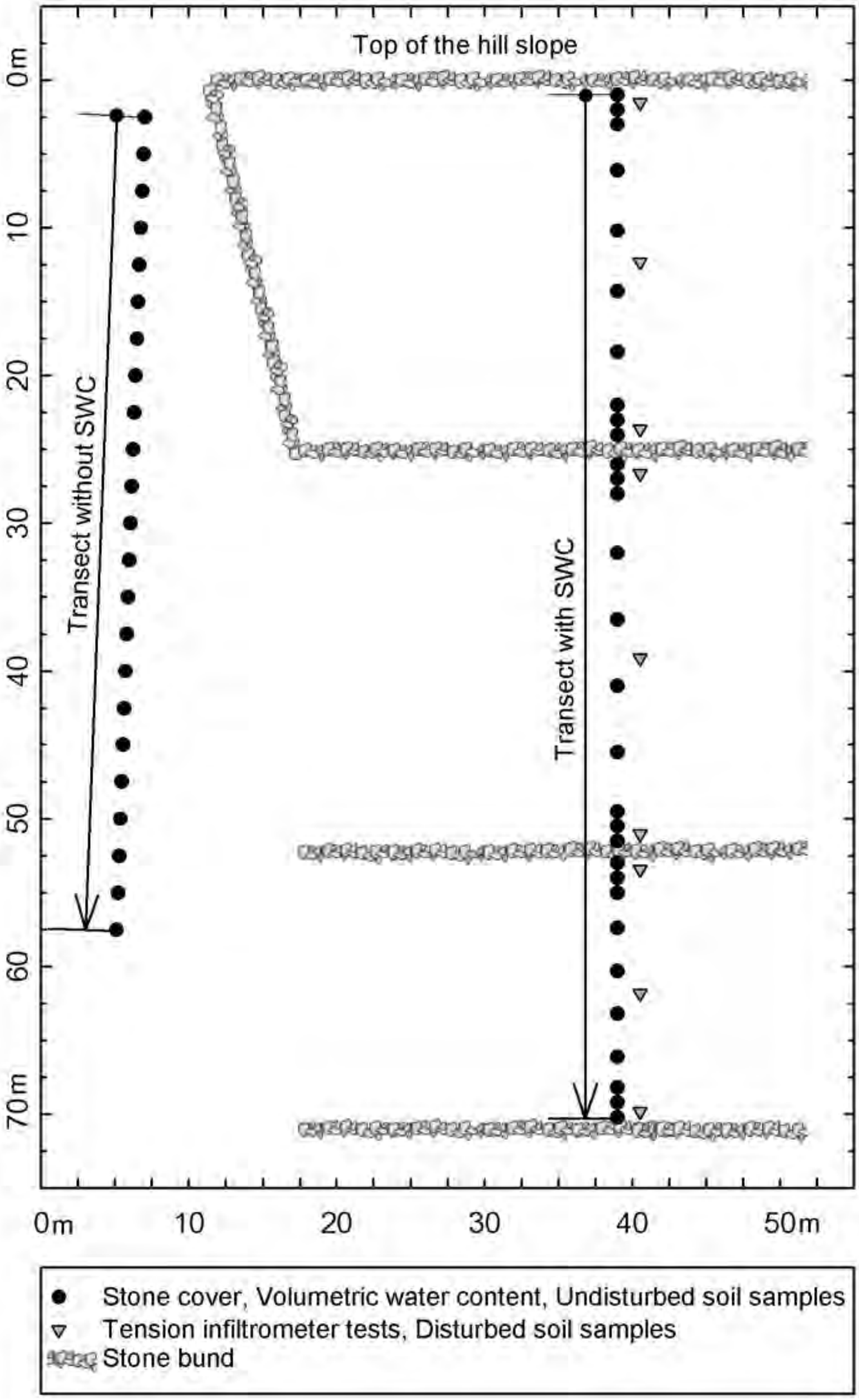

Figure 4.6: Scheme of the experimental site. The stone bunds are indicated by gray textured bars. The arrows show the direction of the transects with and without SWC down the hill slope. The positions of the performed measurements and samplings are represented by the black dots and gray triangles

Time for field experiments was a limiting factor in this work. The main aim on a temporal basis was to gain at least data for the initial, the mid, and the end phase of the rainy season. When possible, additional measurements were performed. Table 4.1 shows a time line for the measurements and samplings performed during the rainy season 2012. At least for the transect with SWC data sets for the initial, mid, and end phase of the rainy season are available. The measurements along the transect without SWC started later, with first measurements on July 11th 2012. The stone cover was assumed to remain constant over the whole rainy season and therefore was assessed only once. At the end of the rainy season we performed a land survey over a time period of two weeks. Within this survey measurements were taken that included the locations of the two transects.

Table 4.1: Time line of the measurements and samplings performed along the two transects in the rainy season of 2012.

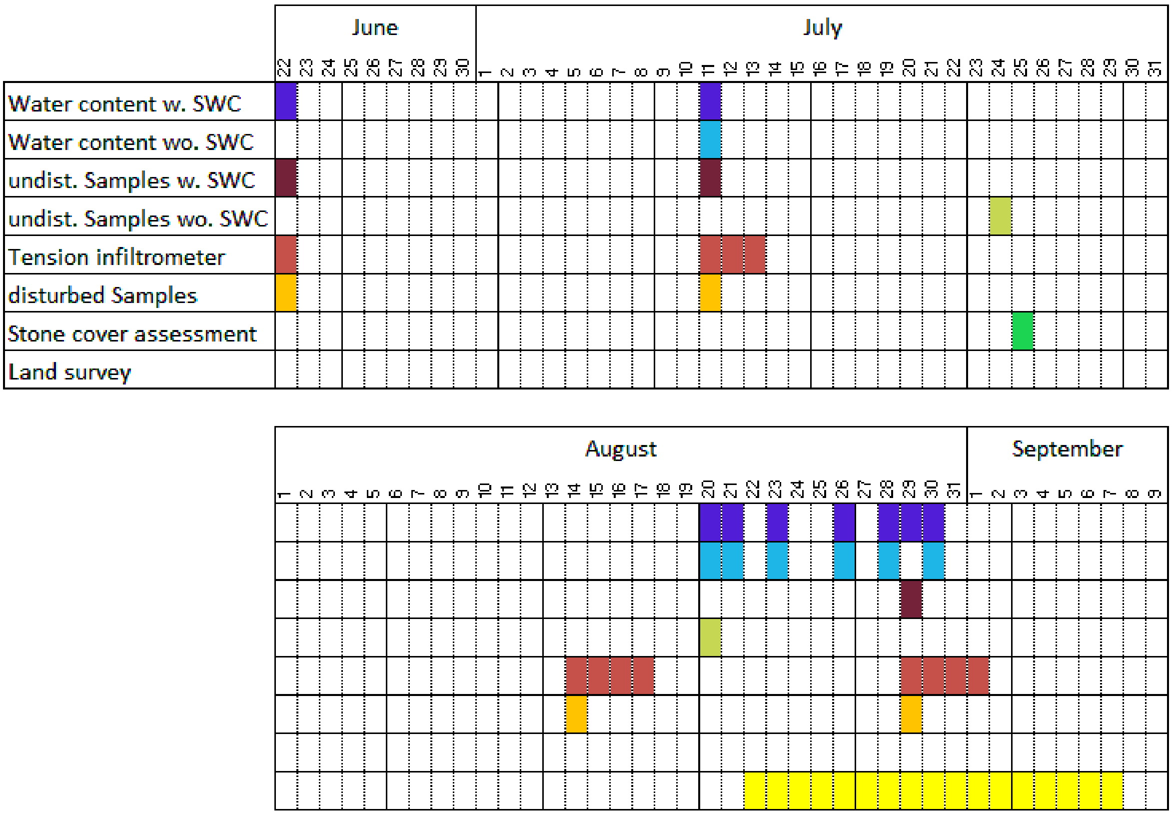

4.3 Near surface volumetric water content

The near surface volumetric water content was determined for the upper 5 cm of the soil layer. As the used method was quick in operation the measurements were performed in the dense sampling intervals and along both of the transects. For the measurement of the near surface volumetric water content the Hydra Probe® Soil Sensor from Stevens® Water Monitoring System, Inc. was used. The sensor applies an indirect measurement method that is based on the different values of dielectric permittivity of air, soil, and water. As this measurement principle does not determine the water content directly a relationship between the measured physical quantities and the volumetric water content must be established. This requires calibration of the measured data. This section involves a short introduction into the measurement principle of this method, as well as a short section about the sensor data calibration.

Figure 4.7: The Stevens® Hydra Probe® in combination with the POGO® Accumulator pack and the pocket PC for data logging (© Stevens® Water).

Figure 4.8: Measurement in the field with the used measurement set up (photo: C. Schürz).

4.3.1 Measurement principle

For a measurement the needles of the probe are entirely pushed into the soil. When inserting the probe the development of voids between the probe needles and the soil due to inaccurate handling must be avoided to minimize measurements errors. The measurement principle is based on the physical characteristic of water. Its dielectric permittivity is, with a value of approximately 80, significantly larger compared to soil or air that show values of approximately 4 and 1 respectively (Gaskin and Miller, 1996). The permittivity or dielectric constant is a terminus used in context with electromagnetism. It represents the proportion of the capacity of a capacitor filled with an isolating material to the case of vacuum (Meschede, 2006, p. 312). It basically describes to which extent an isolating material is polarized by an electrical field (Xu et al., 2012).

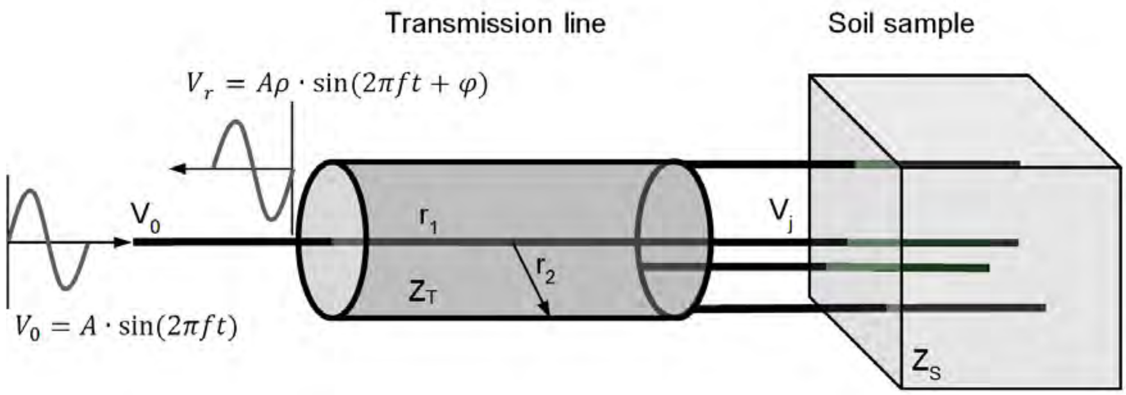

Figure 4.9: Scheme of the electrical function principle of a FDR sensor (based on Gaskin and Miller, 1996).

In an alternating electromagnetic field the dielectric constant is characterized by following complex relationship (Xu et al., 2012):

$$\varepsilon = \varepsilon_r - i\varepsilon_i \tag{4.1}$$

where ε is the complex dielectric permittivity, ε_r is the real part of the dielectric permittivity that represents the capacitive behavior and ε_i describes the imaginary part that is induced by polarization losses. The impedance (complex resistance) of a radial arranged transmitter (as it is the case for the soil probe, but also for the transmission line) is influenced by the dielectric permittivity of the material in-between the two conductors (Gaskin and Miller, 1996).

$$Z = \frac{60}{\sqrt{\varepsilon}} \cdot \ln\left(\frac{r_2}{r_1}\right) \tag{4.2}$$

where Z is the impedance, ε is the complex dielectric permittivity, and r_1 and r_2 are the radius of the inner and the outer conductor. With the propagation of periodic signals reflection of the signal can occur, where the impedance of the conductor changes. For the case of the FDR sensor (Figure 4.9) a change in impedance occurs at the junction of transmission line and sensor. The reflectance of the signal is described by a ratio as follows:

$$\rho = \frac{Z_S - Z_T}{Z_S + Z_T} \tag{4.3}$$

where ρ is the reflection coefficient and Z_S and Z_T are the impedances of soil probe and transmission line. By choosing the length of the transmission line right, the superposition of the original signal and the reflected signal leads to partly amplification at the junction between transmission line and soil probe, but to a partly extinction of the signal at the beginning of the transmission line. The voltage difference of these two points is directly proportional to the reflectance coefficient and therefore proportional to the dielectric permittivity to the sampled medium (Gaskin and Miller, 1996).

$$V_j - V_0 \sim \frac{Z_S - Z_T}{Z_S + Z_T} \tag{4.4}$$

where V_0 and V_j are the voltages at the beginning and at the junction and Z_S and Z_T are the impedances of soil probe and transmission line.

Using the Stevens Water® Hydra Probe® the processing of the voltages is done internally by a microprocessor. The output of the sensor data is given in digital format (Stevens Water, 2007). In combination with the POGO® data logger the output of the sensor was directly displayed and stored for post-processing.

4.3.2 FDR sensor calibration

The output of interest given by the measuring device is the temperature compensated real dielectric permittivity of the air-water-soil continuum of the probed soil volume (Stevens Water, 2007). To derive the volumetric water content a relationship with the dielectric constant is required. Stevens Water (2007) specifies the mathematical shape of the calibration curves in the appearance of an equation (4.5) or (4.6).

$$\theta = A + B \cdot \varepsilon_r + C \cdot \varepsilon_r^2 + D \cdot \varepsilon_r^3 \tag{4.5}$$

$$\theta = A \cdot \varepsilon_r^{\frac{1}{2}} + B \tag{4.6}$$

where θ is the volumetric water content, ε_r is the real dielectric permittivity and A,B,C, and D are coefficients. In this work, equation (4.6) was used for the calibration. For the coefficients A and B various soil specific standard calibration values are available. However, known standard calibrations were incapable of covering the determined relationship of volumetric water content with the measured real dielectric permittivity values. Therefore, an individual calibration curve was determined for the range of measurements, fitting the parameters A and B applying linear regression (see chapter 5.3.1).

4.4 Undisturbed soil sampling

Undisturbed soil samples were taken along both transects in the dense sampling intervals mentioned above. For the sampling the core method was applied. Subsequently, the samples were analyzed for parameters such as bulk density, volumetric water content and total porosity.

4.4.1 Measurement principle

For the core method a cylindrical sampling ring is fully driven into the soil with the sharpened end first. The coherence-characteristics determine if the soils is likely to stay inside the cylinder when it is withdrawn. When taken out, the soil that exceeds the volume of the cylinder is carefully chopped off. Stones in the sample might present difficulties and handling them follows its own rules (Grossman and Reinsch, 2002, p. 207). The samples are then closed with caps to prevent evaporation along with transport. In particular, for the determination of the bulk density the geometry of the sampling rings play an important role. The diameter is recommended to be between 75 and 100 mm and should be greater than the height of the cylinder (Topp et al., 1993, p. 570). Page-Dumroese et al. (1999) found in their work, that sampling rings with smaller diameters led to higher results for bulk density. For this work sampling rings with a volume of 200 cm^3 were used. The height and the inner diameter of the sampling rings were 50 and 72 mm respectively.

Figure 4.10: Sampling equipment including sampling ring, plastic caps, ram and hammer for installation, and shovel for excavation (photo: C. Schürz)

Figure 4.11: Taking undisturbed soil samples in the field. Extracted sampling ring with soil sample and excess soil (photo: C. Schürz).

4.4.2 Analysis

For the analysis of the soil samples the thermogravimetric method was applied. With this method the samples are weighted in moist condition including the sampling ring. The standard procedure then is to dry the samples in the oven at 105°C until the mass change over time is negligible (Topp and Ferré, 2002, p. 419). The samples are reweighted. The bulk density is defined as the mass of a soil sample divided by its volume including the volume of the voids in the sample (Grossman and Reinsch, 2002, p. 207). For the determination of the of the bulk density following relationship was used:

$$\rho_b = \frac{m_{dS+SR} - m_{SR}}{V_{SR}} \tag{4.7}$$

where ρ_b is the bulk density, m_{dS+SR} is the mass of the dried soil sample including the sampling ring, m_{SR} is the mass of the empty sampling ring and V_{SR} is the volume of the sampling ring. The volumetric water content is defined as the volume of the water initially contained in the sample divided by the total sample volume. As the gravimetric method determines masses and no volumes the water volume is calculated using the density of water (Topp and Ferré, 2002, p. 423). The density of water was defined as 1000 kg m^{-3} in this work, which is accurate enough for the analysis.

$$\theta = \frac{(m_{wS+SR} - m_{dS+SR}) \cdot \frac{1}{\rho_W}}{V_{SR}} \tag{4.8}$$

where θ is the volumetric water content, m_{wS+SR} is the mass of the wet soil sample including the sampling ring, m_{dS+SR} is the mass of the dried soil sample including the sampling ring, ρ_W is the density of water and V_{SR} is the volume of the sampling ring. For the estimation of the total porosity a rough approximation was done by assuming a particle density of 2.65 g cm^{-3}.

$$n = 1 - \frac{\rho_b}{\rho_p} \tag{4.9}$$

where n is the total porosity ρ_b is the bulk density and ρ_p is the particle density (Flint and Flint, 2002, p. 242).

4.5 Tension infiltration measurements

Tension infiltration measurements were performed in the initial phase, the mid and the end of the rainy season. As the method is time consuming in its operation only measurements along the transect with SWC and only in three characteristic positions per field were possible to perform. For the measurement a tension infiltrometer from Soil Measurement Systems® Inc. was used. Further on, the measurement principle and the device characteristics are explained, as well as the analysis of the measured data applying Wooding's method and inverse parameter estimation using the software package DISC.

4.5.1 Measurement principle

The design of the used tension infiltrometer is described by Ankeny et al. (1988) and Casey and Derby (2002). It basically consists of a bubble tower, a water reservoir and an infiltration disc that establishes the contact to the soil for water infiltration. The water supply from the water reservoir employs the Boyle Mariotte principle, where only water is supplied to the infiltration disc when air intrudes the reservoir. The only point where air can enter the device is the air entry tube of the bubbling tower. To enter the air must overcome the preset water tension that results from the height difference of the water table in the bubbling tower and the lower end of the air entry tube. The driving force that leads to entering air is the pressure difference of the atmospheric pressure to the air pressure in the bubbling tower. When air enters the bubbling tower it expands and establishes equilibrium in air pressure with the water reservoir by air bubbling into the reservoir via the bubbling tube.

The used tension infiltrometer had an infiltration plate with a diameter of 20 cm with 2 mm holes in the bottom that allow sufficient water flow. To prevent air intrusion via the holes a wetted nylon cloth with a specific air entry point was attached to the base of the disc. To reduce the risk of damage to the cloth and to ensure proper hydraulic contact a plane surface using soil from the experimental site was established and any sharp fragments were removed. Usually filter sand is used for this purpose. However, no such material was available. The bubbling tower and the water reservoir had diameters of 2.56 and 5.1 cm respectively. In both tubes scales were attached to the tube wall to adjust the water tension in the bubbling tower and to manually read the changes of the water level in the water reservoir (Soil Measurement Systems Inc., 2013).

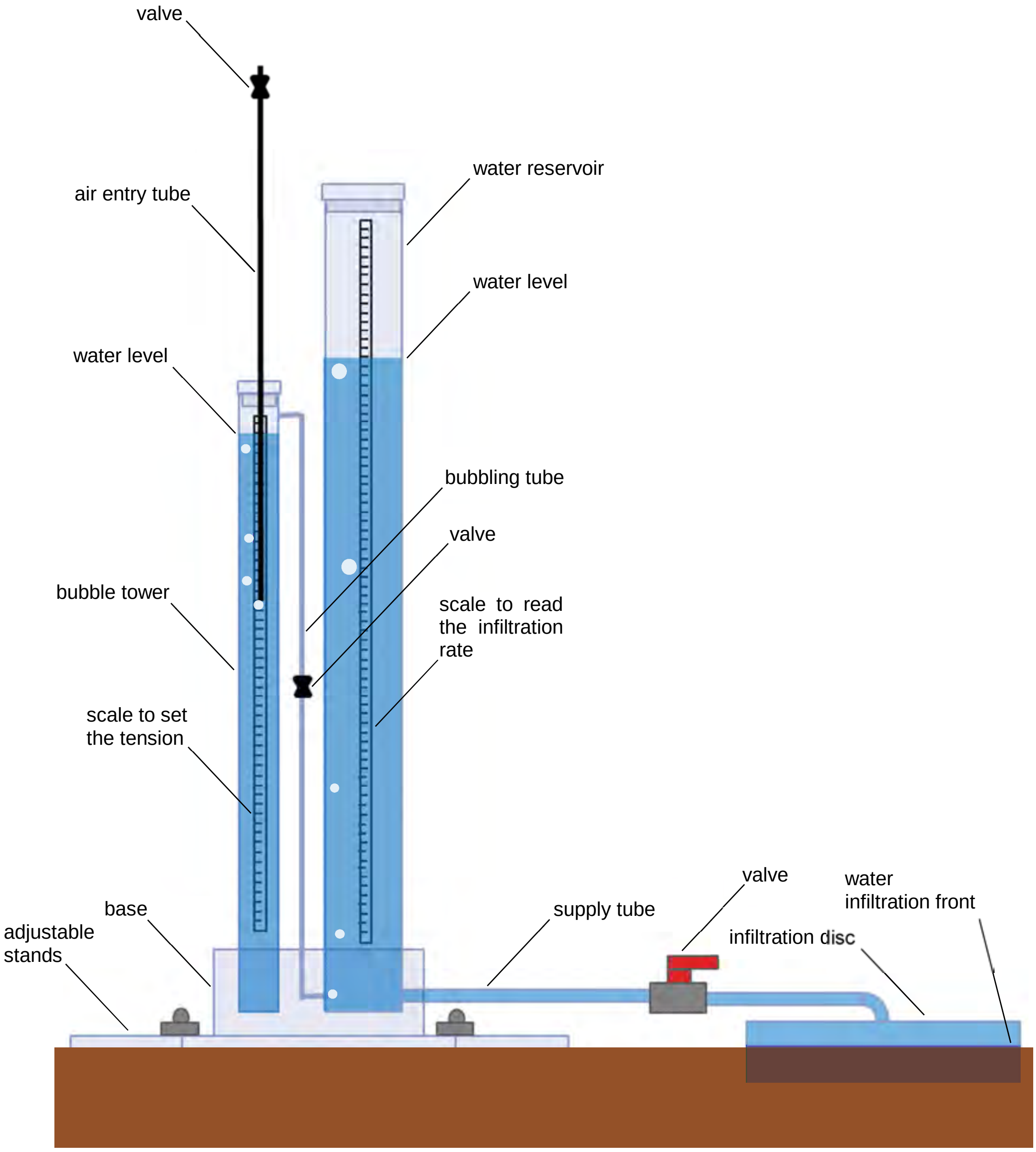

Figure 4.12: Scheme of a tension infiltrometer used for the measurement (based on Casey and Derby, 2002)

The measurements were performed applying three different tension values of -8, -4, and 0 cm starting with the lowest for each measurement. The measurements with each tension were preformed until steady-state flow established (last three differences in water table change per time interval are equal). Before and after each measurement undisturbed soil samples were taken to determine initial and end volumetric water content gravimetrically.

4.5.2 Analysis

The measured tension infiltration data was used to determine the saturated hydraulic conductivity but also water retention characteristics based on the van Genuchten model. The saturated hydraulic conductivity was determined by Wooding's analytical solution (1968) that only requires steady state infiltration rates for at least two different tension settings. Whereas, the approach of Šimůnek and van Genuchten (1996, 1997) considers the entire cumulative infiltration over time to inversely estimate water retention parameters (Hopmans et al., 2002). The software to solve the inverse parameter estimation is called DISC which is based on Hydrus 2D/3D, but designed especially for the analysis of tension infiltration data. It was developed and documented by Šimůnek and van Genuchten (2000).

4.5.2.1 Wooding's analytical solution

Wooding's analytical solution was used to determine the saturated hydraulic conductivity. The approach of Wooding (1968) solving analytically the steady infiltration from a shallow pond has been adapted to steady tension infiltration (Angulo-Jaramillo et al., 2000; Ankeny et al., 1991; Reynolds and Elrick, 1991; and many others). Wooding's solution is stated as follows (Ankeny et al., 1991):

$$Q_\infty = r^2\pi\, K_{fs} + 4r\, \Phi \tag{4.10}$$

where Q_∞ is the steady state infiltration flux, K_{fs} is the saturated hydraulic conductivity, r is the radius of the water source and Φ is the matric flux potential that is defined as the integral of the unsaturated hydraulic conductivity $K(h)$ over the matric potential h: $\Phi(h) = \int_{h_0}^{h_1} K(h)dh$ (Gardner, 1958). Assuming a constant ratio $\alpha = {K(h)}/{\Phi(h)}$ for the pressure range h_1 to h_2 (Ankeny et al., 1991; Philip, 1985) and using the exponential model for the unsaturated hydraulic conductivity after Gardner (1958):

$$K(h) = K_{fs}e^{\alpha h} \tag{4.11}$$

where $k(h)$ and k_{fs} are the unsaturated and the saturated hydraulic conductivities, α is a constant and h is the pressure head, substituting and transforming Equation (4.10) logarithmically leads to following linear relationship (Reynolds and Elrick, 1991):

$$\ln(Q_\infty) = \alpha h + ln\left[\left(r^2\pi + \frac{4r}{\alpha}\right)K_{fs}\right] \tag{4.12}$$

where Q_∞ is the steady state infiltration flux, α is a constant, h is the pressure head, K_{fs} is the saturated hydraulic conductivity, and r is the radius of the water source. α represents the slope of the linear relationship between steady state flow and pressure head. It can be determined for an interval of two steady flows Q_i and Q_{i+1} for the applied pressure heads h_i and h_{i+1} as follows:

$$\alpha_{i+1/2} = \frac{\ln\left(\frac{Q_i}{Q_{i+1}}\right)}{(h_i - h_{i+1})} \tag{4.13}$$

where $\alpha_{i+1/2}$ is the slope for the interval i to $i+1$ Furthermore, the hydraulic conductivity k_{fs} for the same interval can be determined from the intercept of this linear relationship as follows:

$$K_{fs\ i+1/2} = \frac{4\alpha_{i+1/2} Q_i}{r(1+4\alpha_{i+1/2} r)\left(\frac{Q_i}{Q_{i+1}}\right)^{\frac{h_1}{h_1-h_2}}} \tag{4.14}$$

where $K_{fs\ i+1/2}$ is the saturated hydraulic conductivity determined from the partial intercept of the interval i to $i+1$. Substituting the exponential model after Gardner (1958) with the found $\alpha_{i+1/2}$ and $K_{fs\ i+1/2}$ values, unsaturated hydraulic conductivity for each $h_{i+1/2}$ can be calculated (Reynolds and Elrick, 1991):

$$K\left(h_{i+1/2}\right) = K_{fs\ i+1/2} e^{\alpha_{i+1/2}\, h_{i+1/2}} \tag{4.15}$$

where $K\left(h_{i+1/2}\right)$ is the unsaturated hydraulic conductivity for the interval i to $i+1$.

4.5.2.2 Inverse parameter estimation

For the analysis of the tension infiltration data the software package DISC was used that was developed and documented by Šimůnek and van Genuchten, (2000). Analyzing the data the software uses a numerical solution of the Richards equation modified for radial symmetric Darcian flow (Šimůnek and van Genuchten, 2000; Warrick, 1992):

$$\frac{\partial\theta}{\partial t} = \frac{1}{r}\frac{\partial}{\partial r}\left(r\,K\frac{\partial h}{\partial r}\right) + \frac{\partial}{\partial z}\left(K\frac{\partial h}{\partial r}\right) - \frac{\partial K}{\partial z} \tag{4.16}$$

where θ is the volumetric water content, h is the pressure head, K is the hydraulic conductivity, t is the time, r is the radial coordinate, and z is the vertical coordinate positive in downward direction.

The initial and boundary conditions for solving the Richard's equation are adapted for tension infiltrometer data in the software package (Šimůnek and van Genuchten, 2000; Warrick, 1992):

$$\begin{aligned} \theta(r,z,t) &= \theta_i(z) \qquad t=0 \\ h(r,z,t) &= h_i(z) \qquad t=0 \end{aligned} \tag{4.17}$$

$$h(r,z,t) = h_0(t) \qquad 0 < r < r_0\,, z = 0 \tag{4.18}$$

$$\frac{\partial h(r,z,t)}{\partial z} = 1 \qquad r > r_0\,, z = 0 \tag{4.19}$$

$$h(r,z,t) = h_i \qquad r^2 + z^2 \to \infty \tag{4.20}$$

where $\theta(r,z,t)$ and $h(r,z,t)$ are volumetric water content and respective pressure head dependent on the two spatial coordinates r and z and the time t. θ_i is the initial water content, h_i is the respective initial pressure head, h_0 is the supply pressure head of the tension infiltrometer, and r_0 is the infiltration disc radius.

To define the unsaturated soil hydraulic properties which are required for the numerical solution of the Richard's equation a model must be selected. Šimůnek and van Genuchten (2000) chose the unsaturated soil hydraulic functions of van Genuchten (1980) for implementation in the software which are inversely fitted to the tension infiltration data. The soil water retention $S_e(h)$ and the unsaturated hydraulic conductivity $K(h)$ are given by (Šimůnek et al., 1998):

$$S_e(h) = \frac{\theta(h) - \theta_r}{\theta_s - \theta_r} = \frac{1}{(1 + |\alpha h|^n)^m} \tag{4.21}$$

$$K(\theta) = K_{fs} S_e^I \left(1 - \left(1 - S_e^{I/m}\right)^m\right)^2 \tag{4.22}$$

where S_e is the effective water content, K_{fs} is the saturated hydraulic conductivity, θ_r and θ_s are the residual and the saturated water content respectively, I is a pore-connectivity parameter, and α, n, and m are empirical parameters. The pore-connectivity parameter I was estimated by Mualem (1976) to a value of 0.5. This reduces the number of parameters that are predicted inversely to 5, which are θ_r, θ_s, α, n, and K_{fs}.

The objective function $\Phi(\boldsymbol{\beta}, q_m)$ that is minimized during the parameter estimation was defined by Šimůnek and van Genuchten (1996) as follows:

$$\Phi(\boldsymbol{\beta}, q_m) = \sum_{j=1}^{m} \left(\sum_{i=1}^{n_j} \left(q_j^*(t_i) - q_j(t_i, \boldsymbol{\beta}) \right)^2 \right) \tag{4.23}$$

where m represents in the case of this work the different sets of cumulative infiltration measurements, n_j is the number of measurements in one particular data set, $q_j^*(t_i)$ is a specific measurement at the time step t_i for the j^{th} set of measurements, $\boldsymbol{\beta}$ is the vector of the optimized parameters, $q_j(t_i, \boldsymbol{\beta})$ is the model prediction for a given parameter set $\boldsymbol{\beta}$ at the time step t_i.

For the optimization $K(h)$ was estimated a-priori applying Wooding's analytical solution and was therefore excluded in the parameter estimation of the parameter set $\boldsymbol{\beta}$. To provide further stability to the optimization algorithm the residual water content θ_r was also set to a fixed value of 0.090 m^3 m^{-3} as this was the average prediction determined with the pedotransfer analysis applying ROSETTA light to soil texture and bulk density data. The two pre-definitions led to a reduction of inversely estimated parameters to a number of three, namely θ_s, α, and n. Initial values for the fitting of these three parameters were also estimated using the pedotransfer function ROSETTA (Schaap et al., 2001) with soil texture and bulk density as input parameters. Initial an end values for the volumetric water content were determined with thermo gravimetric method (see chapter 4.4).

4.6 Disturbed soil sampling

The soil texture is an important input parameter for the inverse simulation of the soil water characteristics. Therefore, the disturbed soil samples were taken in the exact same temporal and spatial pattern as the tension infiltration measurements were performed. A sample consisted of a mass of several 100 g taken from a thin layer in the top soil. To analyze the disturbed samples for their soil texture the hydrometer method was applied by the Gonder Soil Testing Laboratory.

4.6.1 Analysis

The hydrometer method is based on Stokes' Law, where the settling velocity of a particle is basically dependent on the square of its radius.

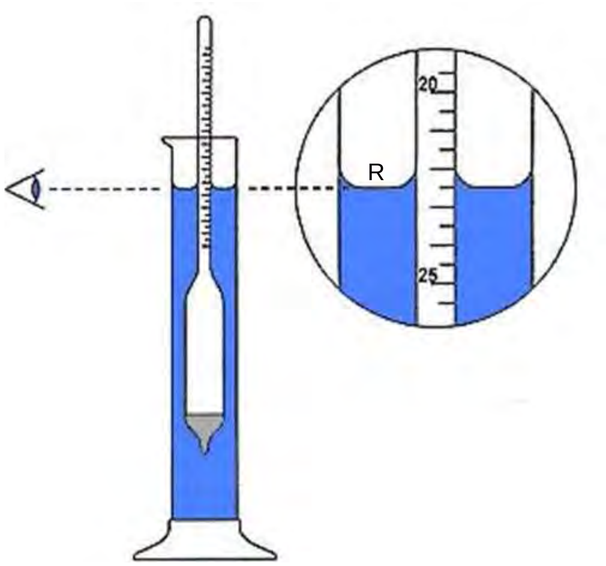

Figure 4.13: Measurement principle of the hydrometer (based on Avogadro Lab Supply).

For the approach of the hydrometer this leads to following relationship:

$$\theta = \sqrt{\frac{18\eta h'}{g(\rho_s - \rho_l)t}} \tag{4.24}$$

where θ is the sedimentation parameter, η is the solution viscosity, h' is the hydrometer settling depth, ρ_s and ρ_l are the particle and the solution density and t is the time (Glendon and Or, 2002, p. 279). For specific hydrometers linear relationships between the scale reading R on the hydrometer and the hydrometer settling depth h' are given. Therefore, the reading R on the hydrometer and the concentration of the soil solution C are directly related to each other at 20°C for most of the hydrometers. The percentage of a specific soil fraction in suspension can be calculated as follows:

$$P = \left(\frac{C}{C_0}\right) \times 100\% \tag{4.25}$$

where C is the concentration determined from the reading R and C_0 is the initial concentration of the soil solution (Glendon and Or, 2002, p. 279). To derive the percentages of the specific soil fractions sand silt and clay, readings must be done at specific time steps according to the sedimentation velocity (Eq. (4.24)) of the specific grain size. The Gonder Soil Testing Laboratory performed readings at 40 s and 2 h.

4.7 Stone cover assessment

On June 25th 2012 photos were taken along both transects in the same interval as the other measurements were performed. For support in the subsequent analysis of the pictures a scale was placed in the pictures as reference. In the analysis a 60 by 60 cm plot was defined in the taken pictures. This represents approximately three times the maximum stone diameter found and was considered as a representative sample size (see Figure 4.14).

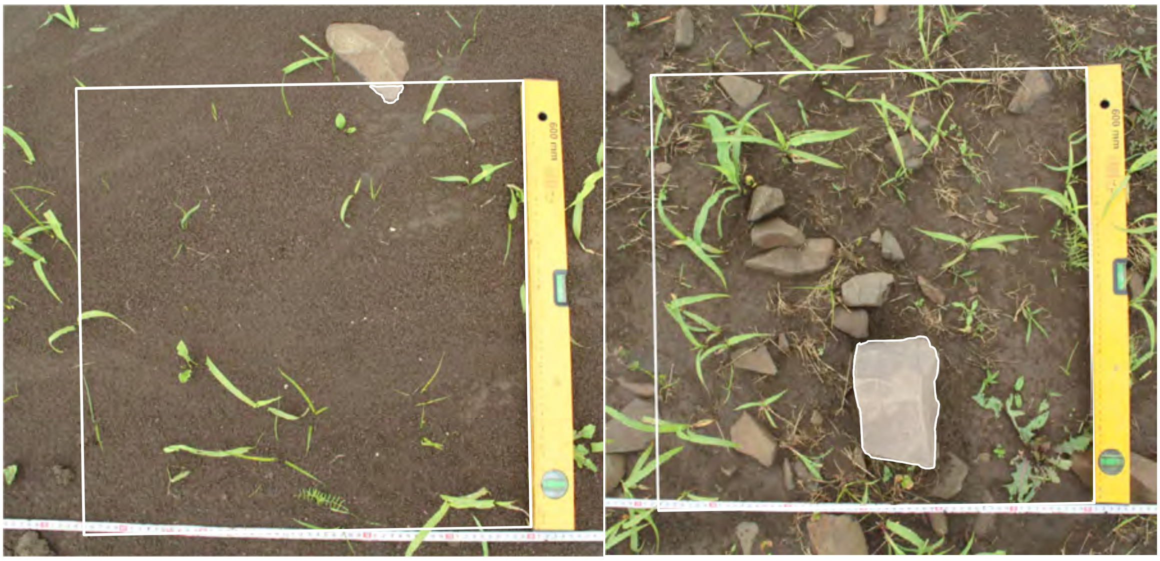

Figure 4.14: Two examples for the taken pictures along the transect with SWC that were assessed. The left picture shows an example for the sedimentation zone above the stone bunds where most of the stones are covered due to sedimentation. Right a typical example of the center zone is shown. In each picture the area of one stone is determined by a polygon (photos: C. Schürz).

The analysis was performed using two different approaches. The first one involved a manual analysis by drawing polygons using the CAD software AutoCad® and summing up the total area of the defined polygons. A second, more sophisticated approach was performed using an image classification tool provided with ArcGIS®. Supervised Classification was performed by selecting training samples for the classes soil, vegetation, and stone in each picture and subsequently classify the picture pixels applying maximum likelihood classification. The total area covered by stones is the sum of the pixels assigned to this class (Brenner, 2013, p. 28). Both approaches led to similar results. For further analysis only the results of the automatized method were used.

4.8 Land survey

In the period from August 22nd 2012 to September 7th 2012 a local surveyor performed a land survey on the hill slope where the two transects were located using a Sokkia® total station. As the work of Claire Brenner (2013) required a fine 1 by 1 meter raster the measurements were available in such resolution for this work too. The relevant measurements that represent the transects were extracted from the whole set of measurements. As the changes in inclination are higher in the areas above the stone bunds these areas required a finer measurement resolution. Further on, small parts of the transects were not covered by the land survey. Therefore, additional measurements were performed manually using a measuring tape and a scale to interpolate and extrapolate relative measurements to the points measured in the survey.

Figure 4.15: Land survey using the total station (photo: C. Schürz).

Figure 4.16: Using several reflectors for faster raster measurement (photo: C. Schürz).

The soil surface was covered by stones of different size and had a rough soil surface. This led to large small scale variations in the measurements. However, for this work only the changes on a larger scale were of interest. Therefore, polynomial splines were fitted to the data points using the function polyfitc() included in the software Mathcad®. The inclinations of both transects were derived by forming the first derivative of the fitted polynomial functions.

4.9 Precipitation

In the Gumara-Maksegnit watershed three rain gauges are located. An additional rain gauge is located in Maksegnit (Figure 4.17). The relevant rain gauging station for the experimental site is located in the Aba-K'aloye sub-catchment approximately 1 kilometer away from the experimental site. The precipitation was measured with a tipping bucket ombrometer, where one tip is equal to 0.2 mm of rainfall. Additionally the air temperature was measured on hourly basis.

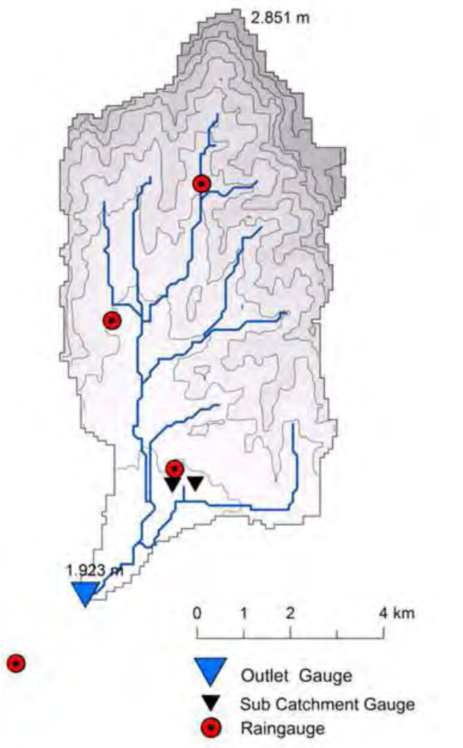

Figure 4.17: Positions of the four rain gauges relevant for the Gumara-Maksegnit watershed (Addis et al., 2013).

Figure 4.18: Reading out the rain gauge in the Aba-K'aloye sub-catchment (photo: C. Schürz).

4.10 Statistical analyses

To proof the visual findings in the data for their significance, statistical tests were required. The following chapter explains in short the tests that were used for the analyses. The statistical analyses were performed with the software R (R Core Team, 2013). The significance level α was set to 0.05 for all the analyses.

4.10.1 Normality of the data sets

Normal distribution of the data is a pre-requisite for various statistical tests. For testing whether a data set is normally distributed or not the one-sample Kolmogorov-Smirnoff test was applied using the function ks.test() from the basic R package ‘stats’ (R Core Team, 2013). It is a nonparametric test to compare a data sample with an assumed distribution function (F_x/F_0). The test quantifies a distance between the empirical distribution function of the sample and the cumulative distribution function of the assumed cumulative distribution function (see (4.28)). It is a very stable test and compared to the χ^2-test works well for small sample sizes (Sachs, 1974, p. 256).

The hypotheses and the test statistic are as follows:

$$H_0 : F_x(x) = F_0(x) \tag{4.26}$$

$$H_1 : F_x(x) \neq F_0(x) \tag{4.27}$$

$$d_n = sup_x | F_x(x) - F_0(x)| \leq d_\alpha \tag{4.28}$$

where $F_x(x)$ is the distribution of the measured data and $F_0(x)$ is the hypothetical distribution function. d_n is the test variable, which represents the maximum distance of the distribution of the data to the assumed distribution function. This value is compared to the critical value d_α. The R function ks.test() obtains exact probability values for a given critical value d_α for the case of a one-sample two-sided test according to the method of Marsaglia et al. (2003).

Additionally the data sets were visually tested by observing the quantile-quantile plots of the data against a normal distribution. For the visualization the R function qqnorm() from the basic R ‘stats’ package (R Core Team, 2013) was used.

4.10.2 Differences of variance

Homogeneity of variances is an important prerequisite for subsequent tests of the mean values. Furthermore, changes in the variability of the soil properties for different spatial and temporal steps were important information. The described tests are separated for the number of samples that are tested for differences.

4.10.2.1 Test for two independent samples

For testing whether the variances of two normally distributed populations (σ_1 and σ_2) differ significantly or not, the test statistic according to equation (4.31) was used (Sachs, 1974, p. 205). The implementation was done with the basic R function var.test(), that is part of the basic ‘stats’ package (R Core Team, 2013). The result of this test criterion follows the F-distribution.

The hypotheses and the test statistic are as follows:

$$H_0 : \sigma_1^2 = \sigma_2^2 \tag{4.29}$$

$$H_1 : \sigma_1^2 \neq \sigma_2^2 \tag{4.30}$$

$$F_{n,m} = \frac{s_1^2}{s_2^2} \leq F_{crit} \tag{4.31}$$

where σ_1 and σ_2 are the standard deviations of the populations from which the samples are taken. $F_{n,m}$ is the test variable. It is calculated forming the quotient of the two sample variances s_1^2 and s_2^2. The R function var.test() determines the probability value according to the given critical F value and the sample sizes of the two data sets.

4.10.2.2 Test for more than two independent samples

Levene (1960) introduced a robust test to test the variances of two or more samples for their equality. Compared to F-test and for example Barlett’s test that is also applicable for more than two samples, Levene’s test is less sensitive to deviations of the sample distribution to normal distribution. Levene uses a classical ANOVA procedure in his approach to compare the deviations in the sample groups to the sample group mean $d_{ij} = \left|x_{ij} - \bar{x}_{i.}\right|$ to the overall mean deviation (Gastwirth et al., 2009). The implementation was done with the R function Levenetest() taken from the package ‘car’ (Fox et al., 2013).

The hypotheses and the test statistic are as follows:

$$H_0 : \sigma_1^2 = \sigma_2^2 = \cdots = \sigma_k^2 \tag{4.32}$$

$$H_1 : at\ least\ one\ sample\ variance\ is\ significantly\ different. \tag{4.33}$$

$$F = \frac{N-k}{k-1} \frac{\sum_{i=1}^{k}(\bar{d}_{i.} - \bar{d}_{..})^2}{\sum_{i=1}^{k}\sum_{i=1}^{n_i} n_i (d_{ij} - \bar{d}_{i.})^2} \leq F_{crit} \tag{4.34}$$

where k is the number of sample groups, N and n_i are the total number of differences and the number of differences in the i^{th} group, and d_{ij}, $\bar{d}_{i.}$, and $\bar{d}_{..}$ are the difference of the j^{th} value in the i^{th} group, the mean difference of the i^{th} group and the total mean of differences respectively. The R function Levenetest() determines the probability value according to the given critical F value.

4.10.3 Differences in mean values

Differences in the mean values of the soil properties for different spatial and temporal steps were one of the major aspects in the descriptive analysis of the data. The described tests are separated for the number of samples that are tested for differences.

4.10.3.1 Test for two independent samples

For testing whether the mean values of two samples of different populations (μ_1 and μ_2) with different sample sizes ($n_1 \neq n_2$) differ significantly or not, the two sample t-test was applied. The result of this test criterion follows a student t-distribution. Normal distribution of the data and assumption of equal variance of the samples are pre-requisites for the use of this test (Sachs, 1974, p. 209). The implementation was done with the basic R function t.test(), that is part of the basic 'stats' package (R Core Team, 2013).

The hypotheses and the test statistic are as follows:

$$H_0 : \mu_1 = \mu_2 \tag{4.35}$$

$$H_1 : \mu_1 \neq \mu_2 \tag{4.36}$$

$$|t_{n,m}| = \left| \sqrt{\frac{n \cdot m}{n+m}} \frac{\bar{x}_1 - \bar{x}_2}{s} \right| \leq t_{crit} \tag{4.37}$$

where μ_1 and μ_2 are the expectation values of the populations from which the samples are taken. In equation (4.37) n and m are the sample sizes,$\bar{x}_1$ and $\bar{x}_2$ are the mean values of the samples and s is the common standard deviation of the two samples. $t_{n,m}$ is the test variable. The R function t.test() determines the probability value according to the determined critical t value.

4.10.3.2 Tests for two or more samples

To test groups of more than two samples two different tests were applied that are differently robust to violations of the assumption of homoscedasticity. The pairwise t-test is according to its prerequisites, hypotheses, and test statistic similar to the two sample t-test. All possible combinations of samples are tested against each other for significances in their mean values. The two major differences are that for the used standard deviation a common value for all samples is used. Second, the probability of not making a type I error is superposed when performing more than one test and the assumed probability of a single t-test does not hold anymore globally. Therefore, the Bonferonni correction (see (4.38)) is applied to adjust the probability of the type I error (Abdi, 2007).

$$p^* = pk \tag{4.38}$$

where p^* is the adjusted probability value, p is the probability value for one pair test and k is the number of samples. The pairwise t-test was implemented by the R function pairwise.t.test() taken from the R package 'asbio' (Aho, 2013). It determines the probability value according to the given critical t value. The resulting probability value is already adapted by the Bonferonni correction.

The pairwise t-test requires the same prerequisites as the two sample t-test. However, homoscedasticity is violated for many groups of samples in the analyses. Therefore, a second test for differences in the mean values was applied. Fisher's least significant differences test allows different sample sizes but also violations of homoscedasticity. The test is based on the pairwise t-test. However, the variance is calculated as pooled variance involving all samples. The significance value is not corrected considering multiple comparisons. This makes the test sensitive for type I errors (Abdi and Williams, 2010). For all analyses the pairwise t-test as well as the least significance test were performed and checked for significances in both tests.

The hypotheses and the test statistic for Fisher's least significance test are as follows:

$$H_{0,ij}: \ \mu_i = \mu_j \tag{4.39}$$

$$H_{1,ij}: \ \mu_i \neq \mu_j \tag{4.40}$$

$$|t_{N-k}| = \left| \frac{\bar{x}_i - \bar{x}_j}{\sqrt{s\left(\frac{1}{n} + \frac{1}{m}\right)}} \right| \leq t_{crit} \tag{4.41}$$

where μ_i and μ_j are the expectation values, n and m are the sample sizes and $\bar{x}_i$ and $\bar{x}_j$ are the mean values of the i^{th} and the j^{th} sample respectively; s is the pooled standard deviation and t_{N-k} is the test variable with $N-k$ degrees of freedom, where N is the total number of observation and k is the total number of samples. The least significance test was implemented by the R function lsdCI() taken from the R package 'asbio' (Aho, 2013). It determines the probability value according to the given critical t value.

4.10.4 Analyzing spatial periodicity in the data

On a spatial basis a periodic behavior was expected, as the spatial pattern of stone bunds repeats three times along the transect with SWC. To visualize the periodic patterns, an autocorrelation analysis was performed and the autocorrelogram plots were evaluated visually. To find the dominant recurrence interval along the spatial domain spectral plots of the data were analyzed visually. To determine whether the visual findings were significant or not Fisher's g-test was performed.

4.10.4.1 Autocorrelogram analysis

A soil property A was sampled at the locations x_i along both transects resulting in n measurements A_i. To determine the autocorrelation coefficient for a set of measurements the covariance of the data set with the same set but shifted by a lag distance h is calculated (Nielsen and Wendroth, 2003, p. 32). For a better interpretation of the value it is normalized by dividing the variances of both data sets as shown in Equation (4.42):

$$r(h) = \frac{cov\big(A_i(x), A_i(x+h)\big)}{\sqrt{var\big(A_i(x)\big) \cdot var\big(A_i(x+h)\big)}} \tag{4.42}$$

where $r(h)$ is the autocorrelation coefficient for the lag distance h The normalization results in a range of 1 to -1 for full positive and negative autocorrelation (Dunn, 2005, p.

354, Wendroth and Nielson, 2002, p. 120). The autocorrelogram is the visualization of the calculated autocorrelation coefficient for different lag distances h, plotted over h. The determination of the autocorrelation coefficients for all h was performed applying the R function acf() from the basic R 'stats' package (R Core Team, 2013).

4.10.4.2 Spectral analysis

Within the spectral analysis the series of data is basically separated into a series of harmonic components. It is based on Fourier analysis, that states that every series of data or signal can be described by a sum of sinusoidal components as shown below (Bloomfield, 2004, p. 2; Nielsen and Wendroth, 2003, p. 196):

$$S(f) = \sum_{h=0}^{\infty} r(h) \mathrm{e}^{-2\pi f i h} \tag{4.43}$$

where $S(f)$ is the is the spectrum of the superposed sinusoidal functions with the amplitudes $r(h)$ from the autocorrelation analysis. The formulation stated is written in the complex form where $i^2 = -1$. To visualize the spectrum, the amplitudes for each wavelength are plotted over the respective wavelengths (Wendroth and Nielson, 2002, p. 125). The algorithm used to perform this analysis was implemented in the R function spectrum() taken from the basic R 'stats' package (R Core Team, 2013). It uses fast Fourier transformation and results in the spectral density of the data.

Finding significance for the dominant frequency in the spectrum Fisher's exact g-test (1929) was performed. The test was performed applying the R function fisher.g.test() from the R package 'GeneCycle' (Ahdesmaki et al., 2012) to the data. It calculates the probability value of one dominant but unknown frequency in the spectrum of a data set.

4.10.5 Cross-semivariogram analysis

Variogram functions can describe spatial correlation. They characterize the differences in the variance of a measured property over several scales as they determine the variance differences of sample values that are separated by the lag distance h. The variance estimator determined from the data is stated as follows (Yates and Warrick, 2002, p. 86):

$$\gamma(h) = \frac{1}{2N(h)} \sum_{i=1}^{N(h)} \left(A_i(x_i) - A_i(x_i + h)\right)^2 \tag{4.44}$$

where $\gamma(h)$ is the semi variance for the lag distance h, $N(h)$ is the number of observations pairs at the lag distance h, and A_i is the observation at the location x_i. To determine the spatial correlation of two variables A_i and B_i the cross-semivariogram was applied. It considers the separation distance of the sample values, as well as the spatial correlation of the two variables and is defined as follows (Schwen et al., 2012; Yates and Warrick, 2002, p. 102):

$$\Gamma(h) = \frac{1}{2N(h)} \sum_{i=1}^{N(h)} \left(A_i(x_i) - A_i(x_i + h)\right)\left(B_i(x_i) - B_i(x_i + h)\right) \tag{4.45}$$

where $\Gamma(h)$ is the cross-semivariance at the lag distance h of the observations of the two variables A_i and B_i at the locations x_i. $N(h)$ is the number of observations pairs at the lag distance h.

Plotting the semi variances and the cross-semivariance of two variables in variograms reveals the spatial behavior of the single variables and the spatial relationship of the combination of the variables. The analysis basically involved a comparison of spatial patterns in the semivariograms and the cross-semivariograms for spatial similarities. The analysis was performed applying the R function variogram() from the R package ‘gstat’ (Pebesma and Graeler, 2013) to the data. The analysis results in a matrix of semivariograms and cross-semivariogram combinations of all considered variables.

4.10.6 Time/space visualization of the volumetric water content data

To show the temporal and spatial behavior of the near surface volumetric water content simultaneously a time space map of the data was plotted. As large spatial and temporal gaps in-between the measurements are present an ordinary kriging algorithm was applied to interpolate values and subsequently create a continuous image. The kriging estimator is stated as follows (Nielsen and Wendroth, 2003, p. 120; Yates and Warrick, 2002, p. 95):

$$A_0^*(x_0) = \sum_{i=1}^{n} \lambda_i A_i(x_i) \tag{4.46}$$

where A_0^* is the estimated value at the location x_0 derived by the summation of the observations A_i at the locations x_i weighted by the factors λ_i. To ensure an unbiased estimator the sum of all weights $\sum_{i=1}^{n} \lambda_i = 1$ (Yates and Warrick, 2002, p. 95). The weights are determined due to the variance between sampled values separated by a lag distance. The experimental variogram is defined as done on the previous page. For the kriging algorithm the experimental variogram was fitted by a theoretical exponential variogram model (Isaaks and Srivastava, 1989, p. 292):

$$\hat{\gamma}(h) = C_0 + C_1 e^{-\frac{|h|}{a}} \tag{4.47}$$

The model is defined by the three parameters C_0, C_1, and a, where C_0 defines the nugget, C_1 the sill and a the practical range of the function. h defines the lag distance. As the interpolation involves space and time, h refers to location in the spatial context, but to time of observation on a temporal basis. The relationship between space on one axis and time on the other one was defined as meters in x direction and days on the y-axis. This approach worked well for CO_2 fluxes shown by Kreba et al. (2013). The variogram analysis was performed visually applying the R function eyefit() to the data. The kriging algorithm was performed using the function krig.conv() involving the previously fitted variogram. Both functions are part of the R package ‘geoR’ (Ribeiro and Diggle, 2012).

5 Results

5.1 Topography of the hill slopes

In the period from August 22nd 2012 to September 7th 2012 a land survey was performed in the area where the two transects were located using a total station. As the measurements covered a larger area the relevant elevation data that represent the two transects were extracted. The survey did not cover the entire length of both transects and the areas above the stone bunds required additional information. Therefore, extrapolation and interpolation with additional manual point measurements were necessary. The measurements also included the small scaled roughness of the soil surface. However, for further analyses the large scale trend of the slope was of major interest. Therefore smoothening the sections in between the stone bunds and the transect without SWC with polynomial splines was an important step.

The elevation measurements of the land survey and the manual measurements are shown in Figure 5.1 as grey circles. The solid lines show the smoothened soil surface of the transect with SWC (left) and without SWC (right). The elevation is displayed superelevated by the factor 10.

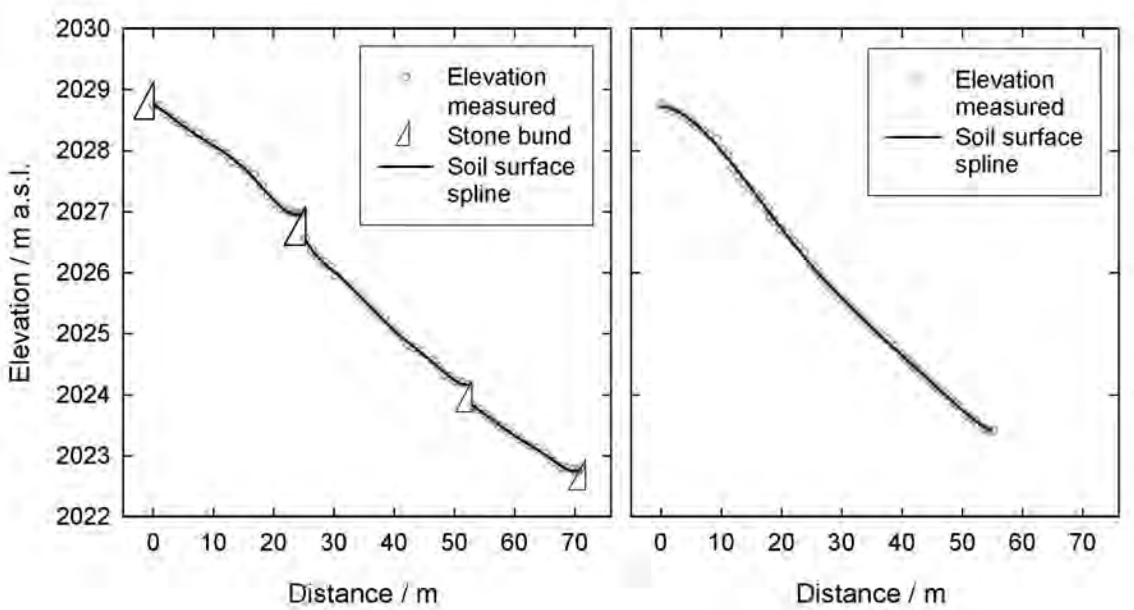

Figure 5.1: Measured elevation levels (gray circles) and smoothened soil surface (solid line) of the transect with SWC (left) and the transect without SWC (right). The elevation is displayed superelevated by the factor 10. The black triangles indicate the positions and the proportions of the stone bunds.

The transect with SWC has a length of approximately 71 meters; whereas the transect without has a length of around 55 meters. As the transects were located in a close vicinity to each other, both had a similar elevation from around 2022.5 meters above sea level to 2028.5 meters above sea level. The transects with SWC and without SWC had a similar average inclination over the total length of approximately 8.4% and 9.7% respectively. However, comparing the two transects field-wise essential differences become visible.

The deviations between measured data and fitted splines are small. However, these small scale fluctuations have a strong influence for deriving the inclination. For results that omit the small scale deviations the inclination was calculated by forming the first derivatives of the spline functions. The results are presented in Figure 5.2 for the transect with SWC (left) and the transect without (right).

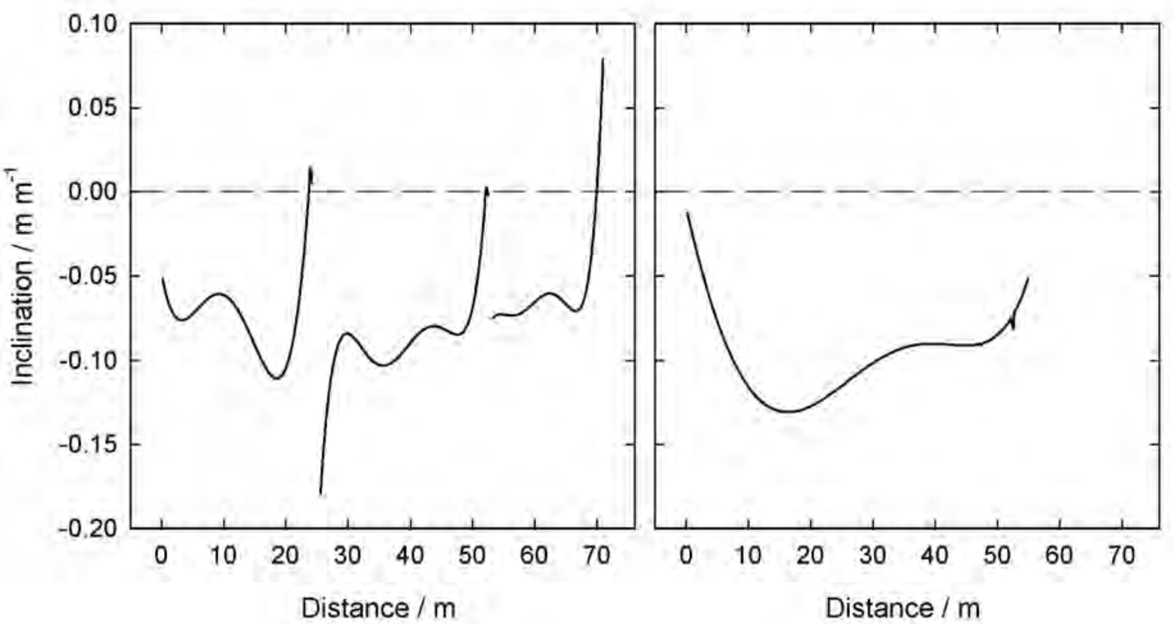

Figure 5.2: Calculated inclination of the transect with SWC (left) and the transect without (right). The inclination results from forming the first derivative of the smoothened polynomial functions of the soil surface.

The use of specific functions for the determination of the inclination predefines a certain shape of the results. Nevertheless, the principal behavior of the inclination becomes visible. The graphs show that the inclination for both transects is in a similar range. However, the areas above the stone bunds show a strong change in inclination towards zero or even positive values. This disrupts the continuum and becomes a strong influence for several processes that are explained further on.

5.2 Precipitation data

The precipitation measurements considered were recorded at the station in the Aba-K'aloye sub-catchment. Figure 5.3 shows the daily precipitation sums, as well as the accumulated precipitation for the year 2012.

The total annual precipitation was 941 mm in the year 2012. As shown in chapter 4.1.2 the long term mean annual precipitation is higher with a value of 1052 mm. Therefore, the year 2012 can be considered as a drier year.

The rainy season started rather late in the year 2012 with regular rainfall starting in the last third of June. The most intensive as well as the largest parts of the annual precipitation sum occurred in July and August. The daily rainfall never exceeded 40 mm during the whole rainy season. Rainfall data from the year 2011 showed daily rainfall sums of up to 130 mm. Therefore, the rainfall in the year 2012 can be considered as less intense, but on a rather regular basis. Surprisingly, the most intensive rainfall occurred in October that is usually rather dry.

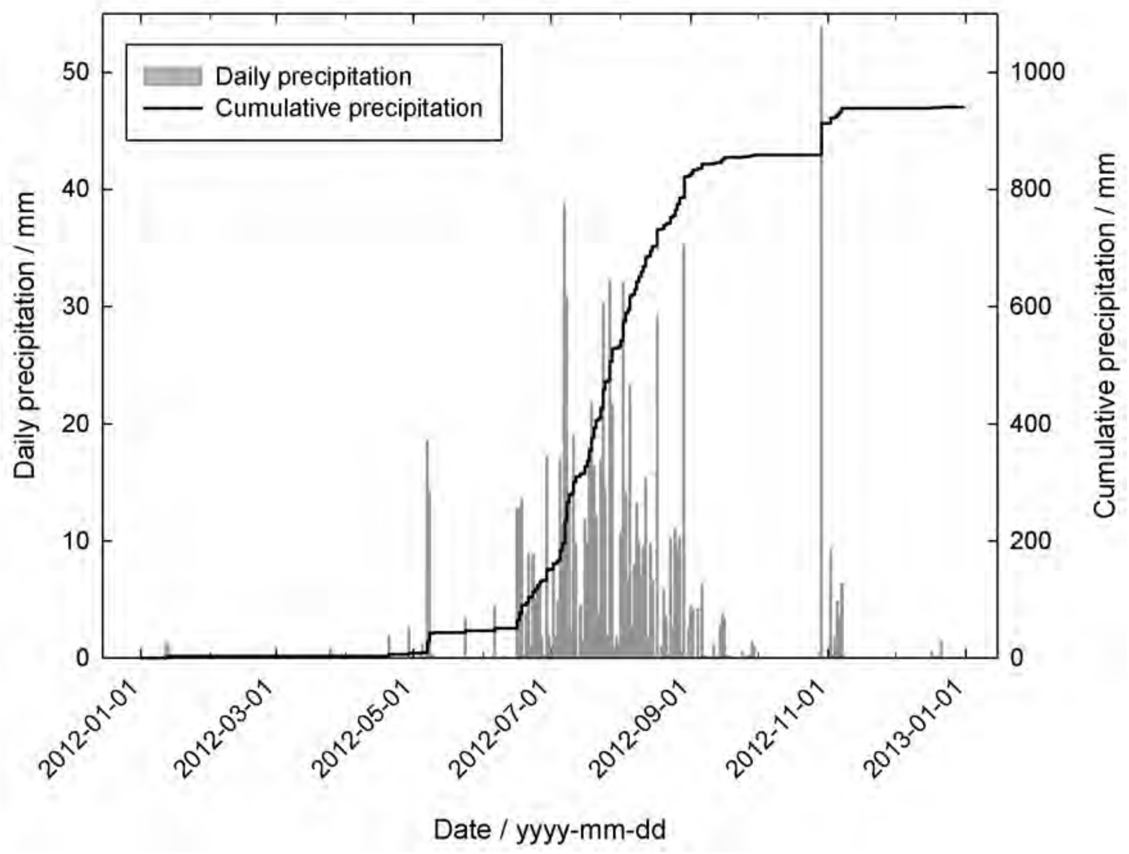

Figure 5.3: Daily and cumulative precipitation in the Aba-K'aloye sub catchment for the year 2012.

5.3 Near surface volumetric water content

The following analyses deal with the data of near surface volumetric water content measurements that we took in the time period from June 22nd 2012 to August 30th 2012. The data for the transect with SWC contains nine sets of measurements for different time steps. One was taken at the begin of the period (August 22nd 2012), the second one on July 11th 2012 and the other 7 in the time period from August 20th 2012 to August 30th 2012. For the transect without SWC water content measurements are available for the same days, except for August 22nd 2012. For the analyses the data sets of the initial phase, the middle phase, and two sets of the end phase were used. As the differences in the volumetric water content are low at the end of the time period further data sets were omitted.

The measurements along both transects were taken in defined patterns of intervals that are described in chapter 4.2. This set up results in 30 measurements along the transect with SWC and 11 or 22 measurements (depending on the used interval) along the transect without SWC.

The used method for measuring the volumetric water content is an indirect method. This indicates that the sensor required calibration (see following chapter 5.3.1). The data for the volumetric water content that is used in this work were calculated according to the results of the calibration.

5.3.1 Calibration of the FDR sensor data

For the calibration 53 undisturbed soil samples were taken along the two transects to cover a certain range for the volumetric water content. We determined the dielectric permittivity value ε_r in at least four points around the sampling rings using the capacitive sensor in the field and calculated the mean electric permittivity for those measurements. Drying the soil samples in the laboratory resulted in the exact volumetric water content for each sample.

Figure 5.4 shows the exact values of the volumetric water content derived with the gravimetric method over the mean values of the dielectric permittivity. To get a linear relationship between those two parameters the square root of the dielectric permittivity was used. The solid line shows the relationship between the square root of the dielectric permittivity and the volumetric water content determined by linear regression. The dotted and the dashed lines represent the prediction and the total confidence intervals respectively.

The data shows variations of up to 5 Vol% in volumetric water content to the determined function. Additionally the measurements only cover a range of 27 to 52 Vol% for the volumetric water content. The physical nature of the dielectric permittivity states that a value of approximately 80 establishes for pure water and around 1 for measurements in air. This does not apply to the determined calibration curve. Additionally, the found relationship does not fit to the various standard calibration curves that are available.

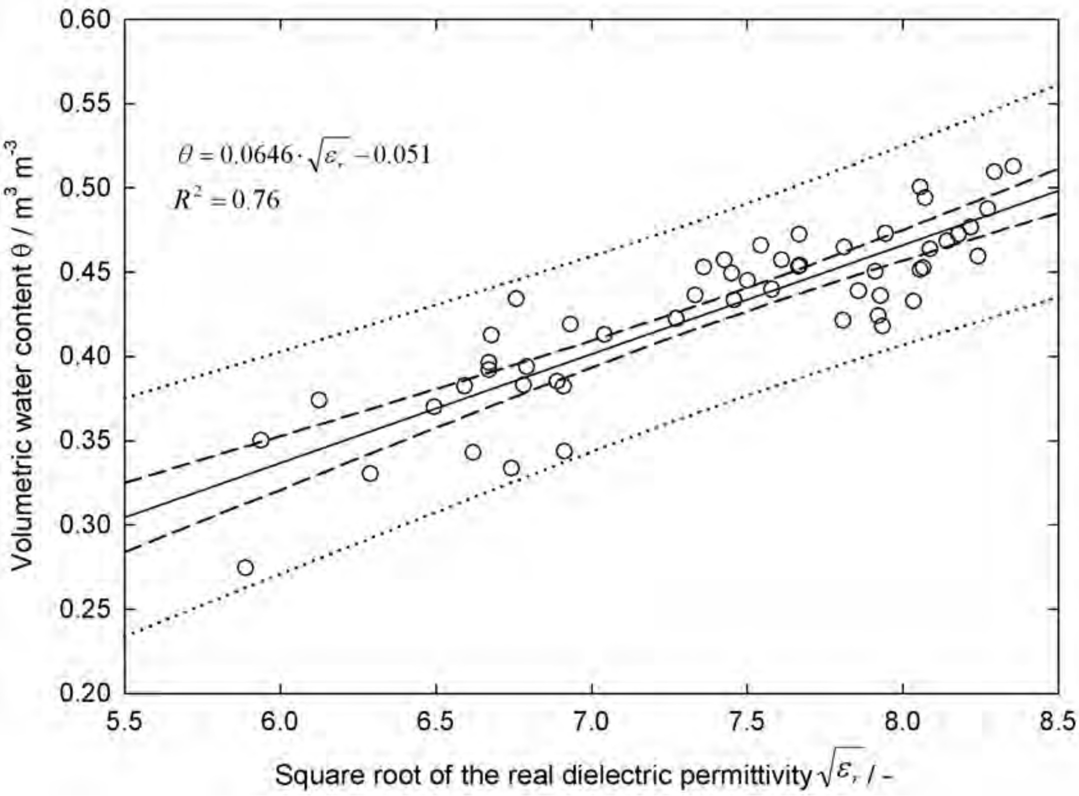

Figure 5.4: The volumetric water content over average value of the square root of the real dielectric permittivity for the used undisturbed soil samples. The volumetric water content was determined by the gravimetric method. The dielectric constant values are average values of at least four point measurements around the soil samples in situ. The solid line shows the linear regression. The dashed and the dotted lines represent the regression and the total confidence intervals (α = 0.05) respectively.

Apart from all those limitations for the determined calibration curve, the found relationship results in more substantial estimations for the volumetric water content than various standard calibrations. Additionally, most of the measurements taken over the whole time period lie in the range that is covered by the calibration curve. For further analyses the exact value of the volumetric water content is only of minor interest. Rather general differences and general trends for the two transects play the important role.

5.3.2 Visualization of the analyzed data sets

The analyses of the volumetric water content involved four data sets of measurements along the transect with SWC, covering the initial phase, the middle phase and the end phase (two data sets) of the rainy season. For the three latter dates, data sets for the transect without SWC are available. These should give a comparison of the effects of the stone bunds to a situation without SWC. In the end phase of the rainy season a more frequent measurement of the volumetric water content was possible. However, additional data from this period of the rainy season add only little further information. Therefore, further data sets were omitted in the analyses. As result seven data sets were used for the analysis of the volumetric water content that are displayed in Figure 5.5.

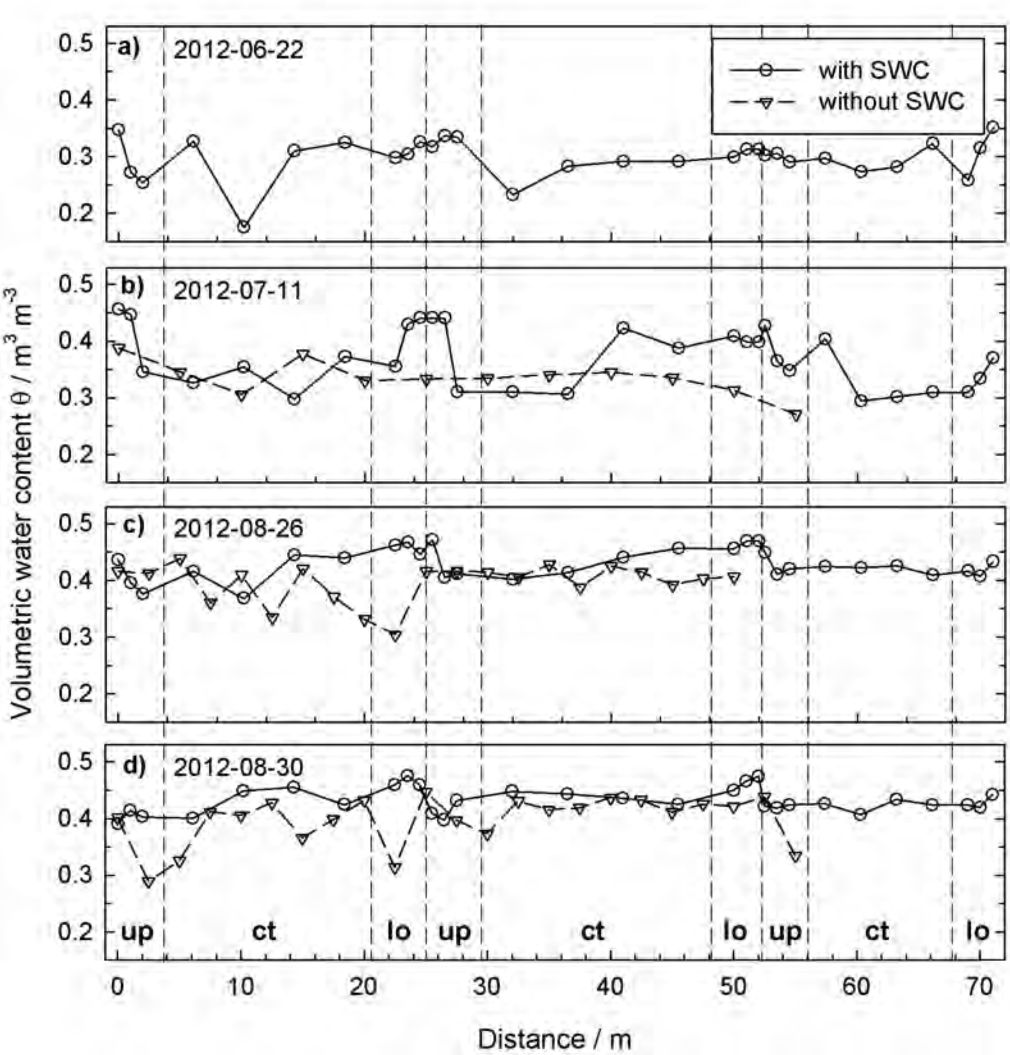

Figure 5.5: The volumetric water content along the transect with SWC (circles with solid line) and without SWC (triangles with dashed line). The figures a) to d) show four different time steps. The vertical dashed lines indicate a hypothetical partition of the transect with SWC into an upper, a center and a lower zone for each field in between two stone bunds.

The graphs a) to d) show the measurements of the volumetric water content along the two transects for the four different time steps. The vertical dashed lines indicate an assumed partition of the transect with SWC. The lines divide each field in between two stone bunds in to a central part of the field (ct), a zone above the stone bunds (lo) where water accumulation is expected and an area under the stone bunds (up).

Graph a) represents the initial phase of the rainy season that started in the mid of June 2012 a week before the measurement shown in the graph was done. The soil precondition in this phase was rather dry and big cracks were present in the soil, due to shrinking processes. Regular rainfall events with average intensity and quantity characterized the precipitation. The graph shows an average volumetric water content of approximately 30 Vol% along the transect with SWC. The variation of the water content is low. Apart from a few random fluctuations a slight rise in the water content in the close vicinity around the stone bunds is visible. This indicates dominant infiltration processes and only a small amount of runoff that accumulated above the stone bunds.

Graph b) illustrates the situation of the middle phase of the rainy season. The soil was already in a wet condition and strong rainfall events took place in this period. The graph shows the measurements along the transects with SWC (circles with solid line) and without SWC (triangles with dashed line). In the center position of the fields (ct) the transect with SWC shows comparable values in water content to the transect without SWC. In the zones around the stone bunds (lo and up) the water content shows large peaks and is much larger compared to the values of the center positions (ct) and the transect without SWC. This indicates that a large part of the rainfall lead to runoff that accumulated above the stone bunds. Additionally, higher values in water content right after the stone bunds (up) lead to the assumption that some part of the runoff spilled over the stone bunds, percolated through them and infiltrated in this zone or accumulated in this zone through interflow processes.

Graph c) and d) represent the end phase of the rainy season. The soil was already saturated to a high degree. Intensive rainfall events were still present. However, the average rainfall and the frequency of rainfall events were lower than in the mid phase of the rainy season. Both graphs show that the variation for the transect with SWC decreased strongly. Still a small peak in the water content in the lower and upper zone along the transect with SWC is visible. Additionally, the water content increases slightly starting in the middle of the center zone towards the lower zone. This indicates that the accumulation zone of soil water expanded strongly. Apart from this slight rises in the water content, the values are similar to the values of the transect without SWC.

5.3.3 Statistical analysis of the data, prerequisites for the data

Normal distribution of the data is an important prerequisite for the majority of statistical tests that were used. To inspect the data visually the data was plotted against the theoretical quantiles of a normal distribution in quantile-quantile plots. Additionally, Kolmogorov-Smirnoff tests show significant differences to the assumption of a normal distribution.

Figure 5.6 shows the quantile-quantile plots of the used data sets where the data is plotted against the quantiles of a normal distribution.

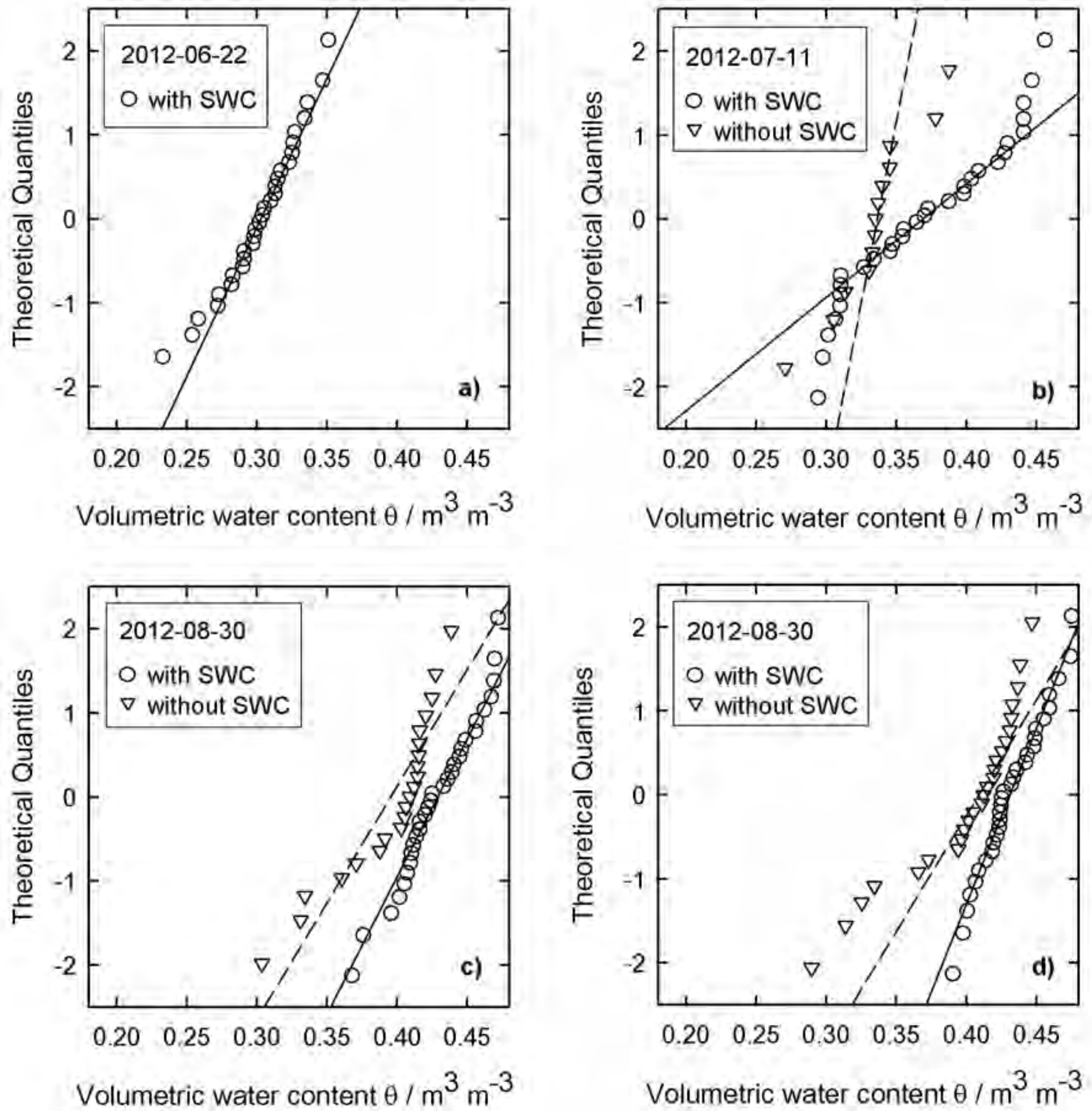

Figure 5.6: Quantile-quantile plots of the data sets for the four different time steps considered. The theoretical quantiles represent a normal distribution. The scale of the volumetric water content was set constant in all four plots to illustrate the shift in water content over time and differences in the variability of the data.

As the central part of each data set has a linear relationship to the theoretical quantiles to a sufficient extent, normal distribution of the data can be assumed. Additionally, the Kolmogorov-Smirnoff tests did not reject the null hypothesis that the data is normally distributed.

As the scale of the volumetric water content on the x-axis was kept constant for all four graphs, they give further on an idea of the changes in the mean and the variability of the data. Over time the graphs show a shift from left to right. This indicates the general rise in the water content for both transects over time. Additionally, the average water content of the transect with SWC is slightly higher for each time step. Overall, all data sets show a similar slope. This indicates that the variations induced by the topographic domain of the stone bunds are similar to the random variations for the initial and the saturated case. The data set of the transect with SWC for June 11th 2012, however, shows a considerably higher variability compared to the other data sets. This is the result of the dominant accumulation processes of the soil water around the stone bunds, as indicated above.

5.3.4 Temporal analysis

For the temporal analysis of the near volumetric water content the sets of measurements for different time steps were compared. The data sets were analyzed for differences in variability and mean value over time applying Levene's test as a variance test and paired t-test and Least significant difference test finding significant differences in the means.

This progressive increase in the volumetric water content that was mentioned previously is again visible in Figure 5.7. The boxplots show the near surface volumetric water content measurements along the transect with SWC (left) and without SWC (right) for the different time steps. The initial, mid and the two end measurements along the transect with SWC show mean values of 29.8, 37.0, 42.9, and 43.2 Vol% respectively. Whereas, the transect without SWC shows mean values of 33.5, 39.5, and 39.9Vol% for the mid phase and the two end phase measurements. The rise in the volumetric water content over time is significant for both transects. However, the changes in the end phase of the rainy season were much smaller than the changes between the previous time steps and were found insignificant.

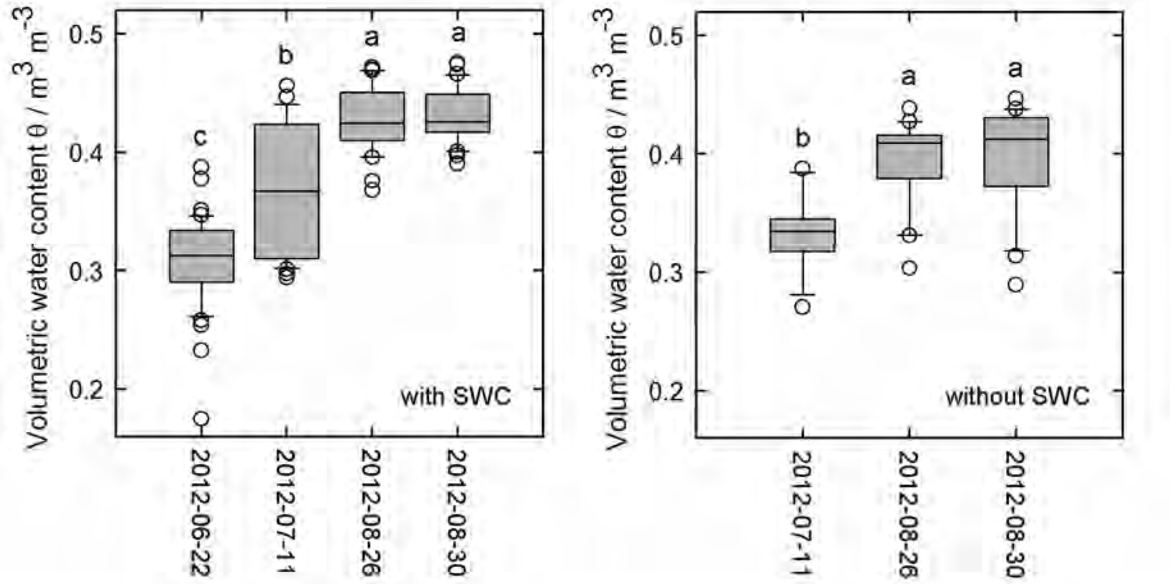

Figure 5.7: Boxplots of the near surface volumetric water content measurements along the transect with SWC (left) and without SWC (right) for the different time steps. The small Latin letters indicate significant differences (p<0.05) between box means giving the largest mean the letter a.

Considering the variance of the datasets a significant difference was found for the measurement along the transect with SWC from June 11th 2012. As already indicated in the previous chapters, the high peaks of accumulated water around the stone bunds lead to a significantly higher variability in the data.

5.3.5 Spatial analysis

In chapter 5.3.2 the topographic domain of the stone bunds on the near surface volumetric water content was considered to be a topic that requires further consideration.

With Figure 5.5 a hypothetical partition of the fields in-between two stone bunds was introduced. The separation should define zones where the different processes runoff formation and accumulation are present to different degrees. Levene's test indicates significant differences in the variability. Paired t-test and Least significance test show significant differences in the mean values.

As the measurements along the transect with SWC covered three fields in between stone bunds the volumetric water content should show a similar behavior on all three fields, if the processes are relevant on a spatial basis. This would lead to a periodic behavior in the data. Autocorrelation analysis can show present periodicities. To find the periodicity and the significance of that periodic behavior a spectral analysis was performed. If one major periodicity is visible in the spectrograms, applying the Fisher's g-test gives information about the significance of this periodicity.

5.3.5.1 Zonal analysis

Figure 5.8 shows boxplots of the sub datasets for the defined zones along the transect with SWC and the datasets of the transect without SWC for the four different time steps.

Graph a) shows the measurement along the transect with SWC for the initial phase of the rainy season. The data for the three defined zones show no significant differences in mean and variance.

Graph b) represents the mid phase of the rainy season. The variance of the data for all three zones increased strongly. The data of upper and the lower zones around the stone bunds differ significantly from the center zones. The center zone shows a similar mean as the transect without SWC; whereas the variance is significantly larger.

Graphs c) and d) illustrate the situation at the end of the rainy season. The variation for each subsample but also between the samples decreased strongly compared to graph b). In graph c) the differences between the three zones of the transect with SWC are insignificant. The values in the upper zone only slightly increased in the same time where a stronger increase for all other zones is shown. However, all zones show significantly larger mean values than the transect without SWC. In graph d) there are again slight changes. The values of the volumetric water content in the upper zone even decreased slightly. Whereas, there was an increase in volumetric water content in the center zone. Still the largest volumetric water content values are found in the lower zones.

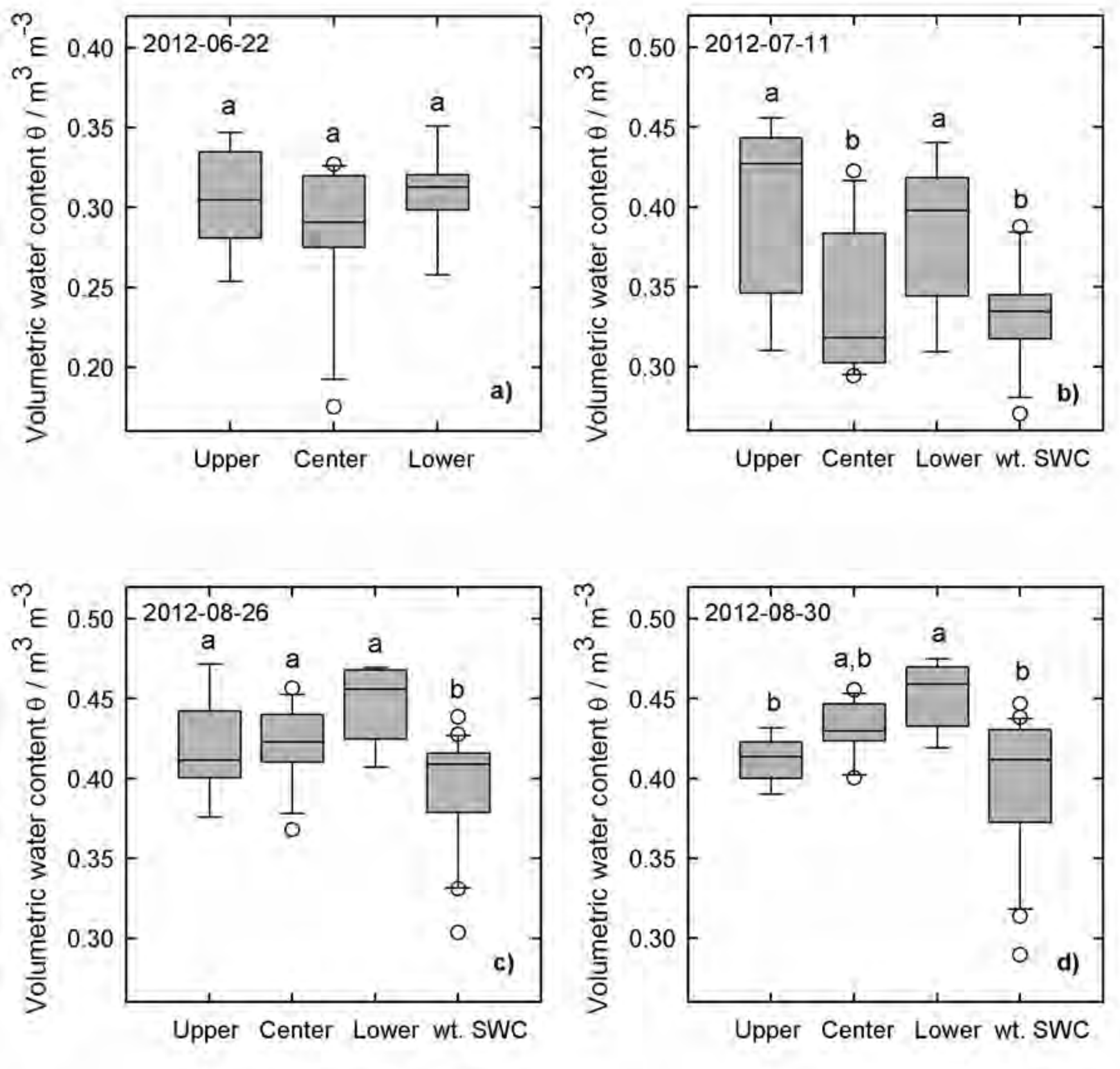

Figure 5.8: Boxplots of the near surface volumetric water content measurements in the upper center and lower zone of the transect with SWC and measurements of the transect without SWC for the four different time steps. The small Latin letters indicate significant differences (p<0.05) between box means giving the largest mean the letter a.

The findings support the definition of different zones in the field where specific processes are dominant. The lower zone shows large values for the volumetric water content for all time steps where runoff processes lead to accumulation in this zone. The upper zone shows a highly variable behavior over the different time steps compared to the other zones. Where the largest values for the water content with a very high variability where found in the most intense phase of the rainy season a homogenization of the variability and the mean of the water content where found towards the end of the rainy season. This finding indicates that interflow might be the dominant process in this zone. Over time the interflow becomes a quasi-steady state process that establishes a constant volumetric water content with low variability. The changes of the water content in the center zone of the fields indicate that the accumulation front of the soil water expands over time and also covers parts of this zone. This puts the widths of the defined zones into question as the accumulation of the soil water is difficult to cover by this approach. However, the findings show that the approach was substantial for the description of the processes.

5.3.5.2 Autocorrelogram analysis

Figure 5.9 shows the autocorrelograms for the measurements along the transect with SWC for four different time steps. For comparison the autocorrelograms of the transect without SWC for two of the time steps are shown additionally.

The initial phase of the rainy season showed a weak influence of the stone bunds on the volumetric water content as only little runoff was accumulated due to the stone bunds. This is also shown by the autocorrelogram (graph a)) where no clear periodic pattern is visible. The graphs of the middle phase and the end phase of the rainy season show a clear periodic behavior in the volumetric water content along the transect with SWC (graph b) – d)), whereas the patterns in the graphs b) and c) are the clearest. To compare the findings with the random variability graphs e) and f) show the autocorrelograms for two measurements along the transect without SWC. Graphs e) and f) show no clear pattern for the autocorrelation coefficient. This indicates that no periodic behavior is induced by random variability of the volumetric water content.

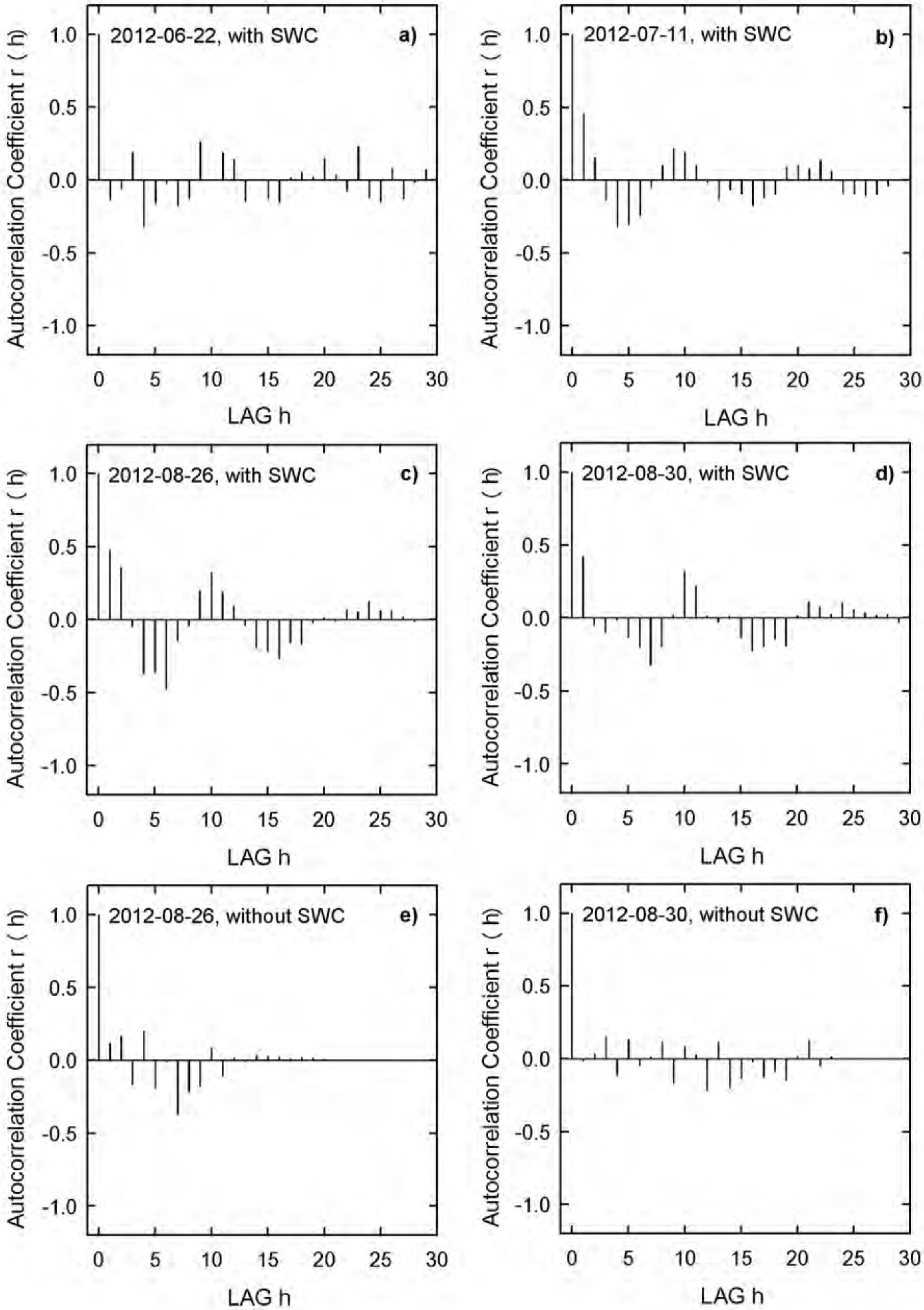

Figure 5.9: Autocorrelogram plots for the transect measurements of the volumetric water content for the four different time steps a) – d). Graphs e) and f) show the autocorrelograms of the transect without SWC for two of the four time steps for comparison.

5.3.5.3 Spectral analysis

Figure 5.10 shows spectrograms for the autocorrelation analysis above. Again the four data sets of the transect with SWC and the two without SWC were used for the analysis.

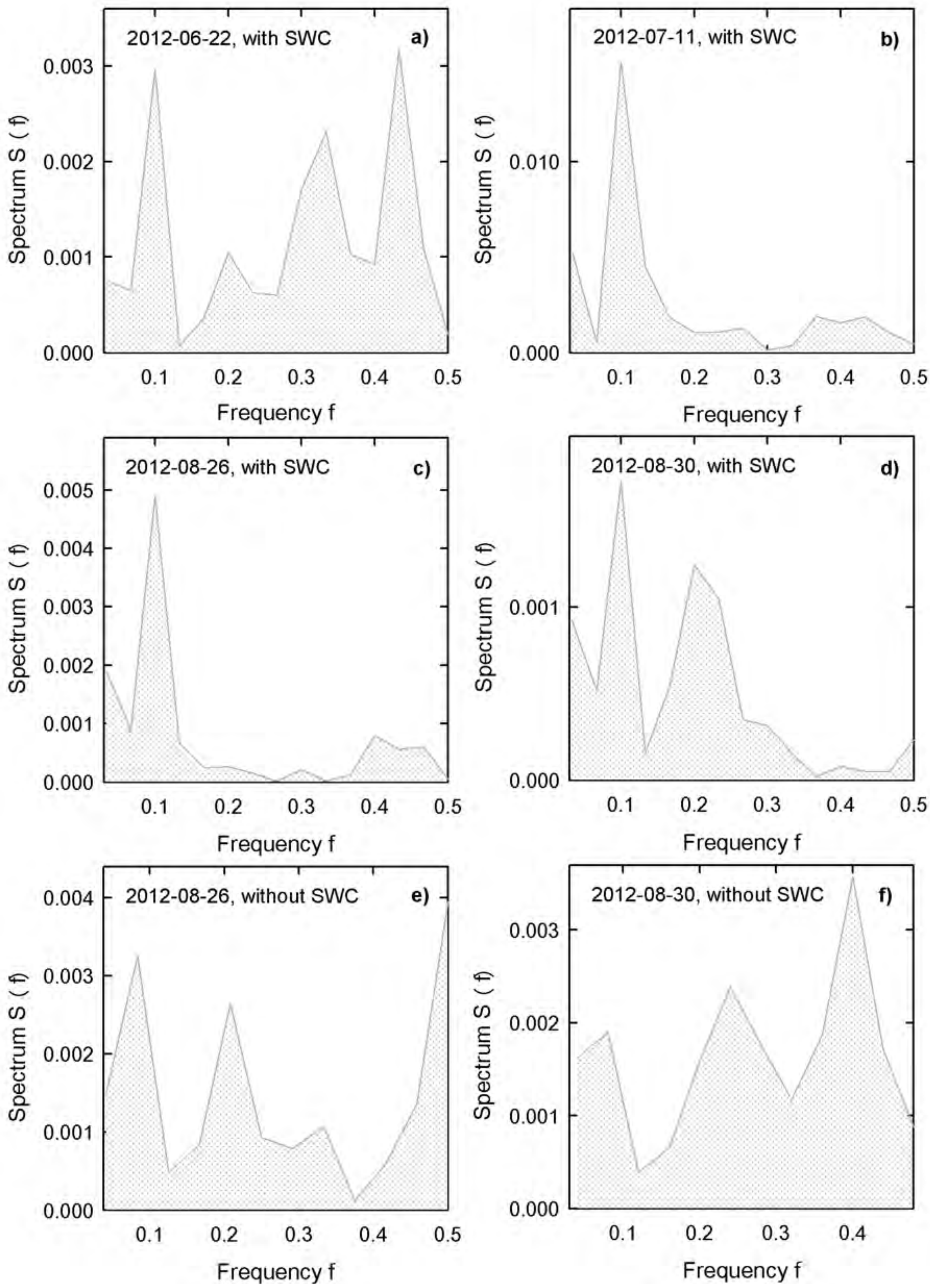

Figure 5.10: Spectrogram plots for the transect measurements of the volumetric water content for the four different time steps a) – d). Graphs e) and f) show the spectrograms of the transect without SWC for two of the four time steps for comparison.

Graphs a) to d) show a high peak for a frequency of 0.1 that is equivalent to a LAG distance of 10. This distance represents exactly the interval for the measurements in-between two stone bunds. However, graphs a) and d) show other peaks of similar amplitude. The significance test supports these findings as the assumption that one significant frequency is contained in the data only holds for the graphs b) and c). In graph d) the peak at frequency 0.1 is the highest, though no significance was found. The comparative plots e) and f) of the transect without SWC show a similar picture as plot a) where almost no influence of the topographic domain was expected.

In the initial phase of the rainy season where almost no accumulation of surface runoff took place in the zone above the stone bunds no strong influence in the spatial domain was found. This was shown by a weak periodic behavior in the analysis. For the time steps where strong rainfall events led to a dominant runoff process and therefore high accumulation above the stone bunds a strong periodic behavior in the data was found. For the transect without SWC where the spatial domain shows only random variations no periodicities were found at all.

5.3.6 Visualization of the findings, time-space plot

The data of the near surface volumetric water content is strongly influenced by spatial and temporal processes that take place parallel. To visualize the development of the water content over space and time and to support the findings from the chapters above a geo-statistical approach was used applying ordinary kriging to the data to find estimates for the missing values in-between the measured values. To do so, the found trends were first quantified by functions and then removed from the data to leave only the random variations for the interpolation. The grid that was used for the prediction spanned over space in one dimension and the time in the second dimension. The relationship between space and time was defined by one meter in space equals one day in the dimension time. At this point I want to emphasize that this assumption is very subjective and is not based on any profound knowledge. The geo-statistical approach was not used to draw physically based correct maps, but it was rather used as a visualization tool. After the prediction the trends were again added to the data and plotted into a 3D map.

5.3.6.1 Visualization of the transect data with SWC

The data showed a significant increase over time and a periodical behavior along the spatial domain. To quantify those trends functions were fitted to the data as represented in Figure 5.11. The left graph shows the temporal trend of the mean values of the data sets. The right graph shows the spatial behavior for one of the data sets exemplary.

The water content changed strongly in the initial phase of the rainy season and increased slowly at the end phase to reach almost a saturated condition. As this trend was assumed to be non-linear an exponential trend was fitted to the data. The spectral analysis showed that periodic trend in space has a periodicity of 10 LAG distances. To fit this trend a cosine function was used.

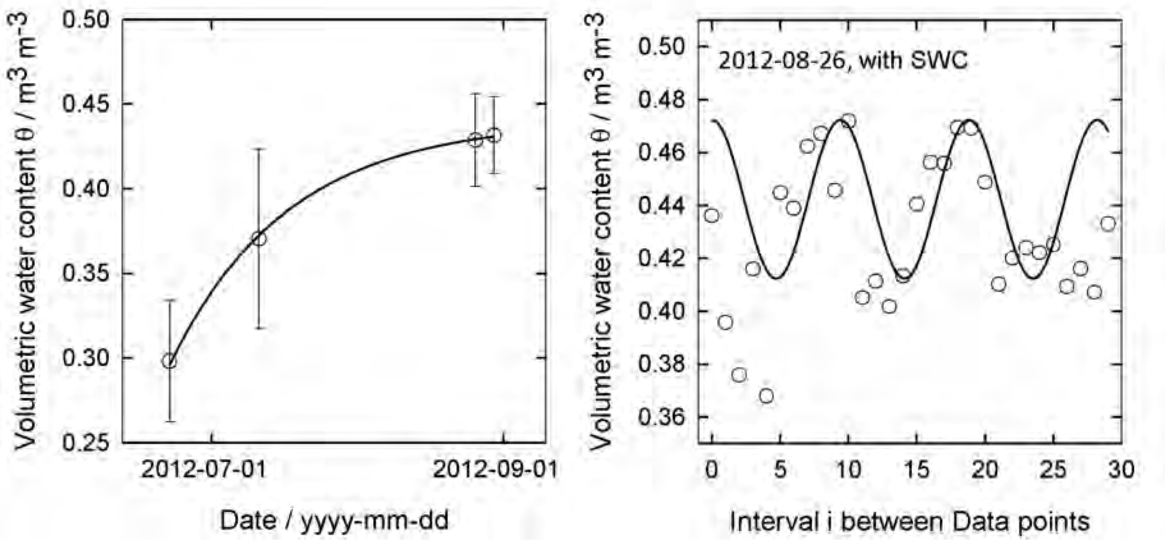

Figure 5.11: Quantification of the temporal (left) and the spatial (right) trends of the near surface volumetric water content data of the transect with SWC. The temporal trend was fitted by an exponential function. The spatial trend was fitted by a cosine function with a period of 10 LAG distances.

Figure 5.12 shows the resulting map of this approach for the data with SWC. The x-axis shows the distance along the transect, whereas the time over the rainy season is represented by the y-axis. The graph clearly indicates the development of the accumulation zones (blue areas) around the stone bunds (gray bars). It clearly illustrates the progressive development of the accumulation zones above the stone bunds and also shows the accumulation of soil water after the stone bunds and the dryer areas in the center positions of the fields.

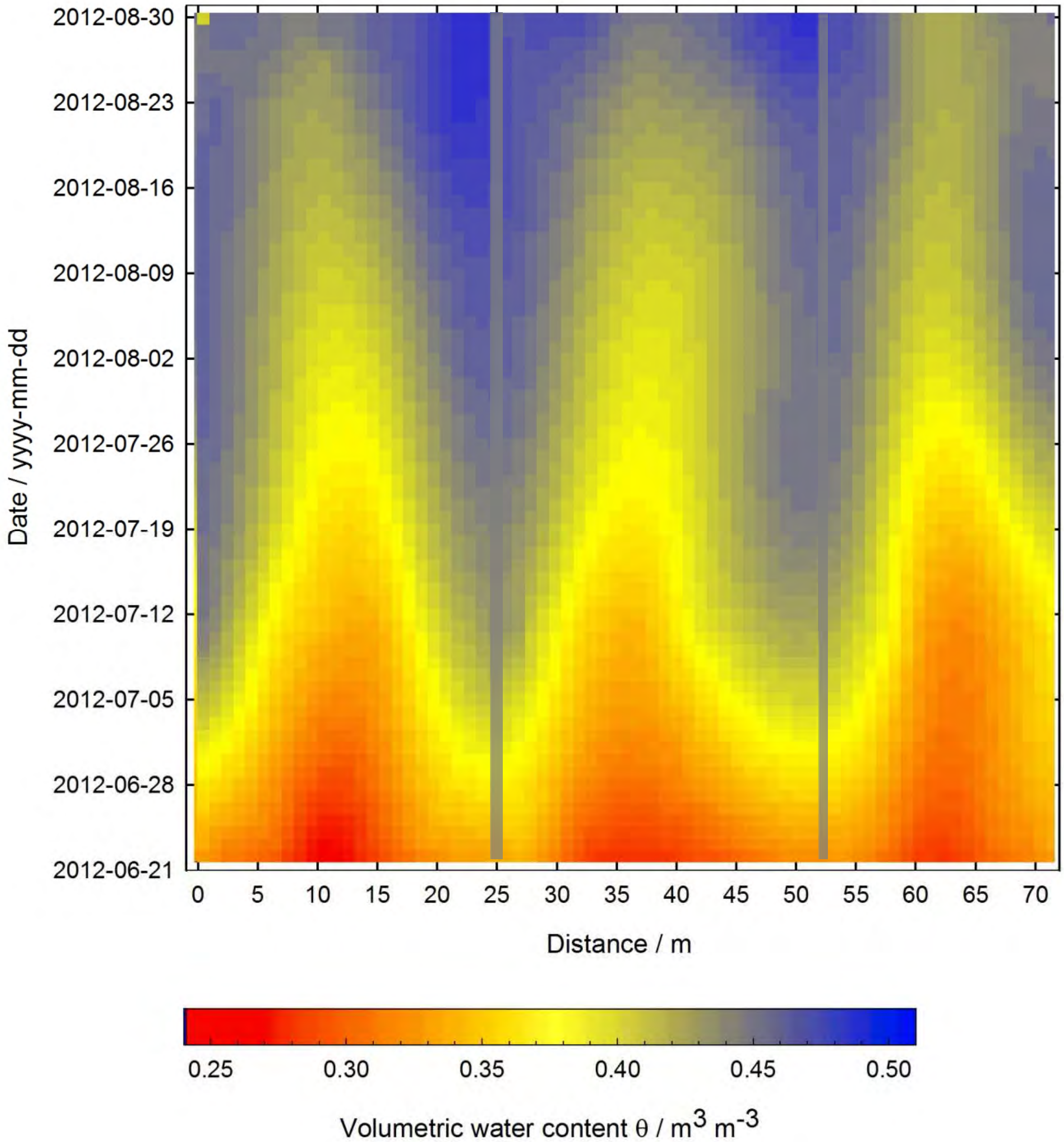

Figure 5.12: Visualization of the near surface volumetric water content along the transect with SWC in a time-space plot. The x-axis represents the distance along the transect. The y-axis represents the time. The relationship between space and time was defined subjectively with one meter equals one day. The colors indicate the volumetric water content in a range from 22 Vol% (red) to 52 Vol% (blue).

5.3.6.2 Visualization of the transect data without SWC

The data showed a significant increase over time, but no significant trends along the spatial domain. To quantify the temporal trend a function was fitted to the data as shown in Figure 5.13. The temporal trend of the mean values of the data sets and the spatial behavior for one of the data sets are represented in the left and the right graph respectively. For the transect without SWC a dataset for the initial phase of the rainy season is missing. The temporal trend was also most likely an exponential one. However, as the graph lacks the information of the initial phase a linear function was fitted to the data. This leads to satisfying results for the visualization. As no spatial trends were found for the transect without SWC a quantification by a function was omitted.

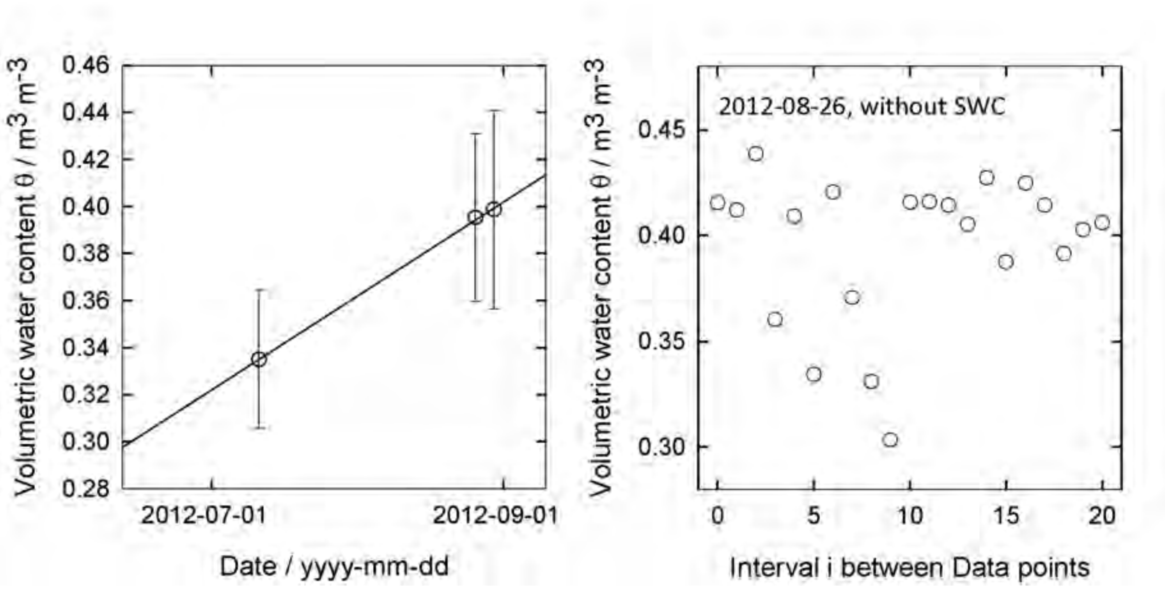

Figure 5.13: Quantification of the temporal (left) trend of the near surface volumetric water content data of the transect without SWC. The temporal trend was fitted by an exponential function. The spatial trend showed no clear pattern.

Figure 5.14 shows the resulting map of this approach for the data with SWC. The x-axis shows the distance along the transect, whereas the time over the rainy season is shown by the y-axis. In the graph only the spatial trend is visible as it was intended to be. Comparing this picture to the visualization of the data with SWC it clearly shows that wet conditions develop much later on the transect without SWC.

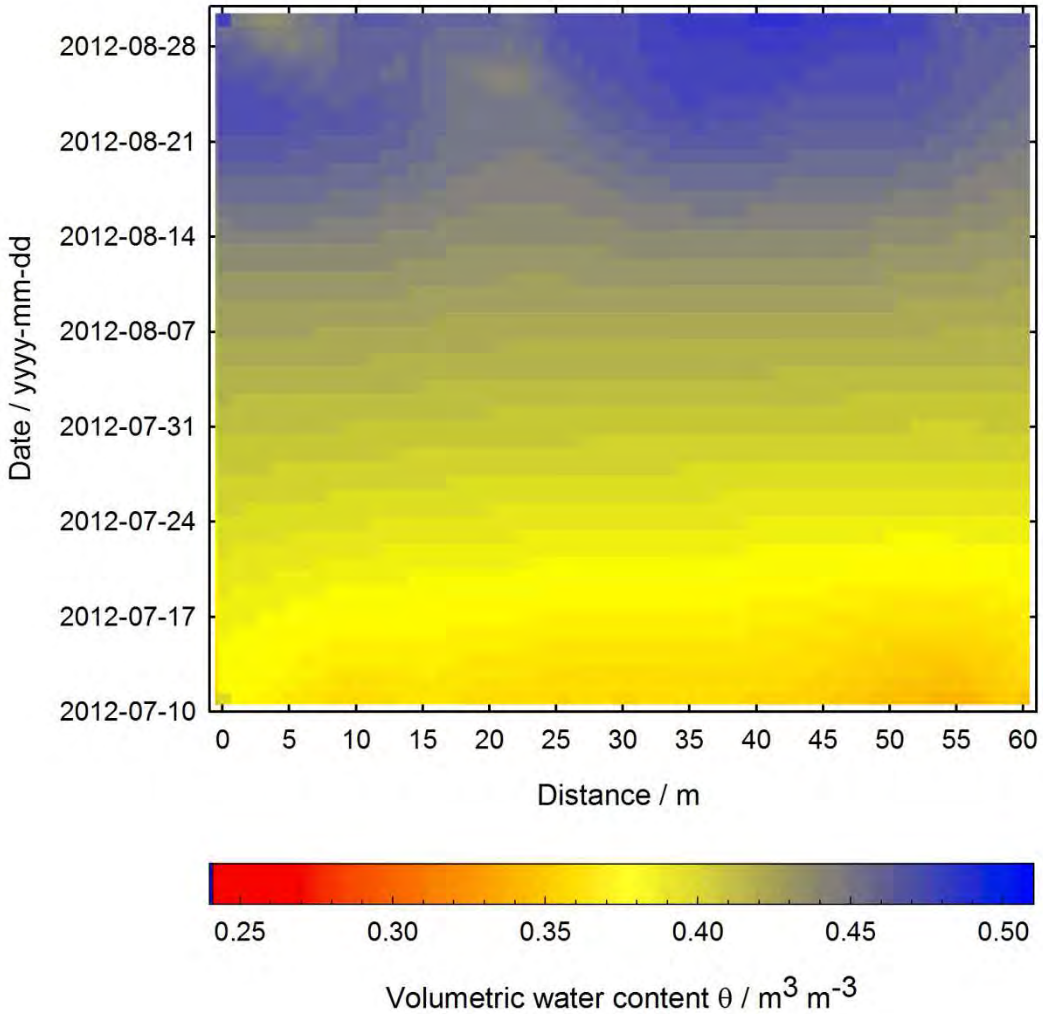

Figure 5.14: Visualization of the near surface volumetric water content along the transect without SWC in a time-space plot. The x-axis represents the distance along the transect. The y-axis represents the time. The relationship between space and time was defined subjectively with one meter equals one day. The colors indicate the volumetric water content in a range from 22 Vol% (red) to 52 Vol% (blue).

5.4 Bulk density

Over the whole rainy season three sets of soil samples were taken along the transect with SWC. The first set was sampled at the beginning of the rainy season on June 22nd 2012, the second in the middle on July 11th 2012 and the third set at the end of the rainy season on August 30th 2012. For comparison two sets of soil samples were taken along the transect without SWC on June 20th2012 and August 29th 2012 respectively.

The measurements along both transects were taken in exact same patterns of intervals as the measurements of the volumetric water content (see chapter 4.2). This set up results in 30 measurements along the transect with SWC and 11 measurements along the transect without SWC.

5.4.1 Visualization of the analyzed data sets

In total 5 data sets were available for the analyses that are displayed in Figure 5.15. The values of bulk density are plotted with their positions along the two transects.

Graphs a) to c) show the measurements along the transect with SWC. The dotted areas indicate a hypothetical partition into zones of different processes, similar to the separation of the volumetric water content data in the previous chapter. The center zones are areas where mostly erosion processes are expected. The graphs show a wide range of bulk density values from high to low in these zones. The accumulation zones are the areas where the sedimentation of the eroded material was expected. The inclination decreases in these parts of the transect with SWC. The graphs show mostly low values of bulk density in these areas as the fresh accumulated material is rather loose. The zones around the stone bunds are influenced by various processes and therefore show a very wide variability in the bulk density. Very high bulk density values in these areas can result due to the construction of the stone bunds and because the areas around the stone bunds are used as walking paths. Very low values are found in the areas around the stone bunds where sedimentation took place very close to the stone bunds and the sediment layer already reached a certain thickness.

The graphs d) and e) show the measurements along the transect without SWC. These measurements show the natural variability of the bulk density when no spatial domain influences the erosion and accumulation processes. Compared to the graphs a) to c) the natural variability has a similar range.

On a temporal basis the graphs show that the bulk density remains rather constant over the rainy season. Even in the accumulation areas where the sedimentation processes take place no changes are shown in the temporal scale of a rainy season in the graphs.

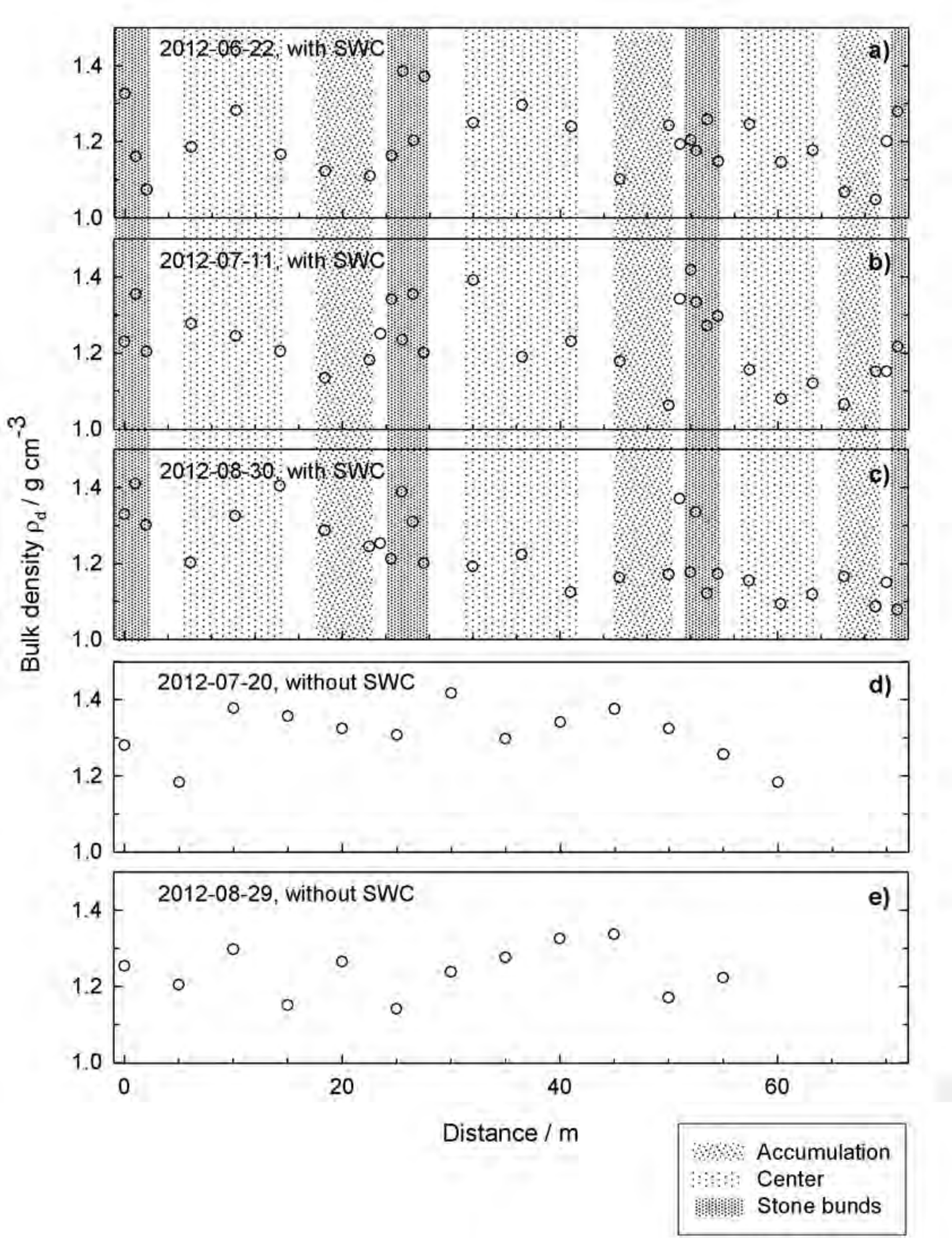

Figure 5.15: The bulk density along the transect with SWC (graphs a) to c)) and without SWC (graphs d) and e)) for the different time steps as indicated. The dotted areas represent a hypothetical partition of the transect with SWC into an accumulation zone, a center zone and a zone around the stone bunds for each field in between two stone bunds.

5.4.2 Statistical analysis of the data, prerequisites for the data

Normal distribution of the data is an important prerequisite for the majority of statistical tests that were used. To inspect the data visually the data was plotted against the theoretical quantiles of a normal distribution in quantile-quantile plots. Additionally, Kolmogorov-Smirnoff tests show significant differences to the assumption of a normal distribution.

Figure 5.16 shows the quantile-quantile plots of the three sets of measurements along the transect with SWC (a) to c)) and the two sets of measurements along the transect without SWC (d)).

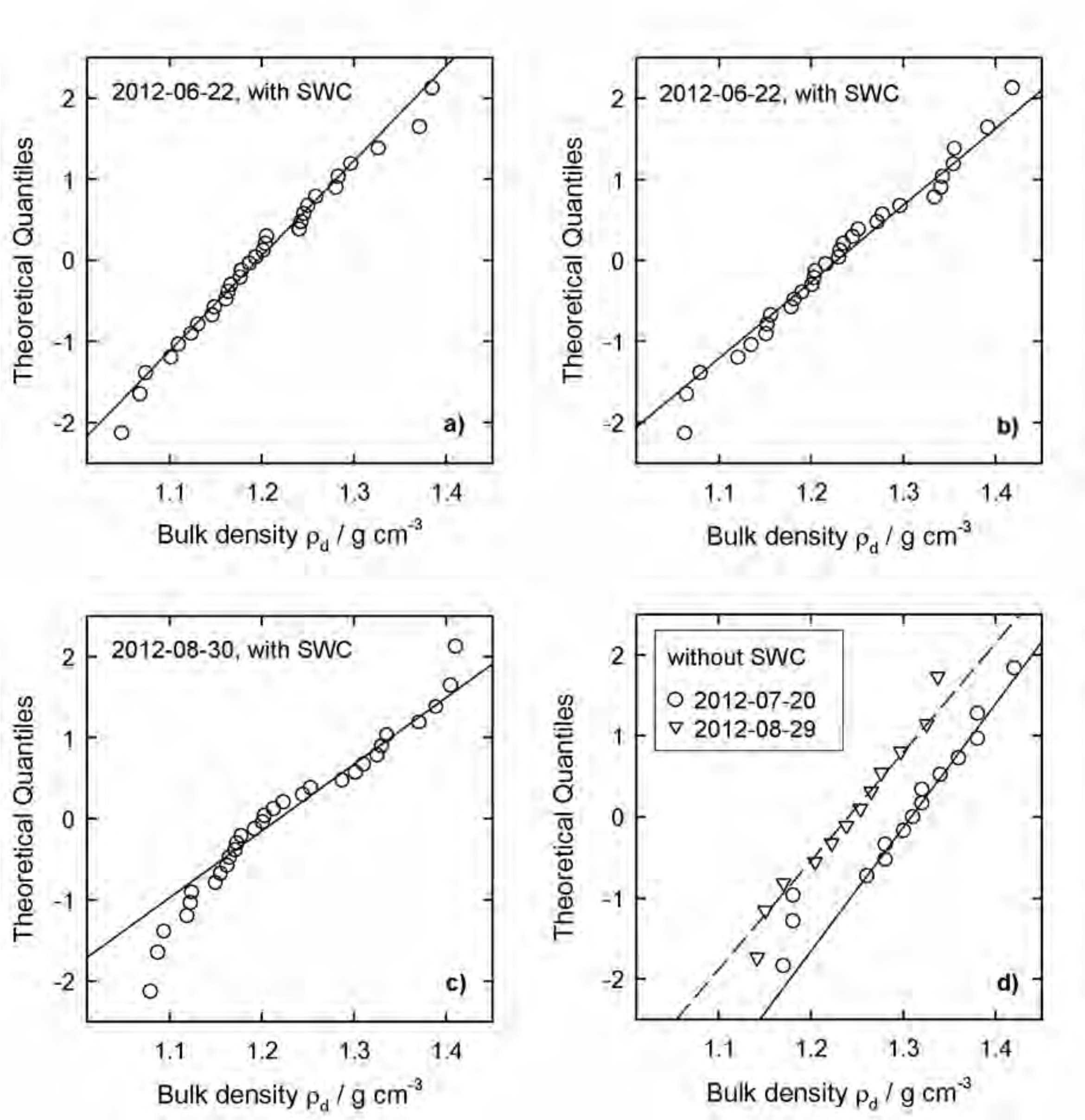

Figure 5.16: Quantile-quantile plots of the data sets for the three different time steps for the transect with SWC and for one sample along the transect without SWC. The theoretical quantiles represent a normal distribution. The scale of the bulk density measurements was set constant in all four plots to illustrate a possible shift of the datasets over time and differences in the variability.

All data follow a linear relationship in the plots. Additionally, the Kolmogorov-Smirnoff tests did not reject the null hypothesis that the data is normally distributed.

The scale of the bulk density on the x-axis remained constant in all four plots. This makes differences in mean values and variability of the data visible. Graphs a) to c) show similar ranges of data values that indicates a steady behavior of the mean value over time. The slopes of the datasets in the graphs a) to c) are similar. Therefore only minimal differences in the variability of the data are expected. The datasets for the transects without SWC show similar values for bulk density in the middle and upper range. However, very low values of bulk density are absent in both datasets. The slope in graph d) is slightly steeper compared to the other graphs. This indicates a slightly smaller variability in the datasets.

5.4.3 Temporal analysis

For the temporal analysis of the near volumetric water content the sets of measurements for different time steps were compared. The data sets were analyzed for differences in variability and mean value over time. Levene's test as a variance test and paired t-test and Least significant difference test were performed to test differences along the transect with SWC as three samples are available. For the two samples of the transect without SWC F-test and t-test were applied.

Figure 5.17 shows boxplots of the bulk density measurements along the transect with SWC (left) and without SWC (right) for the different time steps. The three measurements of the bulk density along the transect with SWC show mean values of 1.20, 1.23, and 1.23 g cm^{-3} respectively. Whereas, the transect without SWC shows mean values of 1.29 and 1.24 g cm^{-3}. For the transect with SWC the differences in mean and variability were insignificant and therefore show no temporal trend. For the transect without SWC the found differences are also only slightly significant to insignificant.

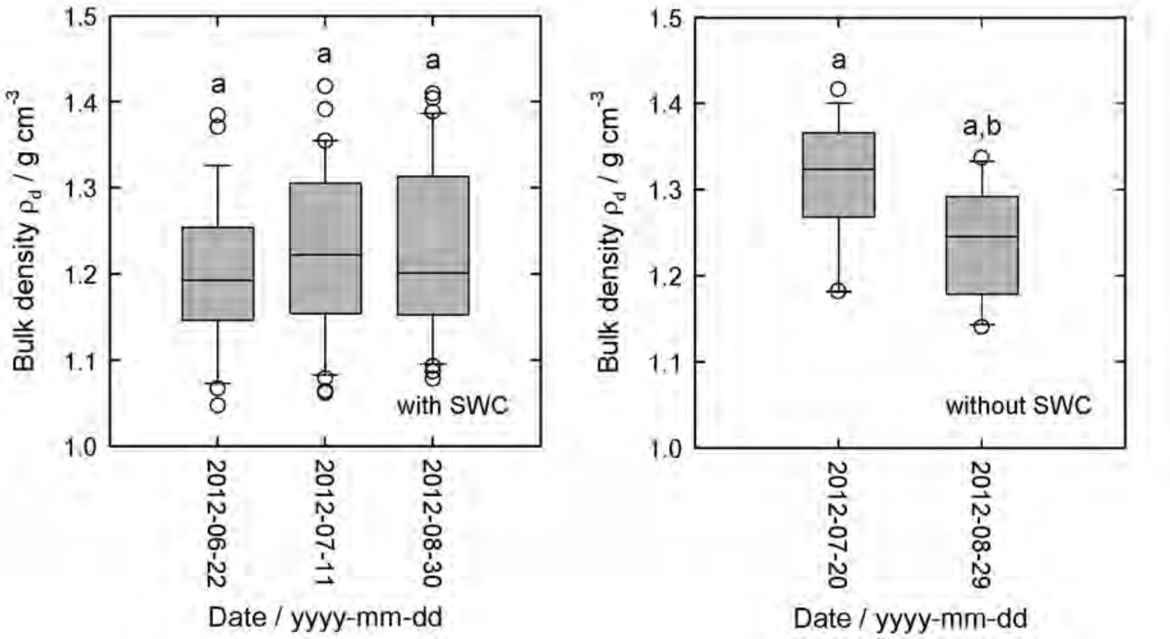

Figure 5.17: Boxplots of the bulk density measurements along the transect with SWC (left) and without SWC (right) for the different time steps. The small Latin letters indicate significant differences (p<0.05) between box means giving the largest mean the letter a.

5.4.4 Spatial analysis

The slightly different hypothetical partition of the fields in-between two stone bunds compared to the volumetric water content should define the zones where the different processes of soil erosion and accumulation are dominant. As the data shows no temporal trend, the data sets were grouped together for the zonal analysis. Levene's test indicates significant differences in the variability. Paired t-test and Least significance test show significant differences in the mean values.

As the measurements along the transect with SWC covered three fields in between stone bunds the bulk density should show a similar behavior on all three fields, if the processes are relevant on a spatial basis. This would lead to a periodic behavior in the data. Autocorrelation analysis can show present periodicities. To find the periodicity and the significance of that periodic behavior a spectral analysis was performed. If one major periodicity is visible in the spectrograms, applying the Fisher's g-test gives information about the significance of this periodicity.

5.4.4.1 Zonal analysis

Figure 5.18 shows boxplots of the sub datasets for the defined zones along the transect with SWC and the datasets of the transect without. The bulk density values for the defined zones differ significantly. The values in the accumulation zone are lowest with a mean of 1.14 g cm^{-3}. The bulk density values for the center zones show a range between the values of the accumulation zone and the values for the stone bunds with a mean value of 1.21 g cm^{-3}. The zone of the stone bunds and the transect without SWC show a similar range in bulk density with mean values of 1.28 and 1.27 g cm^{-3} respectively.

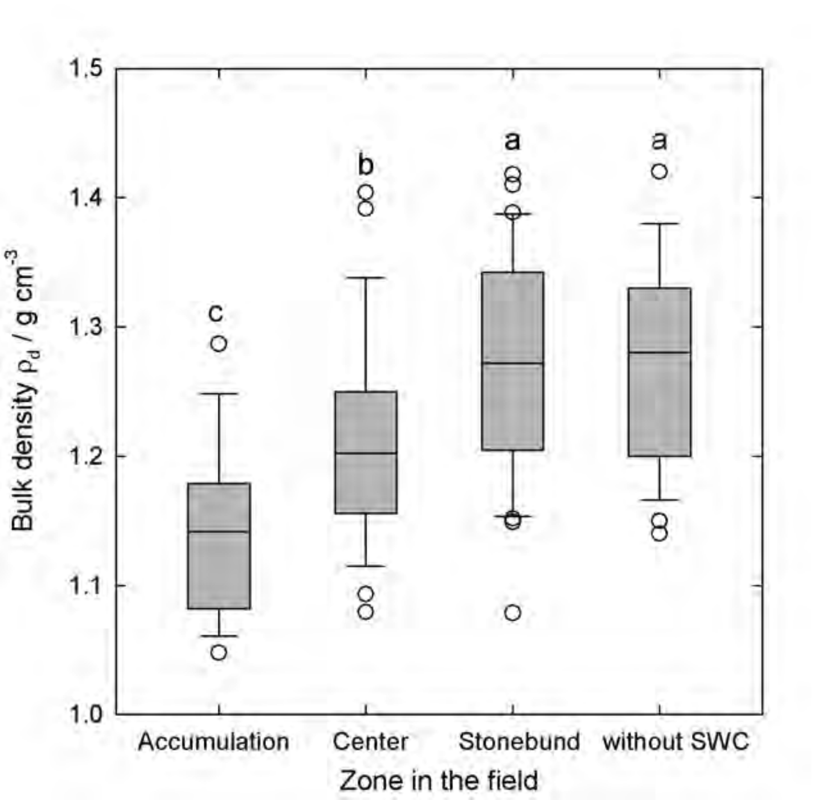

Figure 5.18: Boxplots of the bulk density measurements in the accumulation zone, the center zone, the zone around the stone bunds, and along the transect without SWC. The small Latin letters indicate significant differences (p<0.05) between box means giving the largest mean the letter a.

The findings support the definition of different zones in the field where specific processes are dominant. As the bulk density is significantly lower in the accumulation zone accumulation of looser material is most probably the dominant process in this zone. The bulk density values for the transect without SWC were expected to show a similar range as the values for the center zone. However, the found values are rather high compared to the defined zones.

5.4.4.2 Autocorrelogram analysis

Figure 5.19 shows the autocorrelograms for the measurements along the transect with SWC for the three different time steps. For comparison the autocorrelograms of the transect without SWC for one measurement is shown additionally.

Only graph b) shows a clear periodic behavior of the bulk density measurements along the transect with SWC. For all the other measurements the autocorrelograms show random behavior.

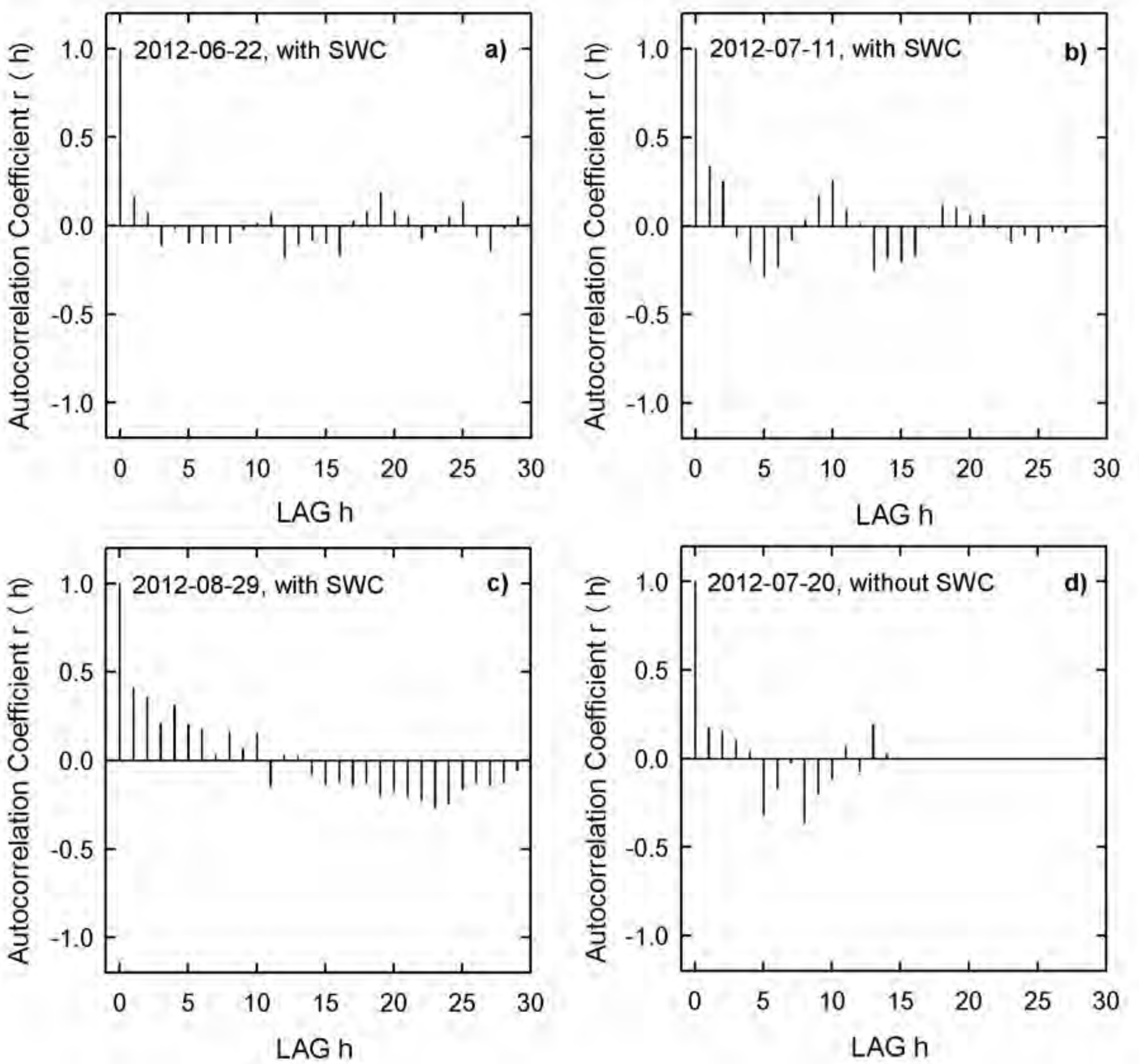

Figure 5.19: Autocorrelogram plots for the transect measurements of the bulk density for the three different time steps a) – c). Graph d) shows the autocorrelograms of the transect without SWC for one measurement for comparison.

5.4.4.3 Spectral analysis

Figure 5.20 shows spectrograms for the autocorrelation analysis above. Again the three data sets of the transect with SWC and one without SWC were used for the analysis.

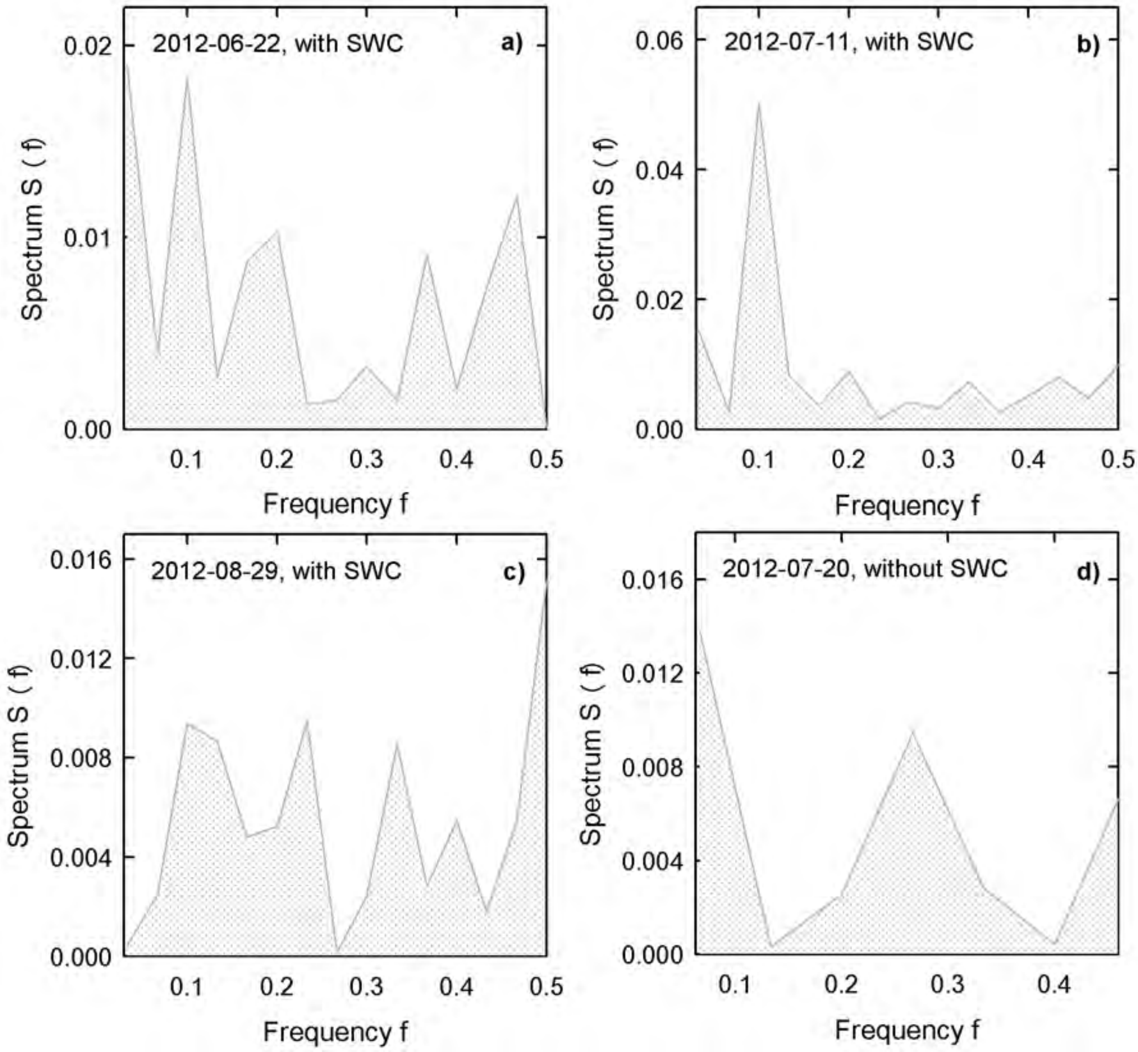

Figure 5.20: Spectrogram plots for the transect measurements of the bulk density along the transect with SWC for the three different time steps a) – c). Graph c) shows the spectrograms of the transect without SWC for one measurement for comparison.

Only graph b) shows a high peak for a frequency of 0.1 that is equivalent to a LAG distance of 10. This distance represents exactly the interval in the measurements in between two stone bunds. However, all other graphs show other peaks of similar amplitude. The significance test supports these findings as the assumption that one significant frequency is contained in the data holds only for the graph b).

The visual impression of the data was that a periodic behavior of the bulk density measurements is present. However, spectral analysis and the autocorrelation analysis show different. The high variations in the zones around the stone bunds, whether a sample was in loose or compacted material might be the reason for the weak findings.

5.5 Stone cover

The stone cover was considered to stay constant within one rainy season. Therefore the assessment of the stone cover was performed only once in the rainy season of 2012. For this work the stone cover was basically assumed to be a good indicator for sedimentation processes. Where accumulation of sediment material takes place a low stone cover was expected as the larger stone fragments are buried under the sediments.

The values of the stone cover were determined by analyzing photographic details with defined scale and area first manually and later on automatized as the differences between the two methods were rather small. The data used for the analyses are the results of the automatized analysis for both transects that was mainly performed by Claire Brenner (2013) for her work in the same test area.

For the assessment of the stone cover along both transects images were taken in exact same patterns of intervals as the measurements of the parameters (see chapter 4.2). This set up results in 30 values along the transect with SWC and 22 values along the transect without SWC.

Table 5.1: Results of the assessment of the stone cover along the transects with and without SWC

Transect with SWC		Transect without SWC	
Distance (m)	Stone cover (m^2 m^{-2})	Distance (m)	Stone cover (m^2 m^{-2})
0.0	0.23	0.0	0.14
1.0	0.12	2.5	0.37
2.0	0.21	5.0	0.41
6.1	0.21	7.5	0.44
10.2	0.28	10.0	0.32
14.3	0.25	12.5	0.43
18.4	0.19	15.0	0.38
22.5	0.08	17.5	0.18
23.5	0.06	20.0	0.18
24.5	0.06	22.5	0.26
25.5	0.25	25.0	0.18
26.5	0.07	27.5	0.09
27.5	0.08	30.0	0.13
32.0	0.13	32.5	0.22
36.5	0.15	35.0	0.16
41.0	0.22	37.5	0.17
45.5	0.13	40.0	0.2
50.0	0.09	42.5	0.19
51.0	0.00	45.0	0.21
52.0	0.03	47.5	0.18
52.5	0.14	50.0	0.17
53.5	0.16	52.5	0.11
54.5	0.15	55.0	0.15
57.4	0.13	57.5	0.18
60.3	0.09	60.0	0.09
63.2	0.12	-	-
66.1	0.06	-	-
69.0	0.07	-	-
70.0	0.02	-	-
71.0	0.07	-	-

5.5.1 Visualization of the data sets

The stone cover shows the expected behavior as illustrated in Figure 5.21. In the zones above the stone bunds that are indicated by dashed vertical lines in the upper graph the stone cover drops significantly to values between 0 and 9% and rises again just after the stone bunds. In the center positions of the fields the stone cover varies between 10 and 28%. The transect without SWC shows large differences in stone cover between the upper and the lower part of the transect. Where the upper part of the transect shows a very high stone cover of up to 44% the stone cover in the lower part varies between 10 and 20%.

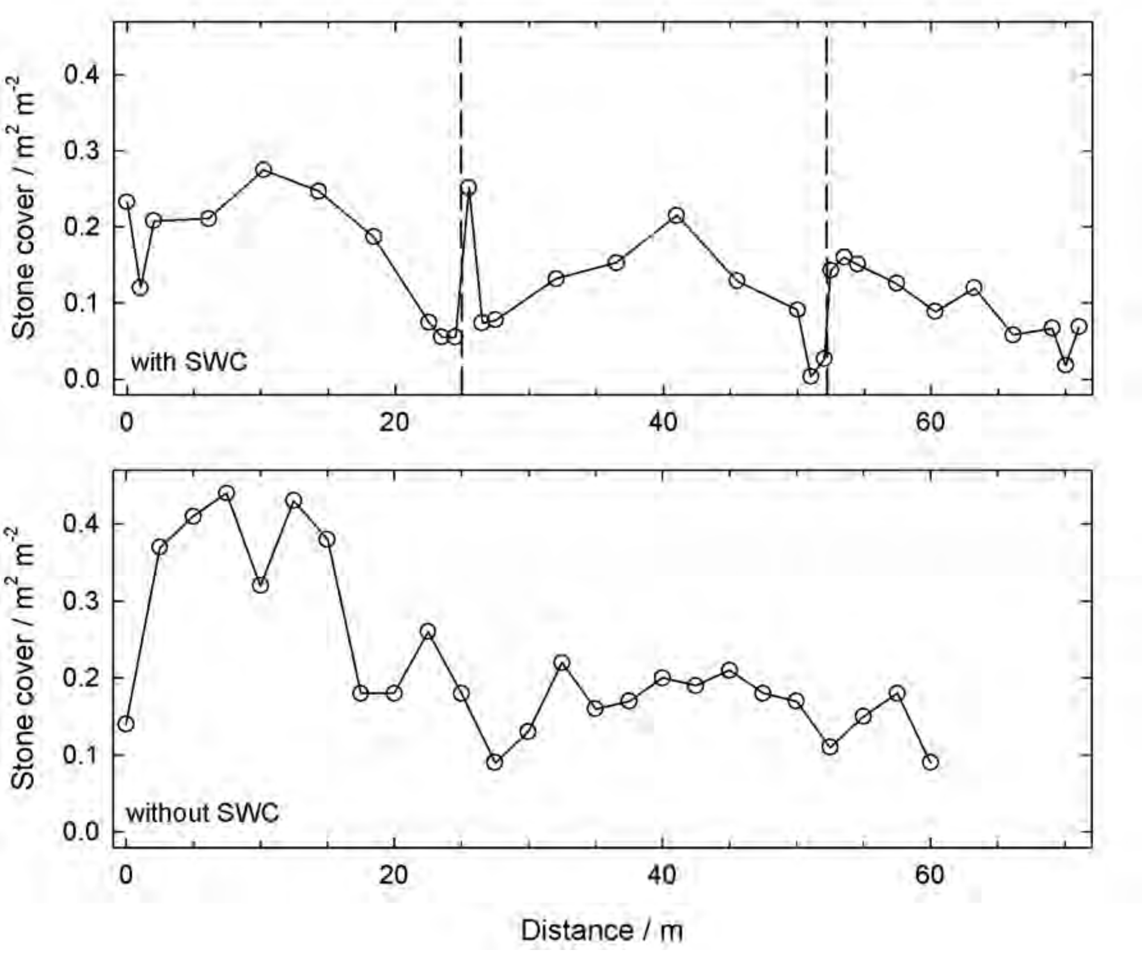

Figure 5.21: The results of the stone cover assessment plotted along the transects with (upper plot) and without (lower plot) SWC. The vertical dashed lines in the upper plot indicate the positions of the stone bunds

5.5.2 Spatial analysis

As the visual inspection of the data indicates different ranges of stone cover in different zones along the transect a spatial analysis was performed similar to the previous parameters. The stone cover and the bulk density are expected to be influenced by the same processes. Therefore, the same partition of the data was used as it was done for zonal analysis of the bulk density. Levene's test indicates significant differences in the variability. Paired t-test and Least significance test show significant differences in the mean values.

As the measurements along the transect with SWC covered three fields in between stone bunds the volumetric water content should show a similar behavior on all three fields, if the processes are relevant on a spatial basis. This would lead to a periodic behavior in the data. Autocorrelation analysis can show present periodicities. To find the periodicity and the significance of that periodic behavior a spectral analysis was performed. If one major periodicity is visible in the spectrograms, applying the Fisher's g-test gives information about the significance of this periodicity.

5.5.2.1 Prerequisites for the data

Normal distribution of the data is an important prerequisite for the majority of statistical tests that were used. To inspect the data visually the data was plotted against the theoretical quantiles of a normal distribution in quantile-quantile plots. Additionally, Kolmogorov-Smirnoff tests show significant differences to the assumption of a normal distribution.

The data sets follow a linear relationship in the plots for most of the values as shown in Figure 5.22. Some of the small values just above the stone bunds, but all of the large stone cover values along the transect without SWC deviate from the assumed normal distribution. However, the Kolmogorov-Smirnoff tests did not reject the null hypothesis that the data is normally distributed.

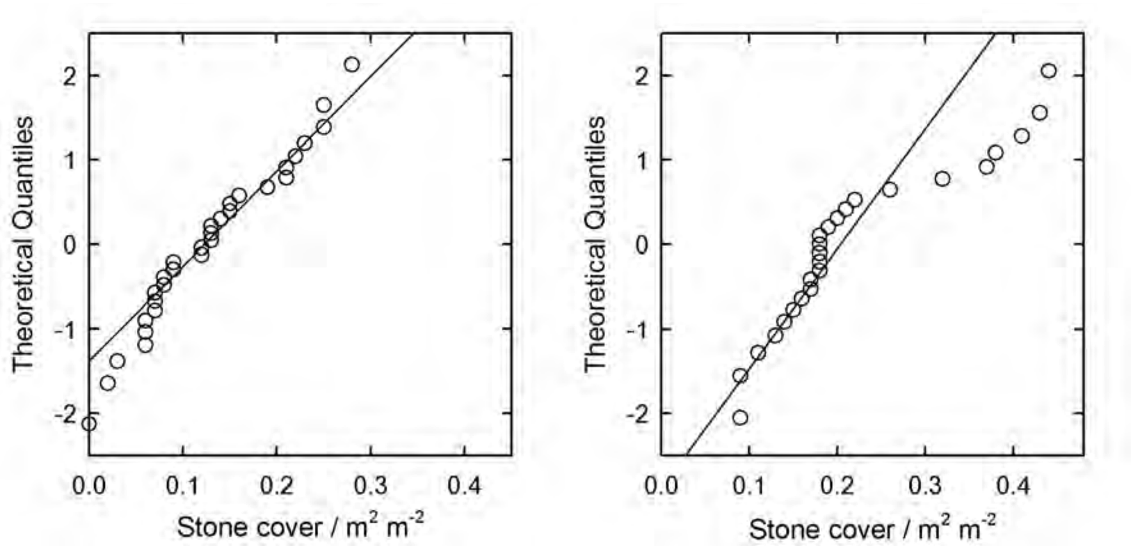

Figure 5.22: Quantile-quantile plots of the data sets with (left) and without (right) SWC. The theoretical quantiles represent a normal distribution. The scale of the stone cover was set constant in the two plots to illustrate general differences between the datasets.

5.5.2.2 Zonal analysis

The partition of the data sets was done similar to the zonal analysis of the bulk density. Figure 5.23 shows the results of the assessment of the stone cover separated in the assumed groups along the transect with SWC. Again the accumulation zone shows the lowest stone cover. However, the zone in the closest vicinity around the stone bunds shows just slightly higher values than the accumulation zone. This can be explained for the points directly above the stone bunds, as the accumulation of sediment started at these points initially. Additionally, for construction of the stone bunds most likely more stones closer to the stone bunds were used than stones farther away from the stone bunds. Therefore, this assumption most probably superposes the decrease in stone cover due to accumulation processes of sediments. The center zone and the transect without SWC show similar values that are significantly higher than the values for the accumulation zone.

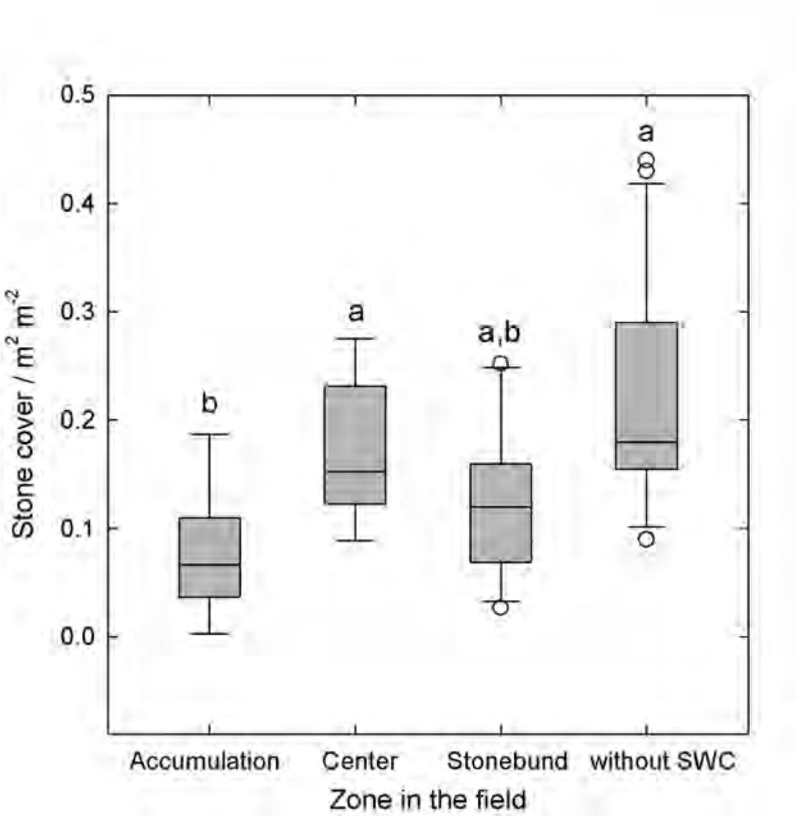

Figure 5.23: Boxplots of the results of the stone cover assessment in the accumulation zone, the center zone, the zone around the stone bunds, and along the transect without SWC. The small Latin letters indicate significant differences (p<0.05) between box means giving the largest mean the letter a.

5.5.2.3 Autocorrelogram analysis

The visual inspection of the data indicated a periodic behavior of the stone cover along the transect with SWC. However, in Figure 5.24 no substantial differences between the two transects were found.

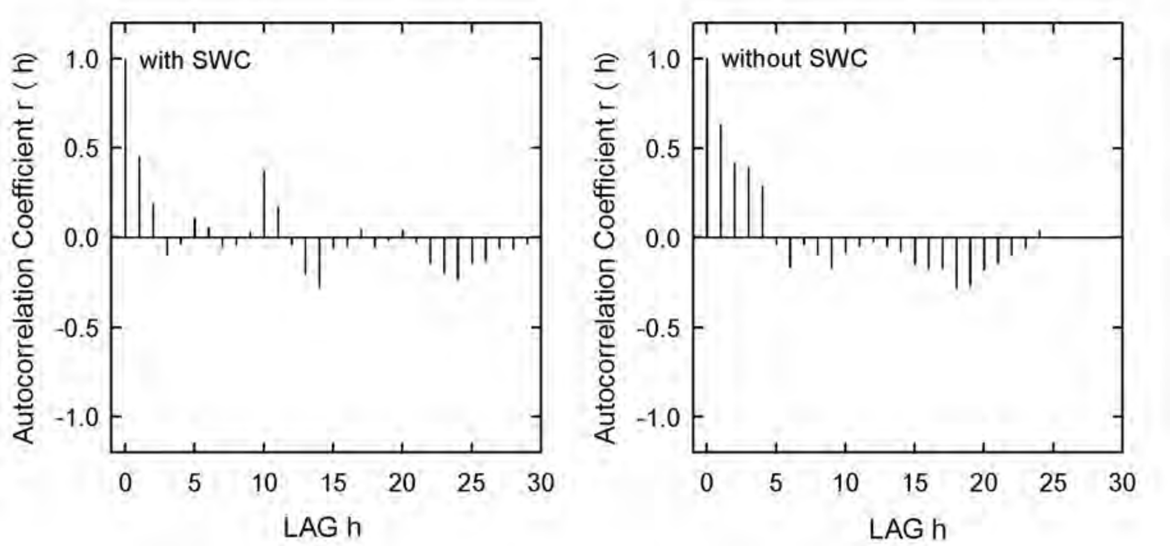

Figure 5.24: Autocorrelogram plots for the results of the stone cover along the transects with (left) and without SWC (right).´

5.5.2.4 Spectral analysis

The spectral analysis shows similar results as the autocorrelograms. The data for the transect with SWC shows the highest peak for a frequency of 0.1 that corresponds to the sampling interval from one field to the other.

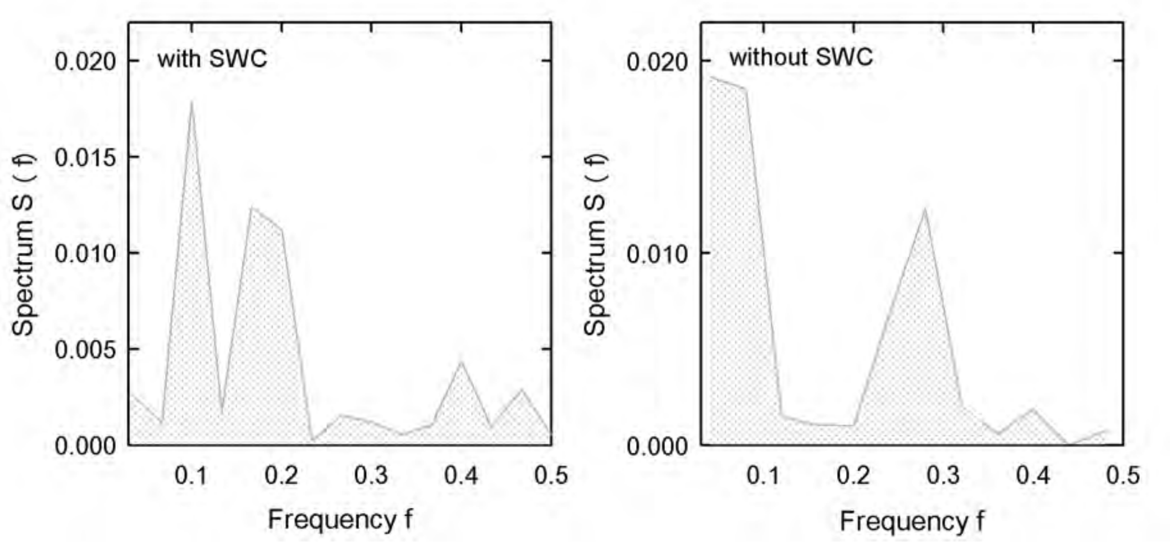

Figure 5.25: Spectral plots for the results of the stone cover along the transects with (left) and without SWC (right).

5.6 Soil water characteristics

This chapter covers the results of the analyses of the tension infiltration measurements. In rainy season of 2012 three sets of tension infiltration measurements were performed along the transect with SWC. The first measurement set was performed in the time from July 11th 2012 to July 13th 2012, the second one from August 14th 2012 to August 17th 2012 and the third from August 29th 2012 to September 1st 2012. Each set of tension infiltration measurements contains nine measurements. On each field in-between two stone bunds three tests were performed; one in the upper position, one in the center zone of the field, and a third measurement in the lower position of each field just above the stone bunds.

The tension infiltration measurements at each point assessed the water recharge rate into the unsaturated soil involving three different pressure heads at the disc device of -8, -4, and 0 cm. Measurements for each supply pressure head setting was performed until steady state water recharge into the unsaturated soil established. Additionally, undisturbed soil samples were taken before and after the tests to determine the initial and end volumetric water content. Disturbed soil samples were taken to determine the soil texture. The results of the soil samples were important input data for the simulation of the soil water characteristics.

The results of the tension infiltration measurements were used to derive the saturated hydraulic conductivity and additional soil water characteristics, such as saturated water content and the van Genuchten parameters α and n.

5.6.1 Results for the soil water characteristics

The saturated hydraulic conductivity was determined using Wooding's analytical solution. To determine soil water characteristics, such as the saturated water content and the van Genuchten parameters an inverse simulation was performed using the software package Disc.

Table 5.2 shows the results for the saturated hydraulic conductivity K_{fs} determined with the Wooding's method and the soil water characteristics residual water content θ_R, the saturated water content θ_S, and the van Genuchten parameters α and n determined by inverse simulation. Additionally the table shows upper and lower confidence values for the simulation results but also the coefficient of determination for the simulation results. As the coefficient of determination only explains the changes in the variance, a visual inspection of the simulated infiltration process was done comparing it to the measured data.

Table 5.2: Saturated hydraulic conductivities calculated using Wooding's method and simulated soil water characteristics using the software package Disc

Date	Pos.	**K_{fs}/Wooding (cm s^{-1})**	**θ_R (m^3 m^{-3})**	**θ_S (m^3 m^{-3})**	$\theta_{S\,lower}$ (m^3 m^{-3})	$\theta_{S\,upper}$ (m^3 m^{-3})	**α (s^{-1})**	α_{lower} (s^{-1})	α_{upper} (s^{-1})	**n (-)**	n_{lower} (-)	n_{upper} (-)	**R^2 (-)**
11.07.2012	1-1	**0.004**	**0.09**	**0.484**	0.479	0.488	**0.134**	0.125	0.142	**1.21**	1.19	1.24	**0.995**
	1-2	**0.015**	**0.09**	**0.471**	0.470	0.472	**0.263**	0.261	0.266	**1.39**	1.37	1.41	**0.999**
	1-3	**0.012**	**0.09**	**0.458**	0.457	0.459	**0.121**	0.116	0.125	**1.35**	1.33	1.37	**0.999**
	2-1	**0.008**	**0.09**	**0.462**	0.458	0.466	**0.206**	0.187	0.224	**1.65**	1.52	1.78	**0.991**
	2-2	**0.013**	**0.09**	**0.480**	0.479	0.481	**0.249**	0.246	0.253	**1.58**	1.55	1.61	**1.000**
	2-3	**0.016**	**0.09**	**0.482**	0.475	0.490	**0.158**	0.123	0.192	**1.21**	1.13	1.30	**0.977**
	3-1	**0.006**	**0.09**	**0.473**	0.472	0.475	**0.210**	0.203	0.216	**1.84**	1.79	1.90	**0.997**
	3-2	**0.009**	**0.09**	**0.512**	0.511	0.513	**0.195**	0.192	0.197	**1.50**	1.48	1.51	**1.000**
	3-3	**0.014**	**0.09**	**0.547**	0.546	0.548	**0.110**	0.106	0.115	**1.46**	1.43	1.49	**0.999**
14.08.2012	1-1	**0.007**	**0.09**	**0.489**	0.487	0.491	**0.198**	0.184	0.212	**1.36**	1.30	1.42	**0.998**
	1-2	**0.012**	**0.09**	**0.481**	0.481	0.481	**0.255**	0.229	0.281	**1.35**	1.27	1.43	**0.995**
	1-3	**0.008**	**0.09**	**0.491**	0.489	0.493	**0.196**	0.182	0.210	**1.37**	1.31	1.44	**0.996**
	2-1	**-**	**-**	**-**	-	-	**-**	-	-	**-**	-	-	**-**
	2-2	**0.009**	**0.09**	**0.498**	0.496	0.500	**0.186**	0.177	0.196	**1.29**	1.27	1.32	**0.998**
	2-3	**0.008**	**0.09**	**0.498**	0.483	0.513	**0.167**	0.167	0.167	**1.30**	1.23	1.36	**0.997**
	3-1	**0.003**	**0.09**	**0.479**	0.477	0.481	**0.167**	0.160	0.175	**1.29**	1.26	1.32	**0.998**
	3-2	**0.005**	**0.09**	**0.463**	0.461	0.466	**0.155**	0.147	0.163	**1.34**	1.31	1.38	**0.997**
	3-3	**0.017**	**0.09**	**0.495**	0.494	0.496	**0.167**	0.164	0.170	**1.43**	1.41	1.45	**0.999**
29.08.2012	1-1	**0.004**	**0.09**	**0.487**	0.486	0.488	**0.143**	0.136	0.150	**1.34**	1.31	1.37	**0.998**
	1-2	**0.008**	**0.09**	**0.494**	0.491	0.497	**0.188**	0.175	0.201	**1.29**	1.24	1.34	**0.994**
	1-3	**0.005**	**0.09**	**0.500**	0.499	0.501	**0.127**	0.123	0.130	**1.39**	1.37	1.41	**0.999**
	2-1	**0.008**	**0.09**	**0.477**	0.474	0.480	**0.163**	0.144	0.183	**1.32**	1.26	1.38	**0.993**
	2-2	**0.010**	**0.09**	**0.509**	0.508	0.510	**0.143**	0.137	0.148	**1.36**	1.34	1.38	**0.999**
	2-3	**0.005**	**0.09**	**0.552**	0.551	0.553	**0.145**	1.420	0.148	**1.45**	1.43	1.47	**0.999**
	3-1	**0.008**	**0.09**	**0.513**	0.512	0.514	**0.112**	0.108	0.116	**1.24**	1.22	1.25	**0.999**
	3-2	**0.009**	**0.09**	**0.530**	0.528	0.532	**0.159**	0.152	0.165	**1.35**	1.32	1.38	**0.997**
	3-3	**0.007**	**0.09**	**0.514**	0.513	0.516	**0.086**	0.080	0.092	**1.24**	1.21	1.26	**0.998**

For validation of the results the calculated saturated water content θ_S was used. It was compared to the pore space determined from the undisturbed soil samples. The saturated water content must be lower than the pore space or at least show a similar value. However, for further analysis this parameter was not considered. The residual water content θ_R was not estimated in the simulation, but set to a constant value of 9.0 Vol% to improve the numerical stability of the simulation due to a decrease of estimated parameters. The van Genuchten parameter n was predicted by the simulation. However, the prediction of this parameter is rather uncertain. Therefore, these two parameters were also omitted in the statistical analyses. For further temporal and spatial analyses only the saturated hydraulic conductivity K_{fs} and the van Genuchten parameter α were used; as these are the most substantial parameters.

5.6.2 Analysis of the saturated hydraulic conductivity

In this chapter the data was analyzed the same way as it was done for previous soil parameters, applying descriptive statistical tests to the data. Normal distribution of the data is an important prerequisite for the majority of statistical tests that were used. To inspect the data visually the data was plotted against the theoretical quantiles of a normal distribution in quantile-quantile plots. Additionally, Kolmogorov-Smirnoff tests show significant differences to the assumption of a normal distribution. Further on, the data sets were analyzed for differences in variability and mean value over time, but also between different zones along the two transects applying Levene-test as a variance test and paired t-test and Least significant difference test finding significant differences in the means.

Figure 5.26 shows the quantile-quantile plots of the saturated hydraulic conductivity values that resulted from Wooding's analytical solution for the three different time periods of tension infiltration measurements. All data follow a linear relationship in the plots to a sufficient extent. Additionally, the Kolmogorov-Smirnoff tests failed to reject the null hypothesis that the data is normally distributed.

Additionally, comparing the three plots a change in the larger hydraulic conductivity values is visible. For the first set of measurements the majority of the hydraulic conductivity was above 0.010 cm s^{-1}. In graph b) only two measurements resulted in a value above this threshold and in graph c) all measurements are below this value. This leads to the assumption that a decrease in the saturated hydraulic conductivity takes place over time.

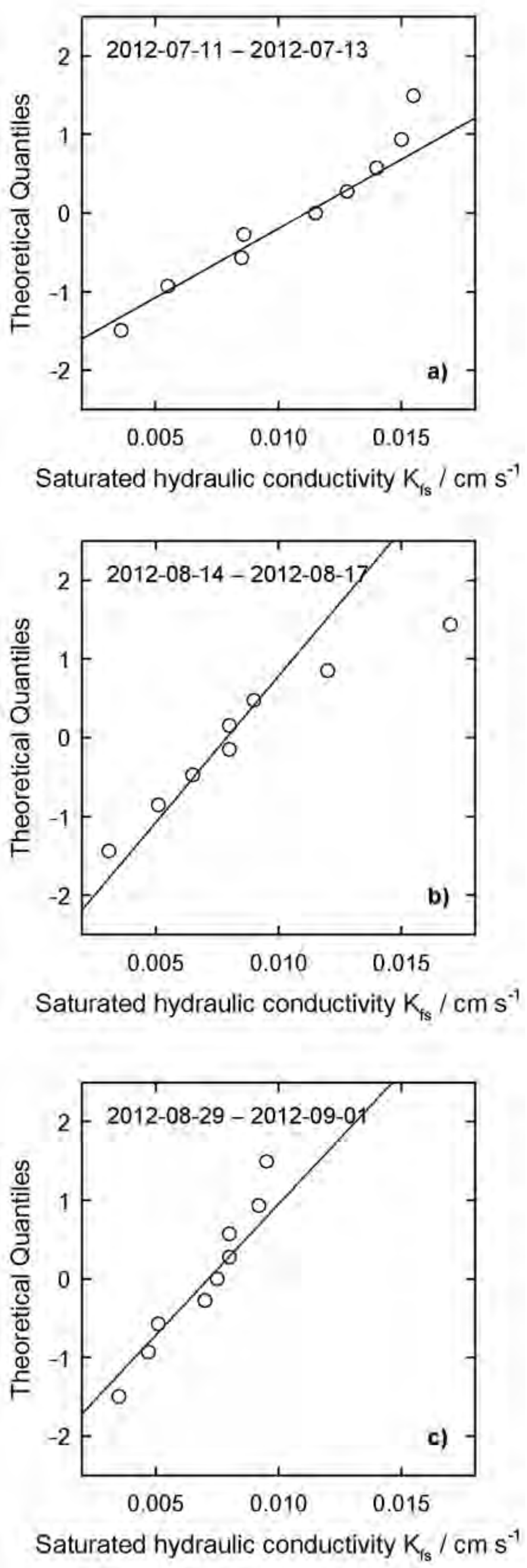

Figure 5.26: Quantile-quantile plots of the data sets of saturated hydraulic conductivity for the three different time steps. The theoretical quantiles represent a normal distribution. The scale of hydraulic conductivity was set constant in all plots to illustrate differences in mean and variability.

5.6.2.1 Temporal analysis

In the previous passage a decrease in the saturated hydraulic conductivity over time was indicated. To get statistical proof for this assumption, the samples for different time step were tested for any significant differences in their statistical parameters.

A progressive decrease in the variability, but also a decrease of the values over time is shown in Figure 5.27. However, in a statistical sense neither the variability of the data sets shows significant differences nor the means of the sets show strong significances.

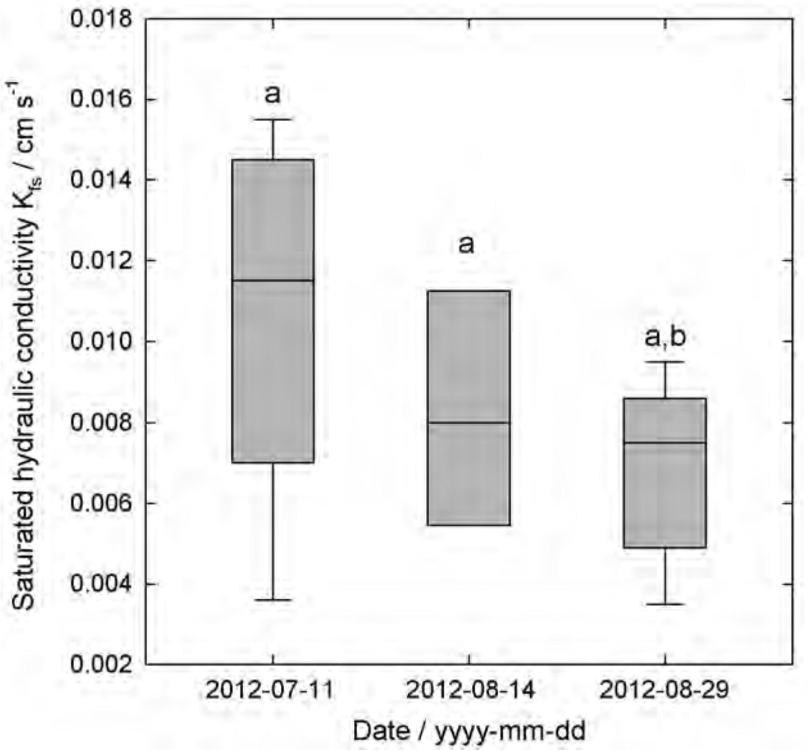

Figure 5.27: Boxplots of the results of the saturated hydraulic conductivity for the three different infiltration test runs. The small Latin letters indicate significant differences ($p<0.05$) between box means giving the largest mean the letter a.

5.6.2.2 Zonal analysis

To get a sufficient number of values in each box the data sets of the three infiltration test runs were added together and the whole set was separated into the three defined zones along the transect with SWC. As the data show a temporal trend this information is included in the analysis. However, general differences between the three zones might become visible.

Figure 5.28 shows the boxplots of the results for the saturated hydraulic conductivity for the three defined zones along the transect with SWC. The upper zone shows a significantly lower mean than the other two zones. Additionally, the variance is much smaller for this zone. Between the center and the lower zone no differences were found in the mean. The lower zone shows a very large variability in the sample set.

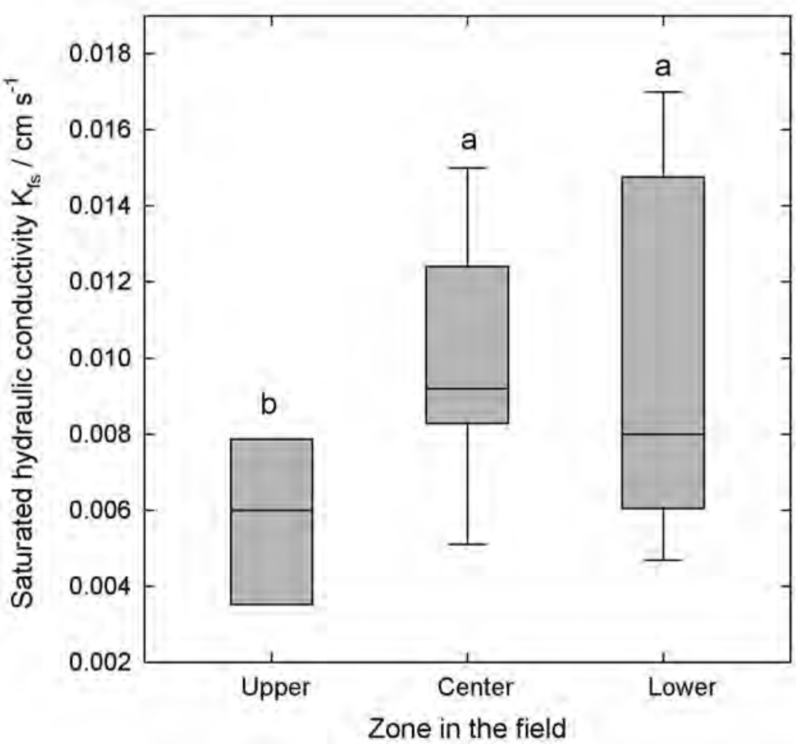

Figure 5.28: Boxplots of the results of the saturated hydraulic conductivity in the upper, center, and the lower zone of the transect with SWC. The small Latin letters indicate significant differences (p<0.05) between box means giving the largest mean the letter a.

To assess where these large differences in the variability of the data sets come from, the samples for the three zones were separated into the time steps of the measurements as shown in Figure 5.29. The lower zone shows the strongest change in the saturated hydraulic conductivity. This is also the zone where the highest variability in the box plot was found. The center zone indicates a slight decrease in the hydraulic conductivity and the values for the upper zone remained rather stable over the whole rainy season.

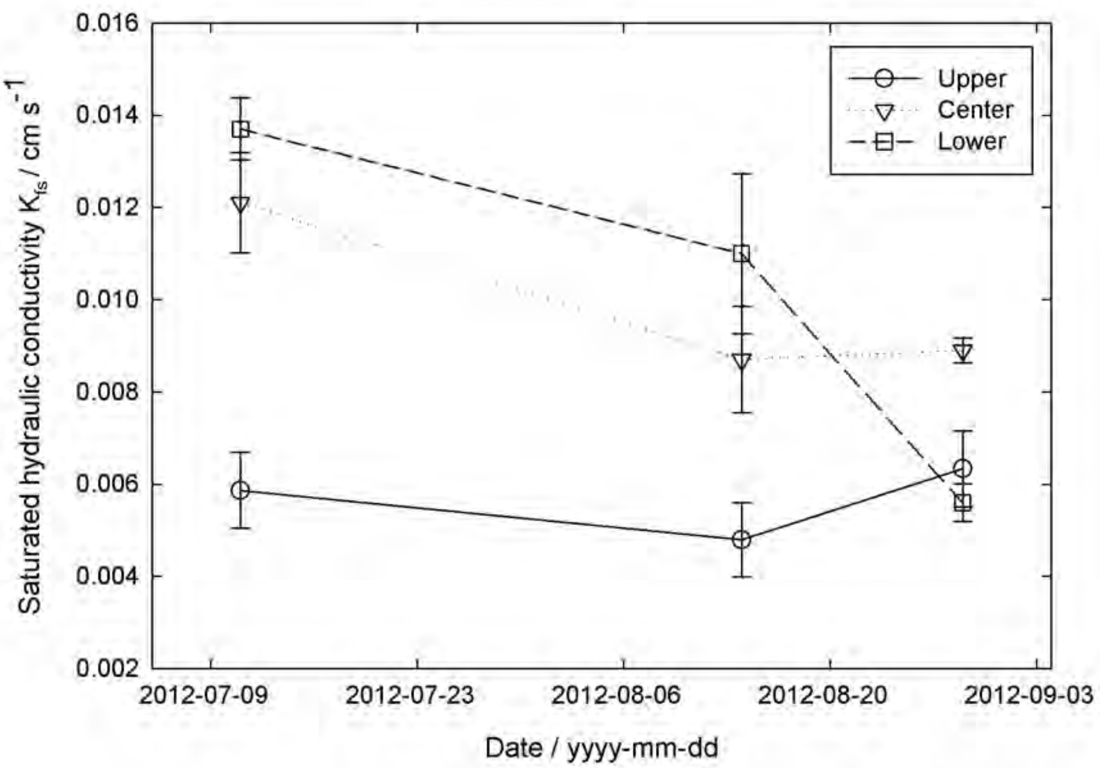

Figure 5.29: Mean values of the saturated hydraulic conductivity for the upper (circles and solid line), center (triangles and dotted line), and lower zone (squares and dashed line) over time. The error bars show the standard error of the data values.

A slight decrease in the saturated hydraulic conductivity was found, where the strongest decrease was found for the zone above the stone bunds. However, the findings are not or only slightly significant. The hydraulic conductivity is a parameter that can vary over several decades depending on the soil type. Therefore in a practical sense a change of approximately 50% of this parameter is negligible.

5.6.3 Analysis of the van Genuchten parameter α

The van Genuchten parameter α is one of the two shape parameters to describe the water retention curve according to the van Genuchten model. The parameter α describes the conditions for the air entry point of the function, where a small α represents a high air entry point in the water retention relationship.

In this chapter the van Genuchten parameter α was analyzed the same way as it was done for previous soil parameters, applying descriptive statistical tests to the data. Normal distribution of the data is an important prerequisite for the majority of statistical tests that were used. To inspect the data visually the data was plotted against the theoretical quantiles of a normal distribution in quantile-quantile plots. Additionally, Kolmogorov-Smirnoff tests show significant differences to the assumption of a normal distribution. Further on, the data sets were analyzed for differences in variability and mean value over time, but also between different zones along the two transects applying Levene-test as a variance test and paired t-test and Least significant difference test finding significant differences in the means.

Figure 5.30 shows the quantile-quantile plots of the van Genuchten value α for the three different time periods of tension infiltration measurements. All data follow a linear relationship in the plots to a sufficient extent. Additionally, the Kolmogorov-Smirnoff tests failed to reject the null hypothesis that the data is normally distributed.

Similar as it was visible in the plots of the saturated hydraulic conductivity the three plots show a change of the values for the three different time steps. The first set of measurements in graph a) show a wide range of different α values. In graph b) almost all values are concentrated in a very narrow range between 0.15 and 0.20 s^{-1}. In graph c) all values lie in the lower half of the range and are below 0.20 s^{-1}.

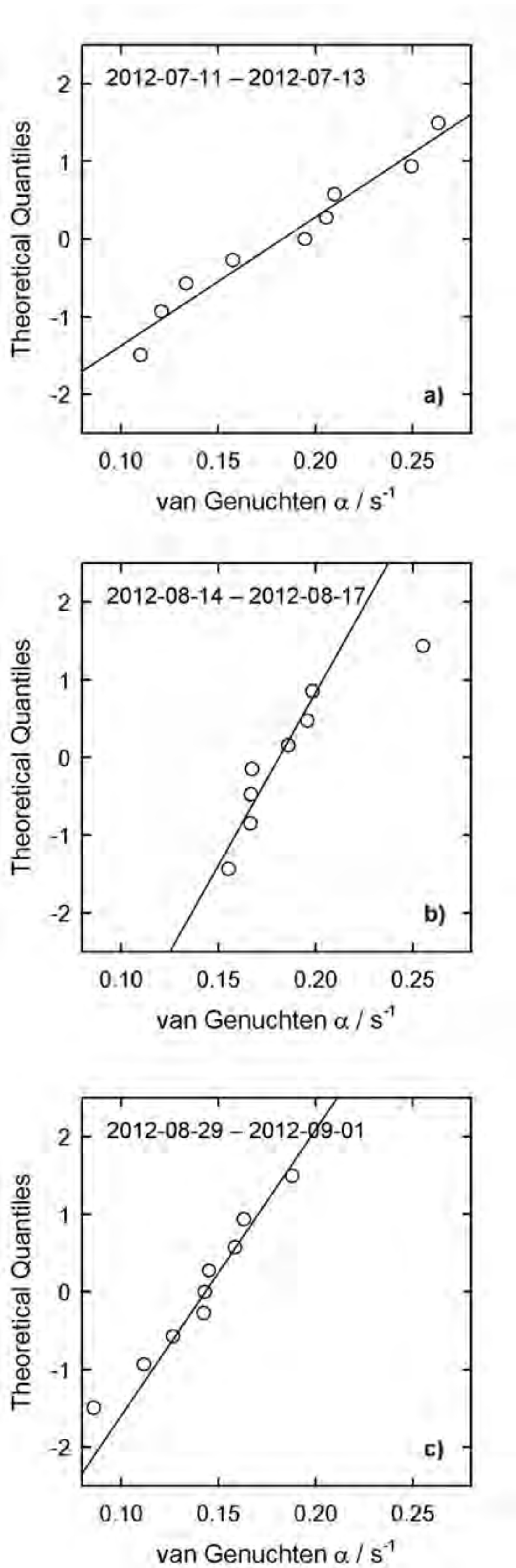

Figure 5.30: Quantile-quantile plots of the data sets of van Genuchten parameter α for the three different time steps. The theoretical quantiles represent a normal distribution. The scale of hydraulic conductivity was set constant in all plots to illustrate differences in mean and variability.

5.6.3.1 Temporal analysis

The quantile-quantile plots indicated a decrease of the van Genuchten parameter α over time, but also strong changes in variability of the data sets.

Figure 5.31 shows the boxplots of the simulated van Genuchten parameters α for the three different sets of tension infiltration measurements. The graph indicates a progressive decrease of the values over time. The variances of the data are strongly variable over time, but show no clear pattern over time. The mean of the data set at the end of the rainy season is significantly lower than the other data sets.

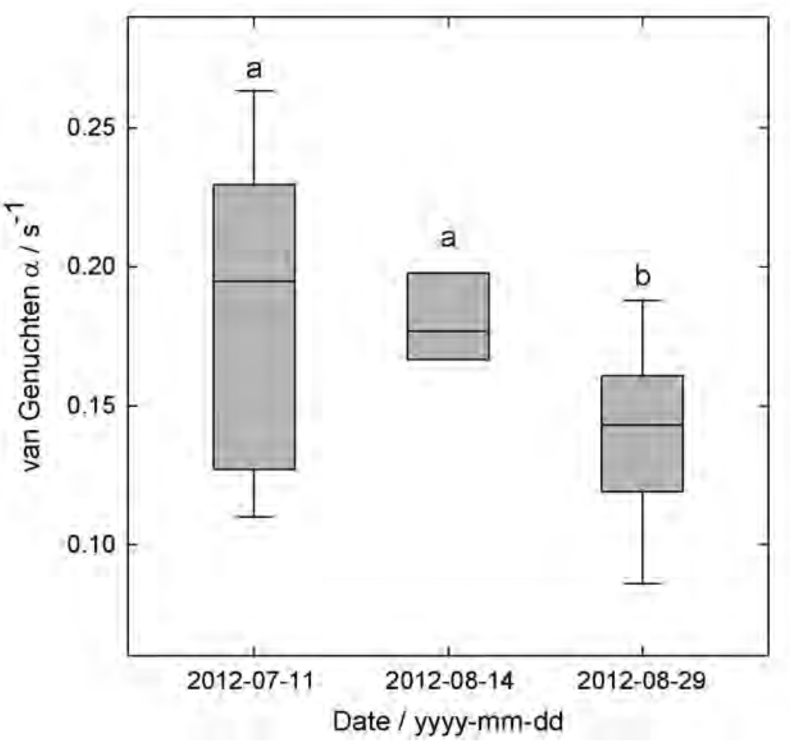

Figure 5.31: Boxplots of the results of the van Genuchten parameter α for the three different infiltration test runs. The small Latin letters indicate significant differences ($p<0.05$) between box means giving the largest mean the letter a.

The parameter α gives information about the air entry point of the water retention curve. In the soil continuum the air entry point is a matter of macro and meso pores. The decrease in mean value of the parameter α over time indicates a decreasing influence of big cracks and a rising effect of the meso pores.

5.6.3.2 Zonal analysis

To get a sufficient number of values in each box the data sets of the three infiltration test runs were added together and the whole set was separated into the three defined zones along the transect with SWC. As the data show a temporal trend this information is included in the analysis. However, general differences between the three zones might become visible.

Figure 5.32 shows the boxplots of the simulated van Genuchten parameter α for the three defined zones upper, center, and lower along the transect with SWC. The graph shows significantly lower values for the parameter α in the lower zones of the transect. The highest values are found in the center zones. The center zones show also the highest variability. The upper zone shows average values for the parameter α.

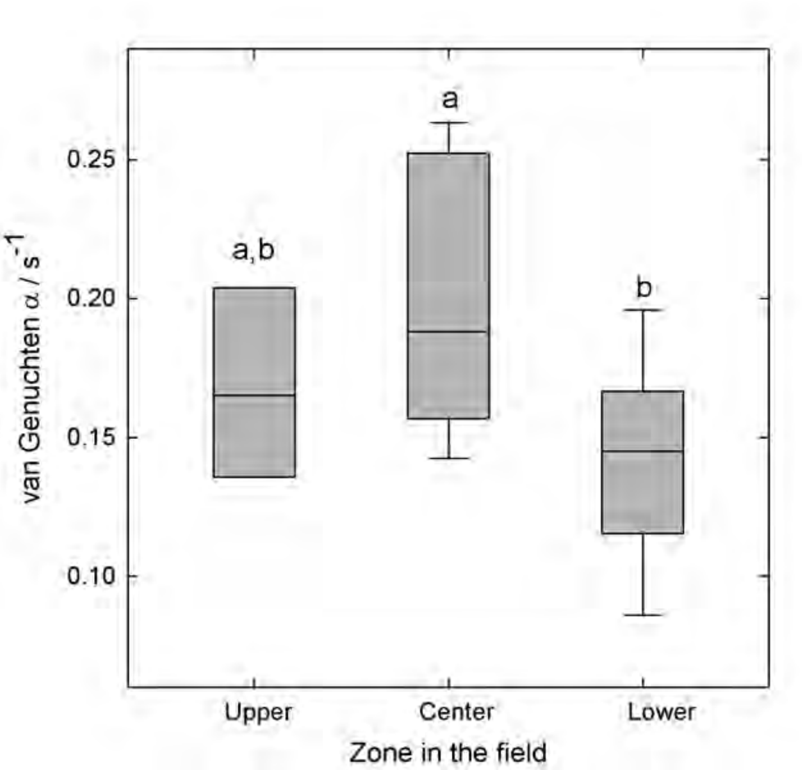

Figure 5.32: Boxplots of the results of the van Genuchten parameter α in the upper, center, and the lower zone of the transect with SWC. The small Latin letters indicate significant differences ($p<0.05$) between box means giving the largest mean the letter a.

To explain the differences in the variability of the data sets over time but also for the different zones the parameter α was plotted over time for the three different zones represented in Figure 5.33. The parameter α decreases constantly over time in the center zone and shows the strongest decrease over the whole time period in this zone. The upper zone also shows a decrease over the whole period. However, this change is not as strong as for the center zone, as the value stagnates in the first period. Surprisingly, the lower zone shows a strong increase from the first to the second time step. This increase explains the very low variability and the absence of low values for the parameter α for the data set from August 14th 2012. After this increase the values strongly decrease to a value lower than the initial value.

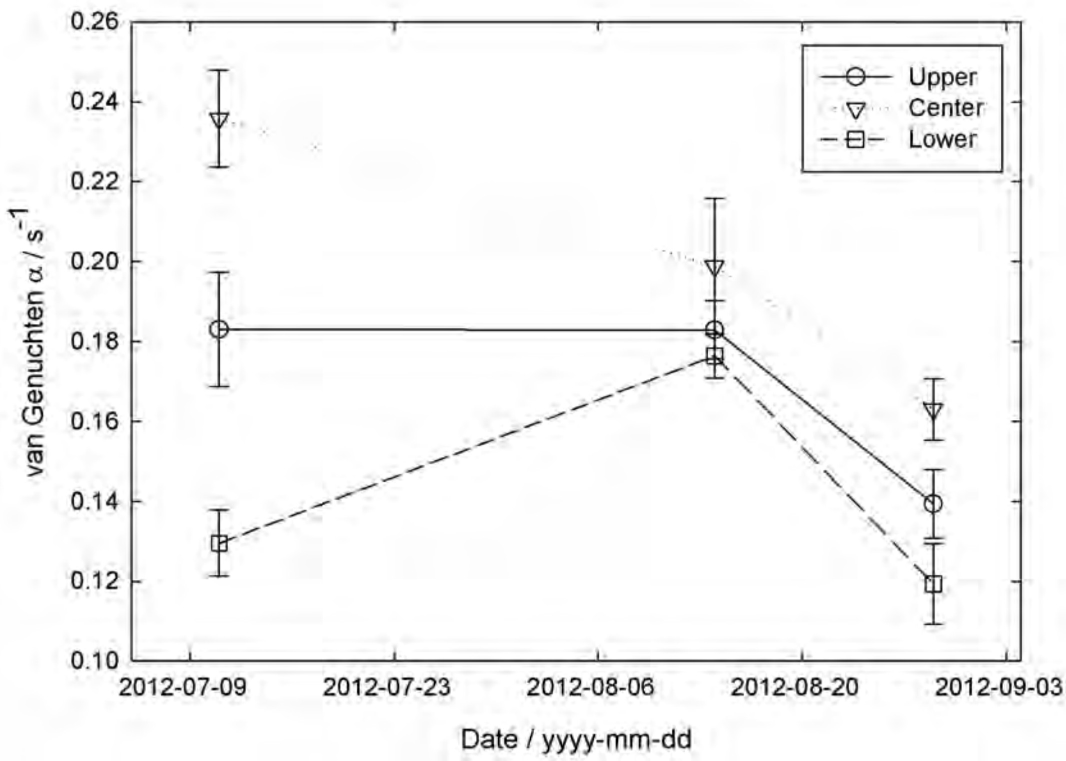

Figure 5.33: Mean values of the van Genuchten parameter α for the upper (circles and solid line), center (triangles and dotted line), and lower zone (squares and dashed line) over time. The error bars show the standard error of the data values.

In the lower zones of the fields just above the stone bunds the values for the parameter α where rather low over the whole rainy season. The center zones showed the highest initial value but also the strongest decrease over the whole period. This might indicate that the influence of big cracks was smaller in lower zone compared to the other zones and did not change that strong over the observed period. In the other zones cracks in the soil were present initially and strongly influenced the water retention behavior of the soil. This influence decreased over the time period, as the soil cracks diminished over time.

5.7 Soil texture

As the soil texture is an important input parameter for the inverse simulation of soil water characteristics, soil samples were taken simultaneously with the tension infiltration measurements in the same locations. The tension infiltration measurements were only performed along the transect with SWC. Therefore, only texture data for this transect is available.

Table 5.3 shows the results of the hydrometer analysis that was conducted by the Gonder soil testing laboratory using the taken disturbed samples. The table shows the fractions of sand, silt, and clay for three sets of samples for June 22nd 2012, July 14th 2012, and August 29th 2012. Comparing the displayed results to the tension infiltration measurements, infiltration tests were performed in the time period from August 14th 2012 to August 17th 2012, but the texture analysis is missing. Unfortunately, the disturbed soil samples for this time period were lost and are not displayed here.

Table 5.3: Results of the hydrometer analysis of the disturbed soil samples in percentages of sand silt and clay for three different time steps.

Date	Pos.	Sand (%)	Silt (%)	Clay (%)
2012 06-22	3-1	28	28	44
	3-2	24	34	42
	3-3	26	32	42
2012-07-14	1-1	22	38	40
	1-2	24	34	42
	1-3	18	38	44
	2-1	24	38	38
	2-2	24	32	44
	2-3	22	34	44
	3-1	22	34	44
	3-2	22	34	44
	3-3	24	32	44
2012-08-29	1-1	28	36	36
	1-2	32	32	36
	1-3	26	34	40
	2-1	30	32	38
	2-2	36	26	38
	2-3	26	32	42
	3-1	30	34	36
	3-2	32	30	38
	3-3	24	38	38

As the set of samples from June 22nd 2012 is rather small in sample size only the sets from July 14th 2012 and August 29th 2012 were used for further analyses.

5.7.1 Visualization of the analyzed data sets

Figure 5.34 shows the results of the hydrometer analysis of the disturbed soil samples taken along the transect with SWC in percentages of sand silt, and clay for the two time steps.

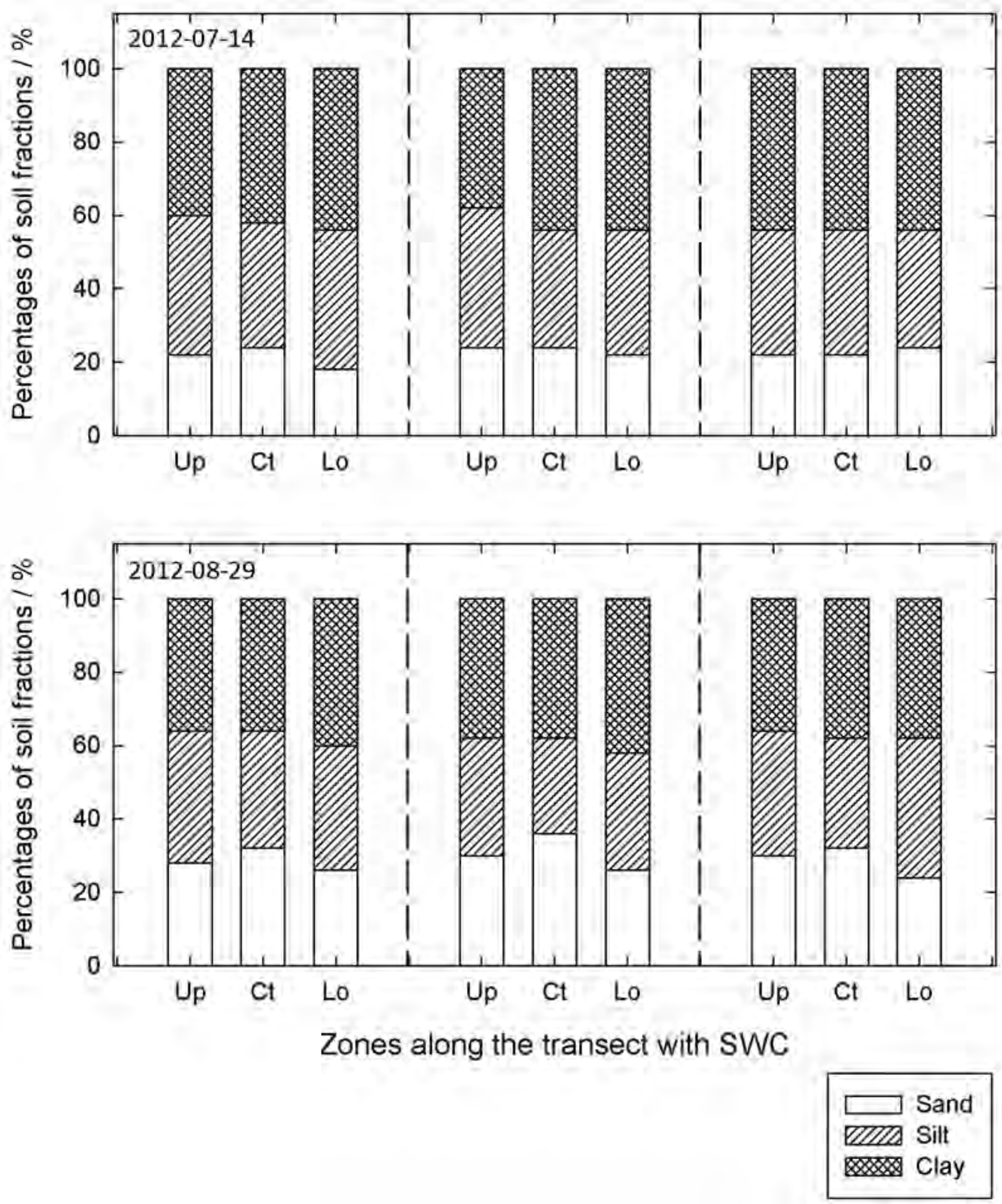

Figure 5.34: Results of soil texture analysis showing the percentages of sand, silt, and clay for the upper (Up), center (Ct), and lower (Lo) positions along the transect with SWC for the two different time steps.

The visual inspection of the data gives no clear differences in the soil fractions. Apart from small deviations all samples show similar fractions of sand silt, and clay for each set of samples. Comparing the two data sets a larger sand content and smaller clay content for all samples taken on August 29th 2012 is visible. As this is shown for all positions along the transect the changes in the soil fractions is not the result of relocation of specific soil fractions. It is rather a result of a systematic error in sampling or analysis.

To classify the soil samples each sample is plotted in a texture triangle according to the sand silt and clay fraction of each sample illustrated in Figure 5.35. As all samples show similar texture the samples are classified as clay or clay loam.

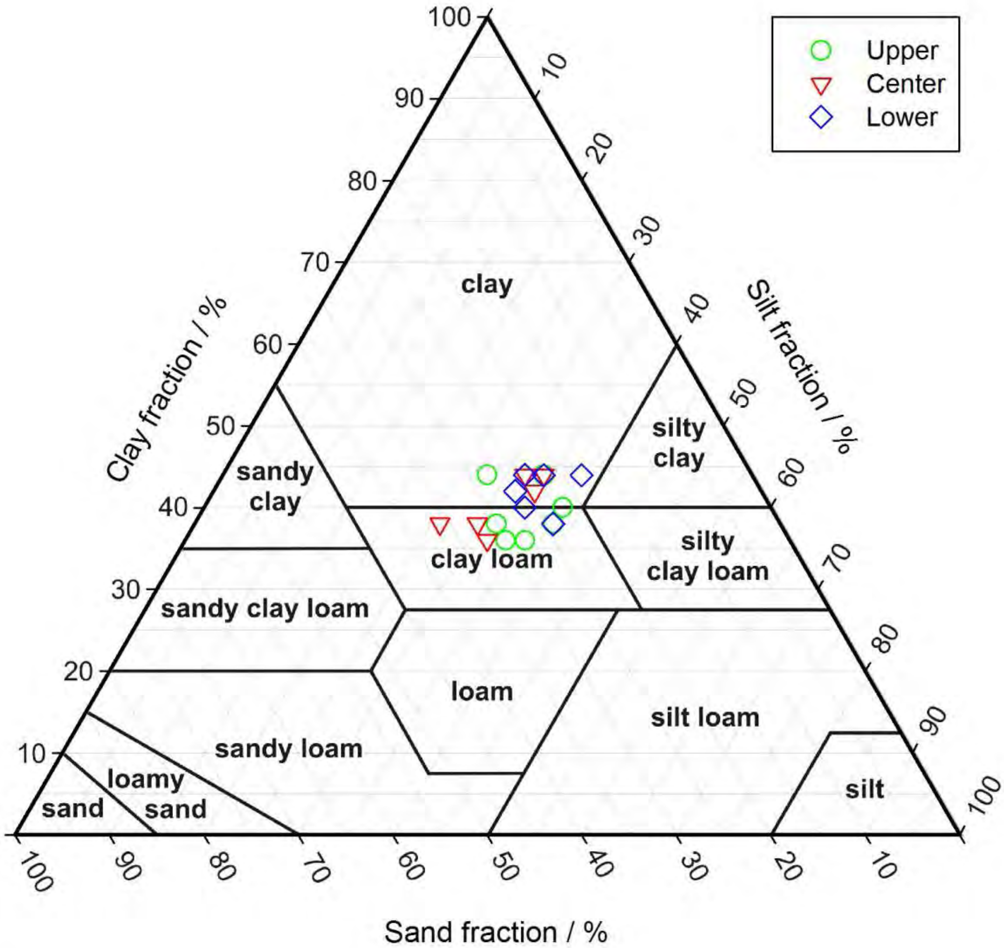

Figure 5.35: Classification of the disturbed soil samples in the texture triangle according to fractions of sand, silt, and clay assessed with the hydrometer method.

5.7.2 Analysis of the soil texture

Similar to other parameters the data sets were compared on a temporal but also on a spatial basis. As normal distribution is an important assumption Kolmogorov-Smirnoff tests should show significant differences to the assumption. Further on, the data sets were analyzed for differences in variability and mean value over time, but also between different zones along the two transects applying Levene-test as a variance tests and paired t-test and Least significant difference test finding significant differences in the means.

For all considered data sets the Kolmogorov-Smirnoff tests failed to reject the null hypothesis that the data is normally distributed.

5.7.2.1 Temporal analysis

The visual inspection of the data assumed a difference for the sand and the clay fraction between the two data sets. Figure 5.36 shows the mean values of the sand, silt and clay fractions for the two different time steps. The assumed differences for the sand and the clay fraction were found significant. However, as mentioned these changes are not expected to be changes due to relocation processes, but rather a result of systematic errors due to sampling or analysis.

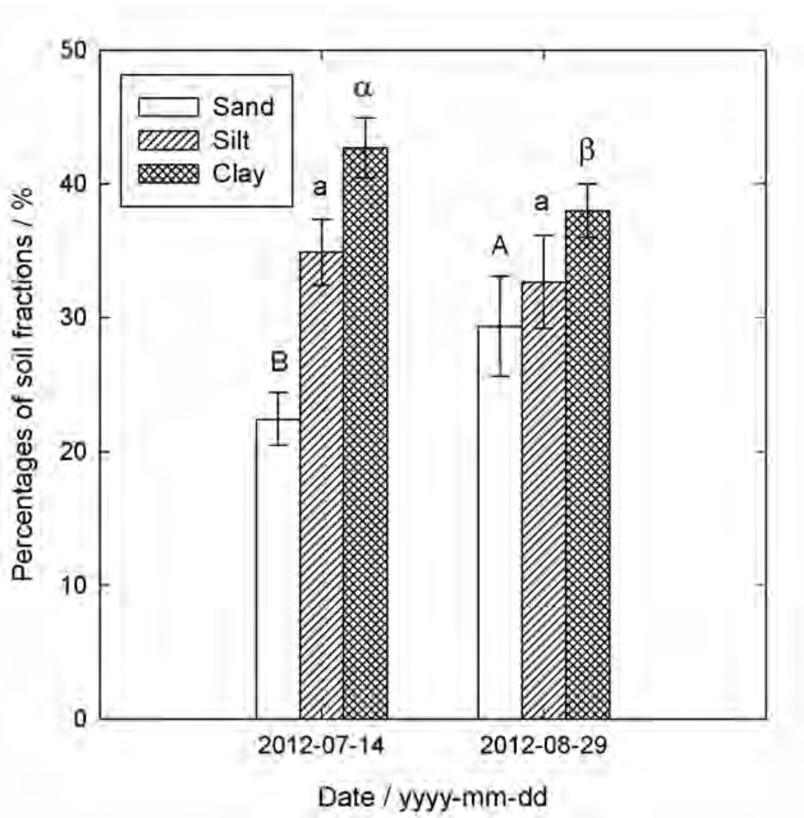

Figure 5.36: Bar chart of the results of soil texture showing the mean percentages of sand, silt, and clay for the two different time steps. The small and capital Latin letters and the small Greek letters indicate significant differences (p<0.05) between means of the same soil fraction giving the largest mean the letter a. The error bars represent the standard deviation of the data.

5.7.2.2 Zonal analysis

Figure 5.37 shows the mean values of the sand, silt and clay fractions for the upper, center, and lower zones along the transect with SWC. The graph shows slight differences for all three soil fractions for the different zones. However, these differences are insignificant.

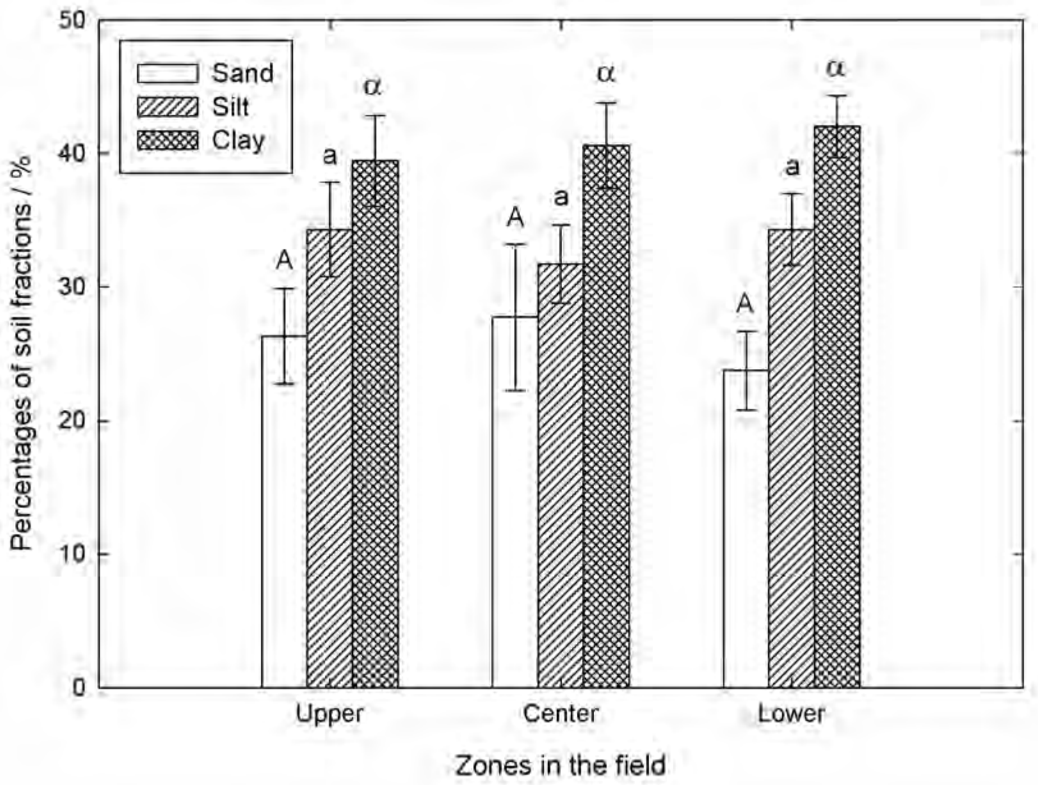

Figure 5.37: Bar chart of the results of soil texture showing the mean percentages of sand, silt, and clay for the defined zones along the transect with SWC. The small and capital Latin letters and the small Greek letters indicate significant differences (p<0.05) between means of the same soil fraction giving the largest mean the letter a. The error bars represent the standard deviation of the data.

5.8 Spatial relationships of the soil parameters

Soil parameters, such as near surface volumetric water content, bulk density, and the stone cover were determined in the exact same pattern along both transects. Additionally, the inclination can be calculated from the fitted splines for the same points. In total four parameters are available to compare on a spatial basis. Three data sets along the transect with SWC and two data sets along the transect without SWC are available for the near surface soil water content and the bulk density for different time steps. For the analysis the semivariance for each parameter and the cross-semivariance for all parameter combinations were calculated for each time step along both transect. The results were plotted and analyzed for similarities in spatial behavior.

5.8.1 Transect with SWC

As data sets for the initial, mid, and end phase of the rainy season are available the analysis was conducted for those three time steps separately. However, inclination and stone cover were treated as constant for all three time steps. Therefore, the relationship between those two parameters remains constant for all three analyses. The major focus lies on the behavior of the water content and the bulk density relative to the other parameters for the three different time steps.

Figure 5.38 shows the results of the cross-semivariogram analysis for the initial phase of the rainy season. The semivariograms of the single parameters are highlighted in gray. The cross-semivariograms of the parameter combinations are arranged in an array below the semivariograms. As the similarity of patterns is of major interest and not absolute values, the display of axis scales was omitted to a large extent. Though, the value zero was indicated by a solid horizontal line in the plots, as the information whether a relationship is positive or negative is vital for the analysis.

The semivariograms of inclination, volumetric water content, and stone cover show a periodic behavior at LAG distance 10 as the semivariance drops at this value. The bulk density shows almost pure nugget behavior for this time step. Although, periodic behavior was found for three of the parameters the cross-semivariograms show only a weak spatial relationship. Only inclination and stone cover show a strong positive spatial relationship.

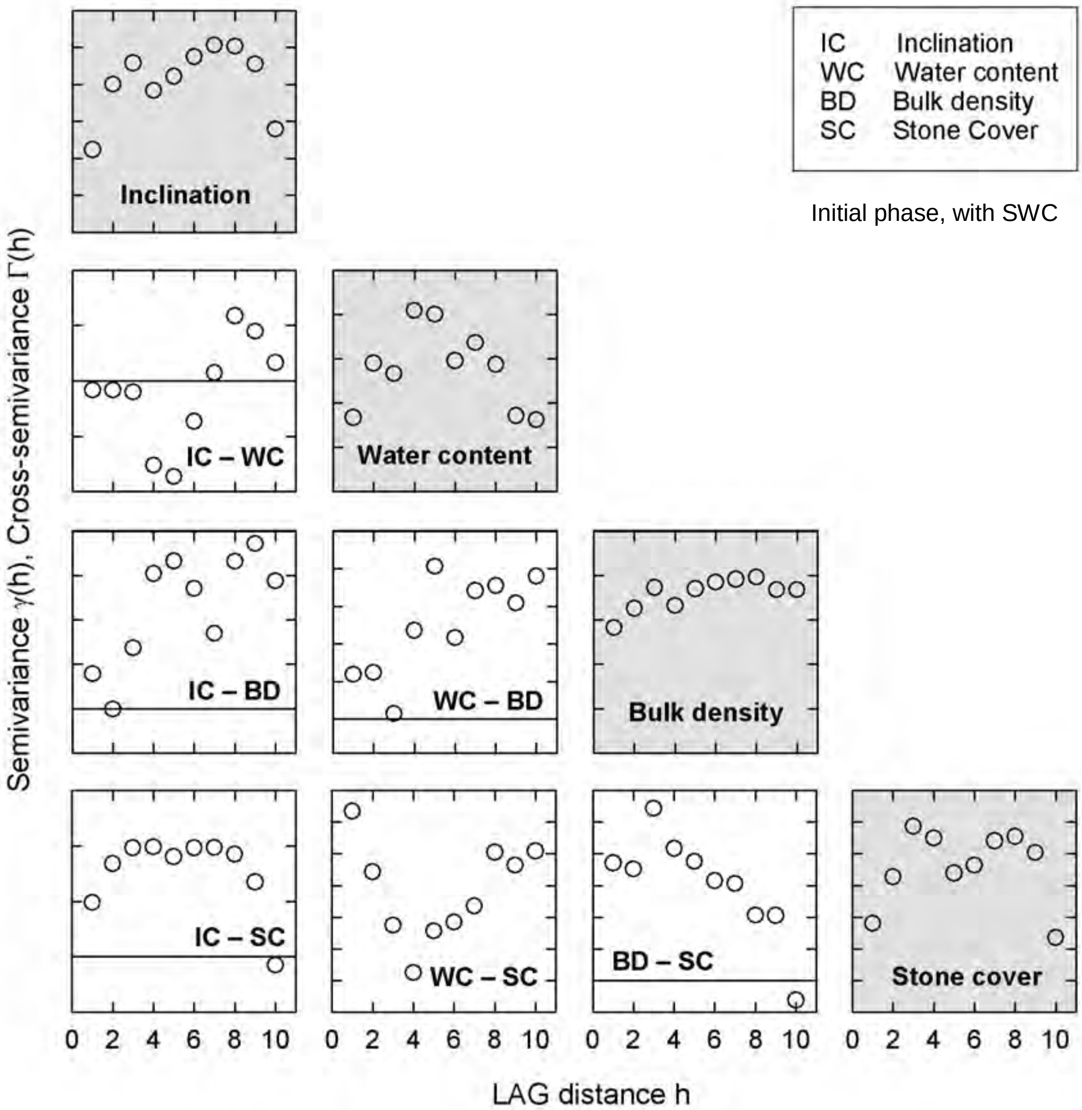

Figure 5.38: Results of the cross-semivariogram analysis for the initial phase of the rainy season along the transect with SWC. The gray graphs show the semivariograms of the single parameters. The cross-semivariograms of the parameter combinations are arranged in an array below.

The mid phase of the rainy season is represented by Figure 5.39. In this case all four parameters show a periodic behavior with a drop in the semivariance at LAG distance 10. Also the cross-semivariograms indicate stronger spatial relationships between the parameters. As the data sets for inclination and stone cover remained the same the relationship shown here is the same as in the previous plot. The volumetric water content shows a strong inverse relationship with the inclination and the stone cover. That means, in areas where the inclination and the stone cover are low the water content is high. As the second data set of bulk density measurements follows the topographic domain of the stone bunds better, also a stronger direct relationship of the bulk density with the volumetric water content was found. However, the relationship of the bulk density with inclination and stone cover seems still rather random.

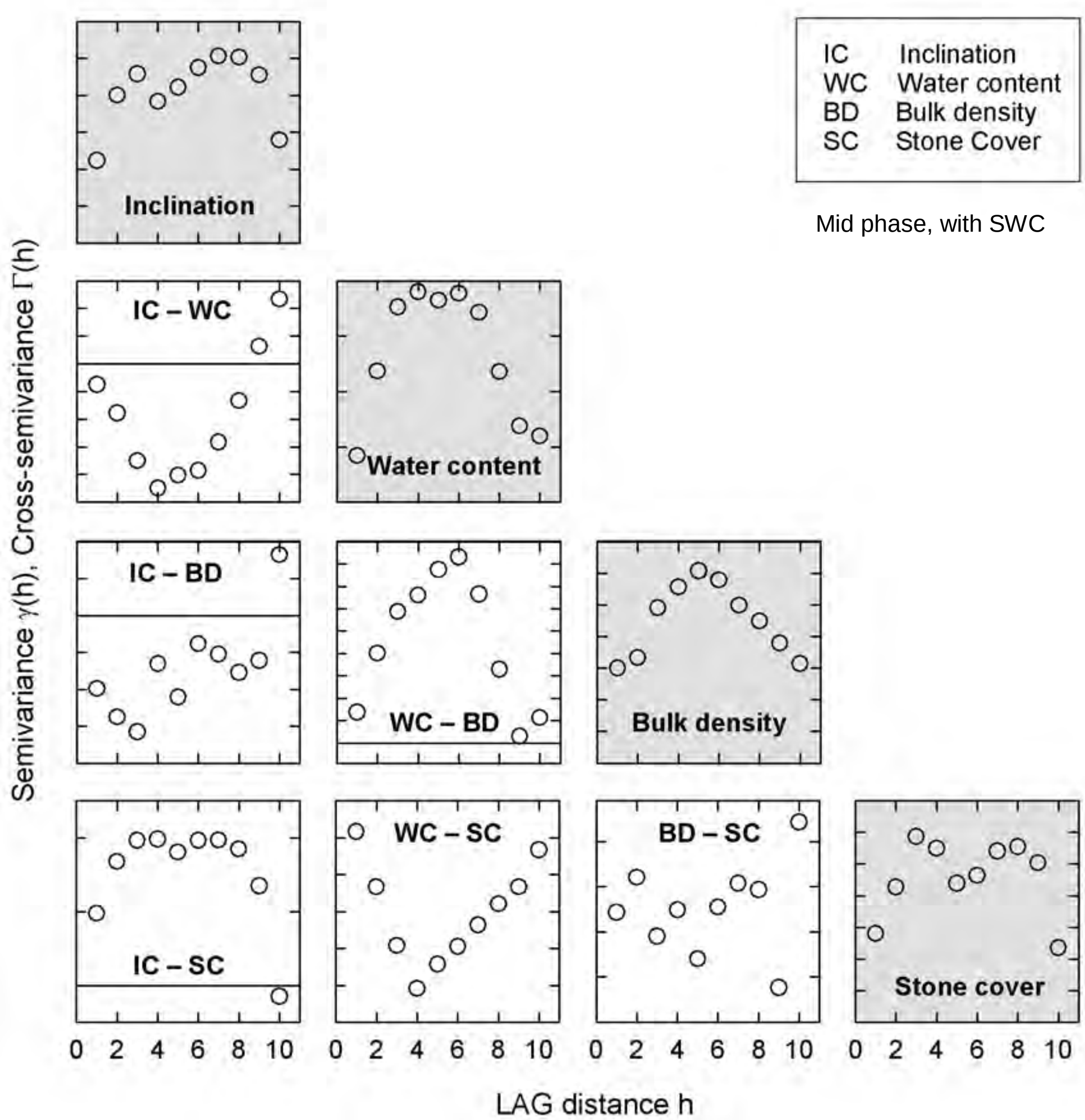

Figure 5.39: Results of the cross-semivariogram analysis for the mid phase of the rainy season along the transect with SWC. The gray graphs show the semivariograms of the single parameters. The cross-semivariograms of the parameter combinations are arranged in an array below.

In Figure 5.40 the results of the analysis for the end phase of the rainy season are represented. Inclination, stone cover, and volumetric water content show a periodic behavior at LAG distance 10. Again the set of measurements of the bulk density indicates a weak spatial relationship. The volumetric water content shows a similar behavior as in the previous analysis and indicates again a strong inverse relationship to the stone cover and the inclination.

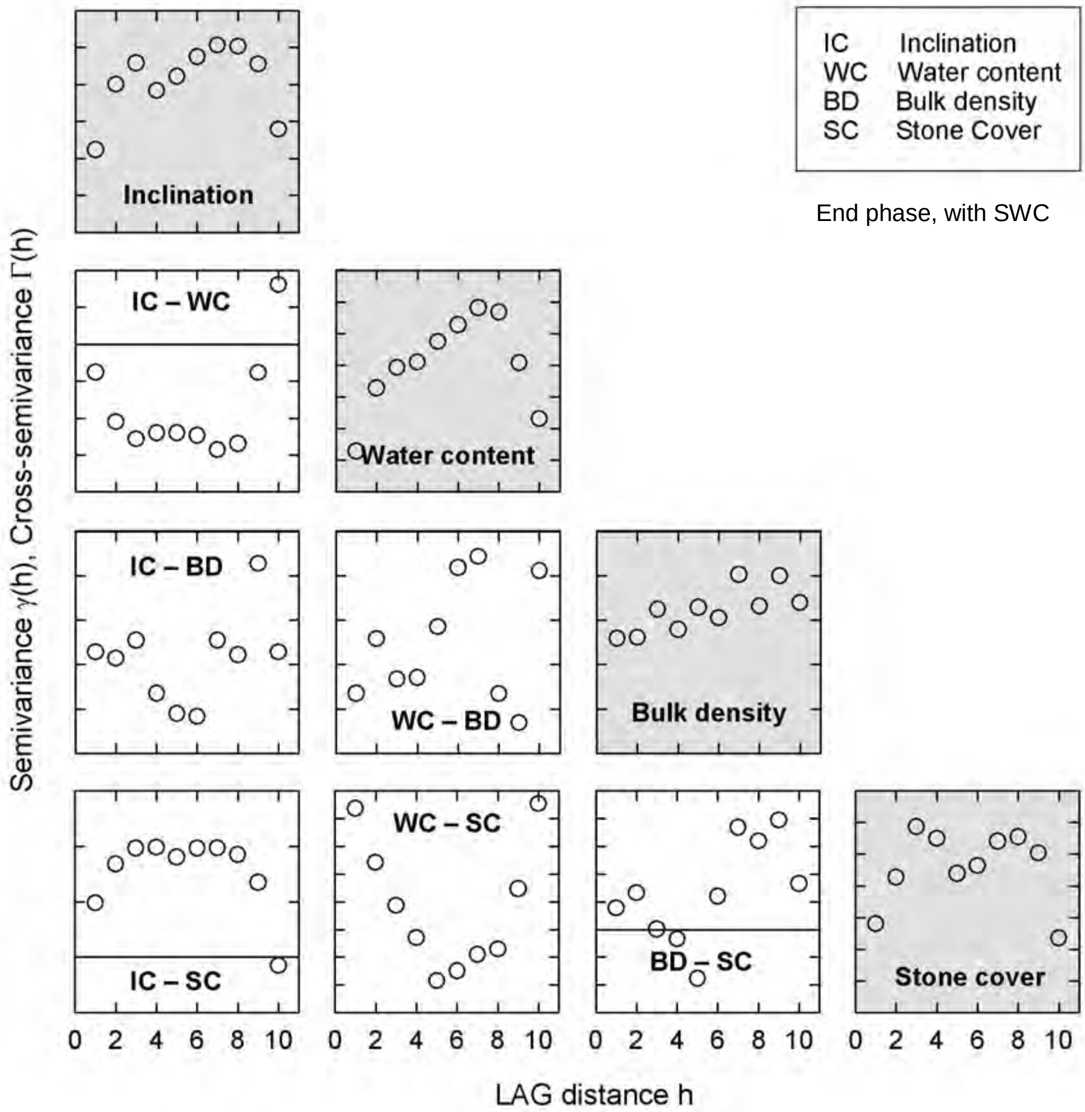

Figure 5.40: Results of the cross-semivariogram analysis for the end phase of the rainy season along the transect with SWC. The gray graphs show the semivariograms of the single parameters. The cross-semivariograms of the parameter combinations are arranged in an array below.

The analysis showed that initially only a relationship for parameters was found where the establishment of the spatial pattern is a long term process. In this case only the inclination and the stone cover show a spatial relationship in the initial phase. The spatial characteristics of those two parameters were already developed prior to the start of the rainy season. The volumetric water content shows a slight periodic behavior initially. However, the relationship to the other parameters is weak. For the mid phase the most substantial spatial relationships between the parameters were found. The strong inverse relationship between the water content and the inclination, but also the stone cover are mainly driven by the runoff accumulation around the stone bunds. In this area the slope decreases due to the accumulated material that also buried the larger stone fragments. In this zone also the major accumulation of soil water takes place. The end phase of the rainy season still showed a good inverse relationship of the water content with the inclination and the stone cover. The bulk density showed a strong dependency on the set of samples used for the analysis. Slight spatial relationships were found only for one time step.

5.8.2 Transect without SWC

To compare the findings of the analysis with SWC to the case of no conservation measure applied the same analysis was performed for the transect without SWC. For the transect without SWC data sets for the mid phase and the end phase of the rainy season were available. Similar to the previous analyses the inclination and the stone cover were treated as constant and the relationship of near surface volumetric water content and bulk density were of major interest.

Figure 5.41 and Figure 5.42 show the results for the cross-semivariogram analysis for the mid and the end phase of the rainy season respectively. In both analyses the parameters indicate no periodic behavior. The semvariograms highlighted in gray mainly show random fluctuations and no sharp decrease over the LAG distance. Additionally, the cross-semivariograms show random fluctuations and no similarities in the patterns of parameters and parameter combinations are visible. This indicates that random spatial characteristics along the transect without SWC did not cause relationships between soil parameters in the spatial domain.

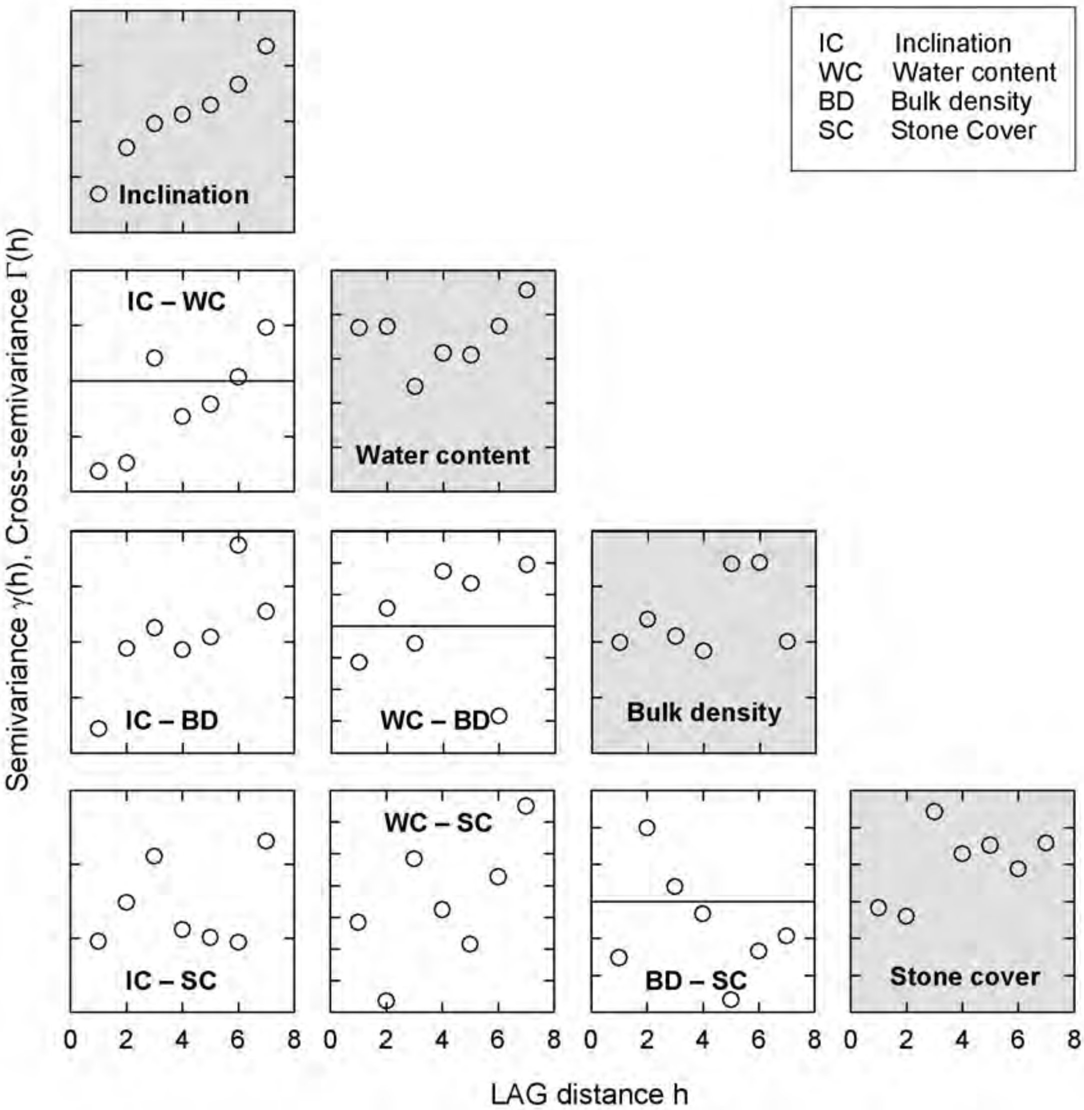

Figure 5.41: Results of the cross-semivariogram analysis for the mid phase of the rainy season along the transect without SWC. The gray graphs show the semivariograms of the single parameters. The cross-semivariograms of the parameter combinations are arranged in an array below.

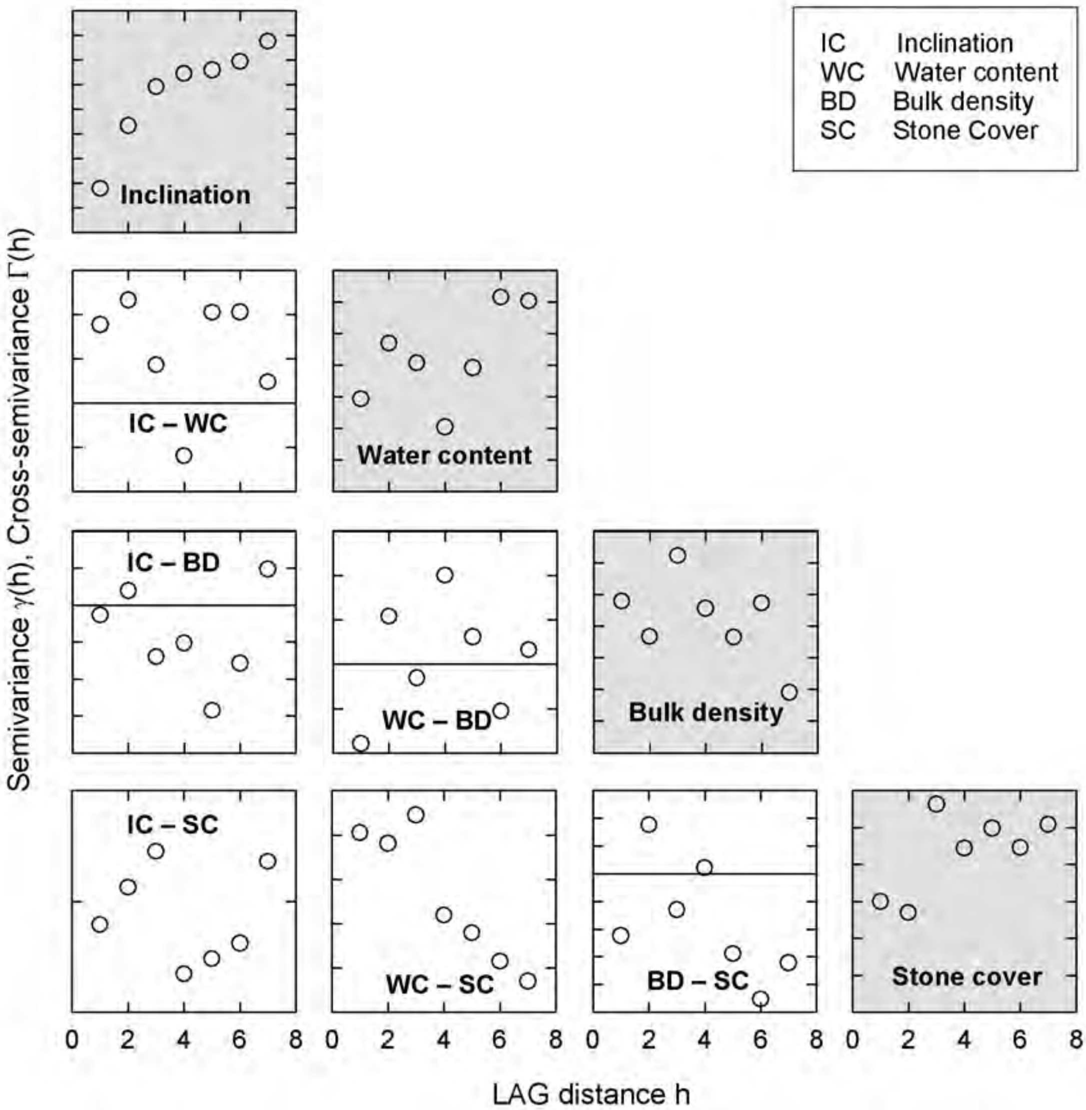

Figure 5.42: Results of the cross-semivariogram analysis for the end phase of the rainy season along the transect with SWC. The gray graphs show the semivariograms of the single parameters. The cross-semivariograms of the parameter combinations are arranged in an array below.

6 Summary and Discussion

The *near surface volumetric water content* showed a positive response to the impact of stone bunds as SWC measure. A temporal increase of near surface soil water was found for both transects with and without SWC. However, the accumulation of soil water was stronger and also happened earlier in the rainy season in the zones around the stone bunds compared to the center zone of the field and the transect without SWC. Especially in the mid phase of the rainy season the areas around the stone bunds showed 15 % higher values in average water content compared to the center position and almost 20 % higher values compared to the transect without SWC. Towards the end of the rainy season the differences decreased. Nevertheless, the transect with SWC still showed higher near surface water contents around the stone bunds. Vancampenhout et al. (2006) found similar results for stone bunds in the Tigray region. Higher soil moisture storage above as well as below the stone bunds were shown in their work. However, Vancampenhout et al. (2006) pointed out that the effect is especially important for greater depths of 1 to 1.5 m and for the dry period after the rainy season. Unfortunately, these facts were not considered in this work.

On a spatial basis the approaches applied in this work were able to visualize the repetitive characteristics of the near surface water content influenced by the topographic domain of the stone bunds. The random behavior of the property in the initial phase of the rainy season, the strongly developed characteristic after the first strong events, as well as the more uniform distribution of soil moisture at the end of the rainy season were shown by these approaches.

Most certainly, the strongest control on the near surface water content was the slope rather than the barrier function of the stone bunds themselves, as the sediment reservoirs behind the stone bunds were almost filled up. The filling up resulted in a strong decrease of the inclination of the slope from 8 % in average to less than 4 %. Similar results were found by Nyssen et al. (2007) for stone bunds in Tigray. Ziadat et al. (2010) found for slopes in a semi-arid area the highest water contents where the slopes were the lowest. This statement supports the findings of this work.

A negative aspect of the retention of runoff is pointed out with Figure 6.1. After strong events the problem of ponding of runoff water above the stone bunds was present. As this happened several times during the rainy season the crop production is drastically reduced towards the stone bunds as visible in the picture.

Figure 6.1: Surface water ponding due to runoff retention above the stone bunds (photo: C.Schuerz)

The *bulk density* showed no clear temporal trend for all positions along both transects. As the preparation of the fields was done before the first measurements, no additional preparations were done that could change bulk density strongly. A visual inspection of the measurements along the transect with SWC showed spatial differences that were found significant. The defined accumulation zone showed the lowest bulk density values with 1.14 g cm^{-3} in average. The center zone, the area around the stone bunds and the transect without SWC showed 5 to 15 % higher values with 1.21, 1.27, and 1.28 g cm^{-3} respectively. Therefore, an impact of the sedimentation process on the bulk density can be seen. The chosen approaches for the spatial analysis however, were not able to show any repetitive behavior of this soil property. The soil around the stone bunds was influenced by sedimentation as well as compaction due to construction of the stone bunds and using the strips on the stone bunds as walking paths. Therefore, a high variability of the bulk density was found in this area that strongly influenced the analysis.

The *stone cover* as a parameter for the previous sedimentation processes showed a similar behavior as the bulk density. Both parameters are influenced by the same processes. Therefore a similar spatial behavior is reasonable. However, the spatial statistical approach did not reveal the similarities found visually due to the influence of the high variability of bulk density above the stone bunds.

The analyses of the *soil water retention characteristics* showed slight differences on a temporal as well as on a spatial basis. The saturated hydraulic conductivity showed the highest initial values for the zone above the stone bunds, but also the strongest decline over the rainy season, with a decrease of 60 % from 0.0137 cm s^{-1} to 0.0056 cm s^{-1}. A similar behavior was found for the center zone of the fields. Surprisingly, the upper zone showed rather low and stagnating levels during the whole rainy season. Additionally, a much larger non saturated flow that was discovered for the measurements in the areas above the stone bunds should be mentioned. In contrast, the van Genuchten parameter α remained rather constant on a low value in the area above the stone bunds. In the center zone the highest initial values were found, but also the strongest average decrease with a reduction of 30 % from 0.236 s^{-1} to 0.163 s^{-1}. The upper position was again stagnating initially, but showed a decrease in the end.

Pachepsky et al. (2001) for example found a relatively strong relationship of the soil water retention characteristics with *soil texture*, especially sand and silt content. However, in this work no spatial as well as temporal differences in soil fractions were found along the transect with SWC. Usually, higher content of sand is found in positions where water erosion takes place that washes out silt and clay. Subsequently silt and clay content are higher in the zones of sedimentation (Ziadat et al., 2010). However, no such effect was shown along the transect with SWC.

Therefore, the found differences in the water retention characteristics are not induced by differences in soil texture. Visual inspection of the transect in the field, however, showed strong differences in soil structure (see Figure 6.2). Where a mainly platy structure was found in the upper and center positions of the transect with SWC, fine to medium grained aggregates were found in the accumulation zones above the stone bunds.

Figure 6.2: Examples for soil structure for the upper and center position of the transect with SWC (left) and the accumulation zone above the stone bunds (right) (photos: C. Schürz).

Therefore, the changes and differences of the water retention characteristics are most likely a result of soil structure. Initially, big cracks between the platy aggregates were dominant for saturated water flow in the center positions of the fields. During the rainy season those cracks closed due to swelling processes of the soil. This led to a decrease of the saturated hydraulic conductivity and also to a larger dominance of the meso pores (lower value for van Genuchten α) in the water retention relationship. As the sedimentation zones showed this fine to medium grained structure throughout the rainy season the van Genuchten α was less influenced by the changes of the cracks. This might explain the rather constant behavior of this parameter throughout the rainy season. The aggregate structure also might have had a large amount of larger pores that strongly contributed to a larger saturated conductivity. Due to swelling processes also those pores most certainly have closed during the rainy season.

7 Conclusion

An impact of stone bunds as a SWC measure on most of the analyzed soil parameters was found on a spatial as well as on a temporal basis. Additionally, similar behavior of soil parameters on a spatial basis was found to some extent with the chosen approach. The most promising parameter to analyze with this approach was the near surface soil water content, where the spatial statistical analyses applied showed the clearest results. In general, this work showed that the chosen statistical methods can reveal temporal and spatial changes of soil properties within the presented context.

8 Outlook

This work only showed the behavior of specific soil properties under the influence of the climatic conditions during one rainy season. Long term monitoring would be important to adequately characterize specific parameters for such a highly variable climate. The parameter that showed the best results within this work, was the near surface soil water content. Therefore, for future monitoring a special focus should lie on this parameter. However, as shown by Vancampenhout et al. (2006) not only the near surface water content, but measurements in deeper soil layers should be performed. Furthermore, the measurements should be extended throughout the dry season afterwards, as the surplus of soil moisture during this period is most crucial and would be an important factor to assess the impact of the stone bunds.

For the measurement of the volumetric water content, also other methods should be considered, as capacitive measurement methods showed difficulties in the calibration that subsequently would result in high uncertainties for the parameter.

The kriging approach to display temporal and spatial changes simultaneously supported the findings very well. However, so far it is only valid as a visualization tool, as a relationship between the spatial and the temporal scale is unknown and was defined in a subjective way. Further frequent measurements of the soil water content in a fine spatial resolution would be necessary to analyze the relationship between the spatial and the temporal scale.

In the rainy season of 2012 the sedimentation reservoirs behind the stone bunds were already filled up to a large extent. Gebremichael et al. (2005) found in their work that the efficiency of stone bunds strongly decreases when the sedimentation storage of the stone bunds is filled up. Therefore, maintenance of the stone bund structures prior to the start of the rainy season would be very important.

References

Abdi, H., 2007. The Bonferonni and Šidák Corrections for Multiple Comparisons, in: Salkind, N. (Ed.), Encyclopedia of Measurement and Statistics. Thousand Oaks, CA.

Abdi, H., Williams, L.J., 2010. Fisher's Least Signifcant Difference (LSD) Test, in: Salkind, N. (Ed.), Encyclopedia of Research Design. Thousand Oaks, CA.

Addis, H.K., Strohmeier, S., Srinivasan, R., Ziadat, F., Klik, A., 2013. Using SWAT model to evaluate the impact of community-based soil and water conservation interventions for an Ethiopian watershed, in: Proceedings of the 2013 International SWAT Conference, Paul Sabtier University, Toulouse, France July 17-19th, 2013. Toulouse.

Ahdesmaki, M., Fokianos, K., Strimmer, and K., 2012. GeneCycle: Identification of Periodically Expressed Genes.

Aho, K., 2013. asbio: A collection of statistical tools for biologists.

Angulo-Jaramillo, R., Vandervaere, J., Roulier, S., Thony, J., Gaudet, J., Vauclin, M., 2000. Field measurement of soil surface hydraulic properties by disc and ring infiltrometers - A review and recent developments. SOIL TILLAGE Res. 55, 1–29.

Ankeny, M.D., Ahmed, M., Kaspar, T.C., Horton, R., 1991. Simple Field Method for Determining Unsaturated Hydraulic Conductivity. Soil Sci. Soc. Am. J. 55, 467. doi:10.2136/sssaj1991.03615995005500020028x

Ankeny, M.D., Kaspar, T.C., Horton, R., 1988. Design for an Automated Tension Infiltrometer. Soil Sci. Soc. Am. J. 52, 893. doi:10.2136/sssaj1988.03615995005200030054x

Bai, Z.G., Dent, D.L., Olsson, L., Schaepman, M.E., 2008. Global Assessment of Land Degradation and Improvement. 1. Identification by remote sensing (Report No. 2008/01). ISRIC - World Soil Information, Wageningen.

Blanco, H., Lal, R., 2008. Principles of Soil Conservation and Management. Springer, New York, NY.

Bloomfield, P., 2004. Fourier Analysis of Time Series: An Introduction. John Wiley & Sons.

Bosshart, U., 1997. Catchment Discharge and Suspended Sediment Transport as Indicators of Physical Soil and Water Conservation in the Mayketin Catchment, Afdeyu Research Unit: A Case Study in the Northern Highlands of Eritrea (Volume 39 of Soil conservation research project: research report). University of Bern, Bern.

Brenner, C., 2013. Monitoring and Simulation of Soil Erosion in the Ethiopian Highlands on a Plot Scale (Master Thesis). University of Natural Resources and Life Sciences, Vienna.

Casey, F., Derby, N., 2002. Improved design for an automated tension infiltrometer. SOIL Sci. Soc. Am. J. 66, 64–67. doi:10.2136/sssaj2002.0064

Dejene, A., 2003. Integrated Natural Resources Management to Enhance Food Security, The Case for Community-Based Approaches in Ethiopia. FAO, Rome.

Dent, D., Asfary, A.F., Giri, C., Govil, K., Hartemink, A., Holmgren, P., Keita-Ouane, F., Navone, S., Olsson, L., Ponce-Hernandez, R., Rockström, J., Sheperd, G., 2007. Land, in: United Nations Environmental Programme (Ed.), Global Environmental Outlook (GEO4): Environment for Development. UNEP, Nairobi.

Dereje Ayalew, 2012. Variability of rainfall and its current trend in Amhara region, Ethiopia. Afr. J. Agric. RESEEARCH 7. doi:10.5897/AJAR11.698

DESA, UN, 2013. World Population Prospects. The 2012 Revision. Volume II: Demographic Profiles (Report No. ST/ESA/SER.A/345). United Nations, Department of Economic and Social Affairs, Population, New York, NY.

Dunn, P.F., 2005. Measurement and Data Analysis for Engineering and Science. McGraw-Hill Higher Education.

Ecologic Institute, SERI, 2010. Establishing an environmental sustainability threshold on soil erosion, Fact sheet on soil erosion., Establishing Environmental Sustainability Thresholds and Indicators. Ecologic institute and Sustainable Europe Research Institute (SERI).

FAO, 1965. Soil Erosion by Water: Some Measures for Its Control on Cultivated Lands. FAO, Rome.

FAO, 2013. Land Resources - Land Dagradation and Assessment [WWW Document]. URL http://www.fao.org/nr/land/degradation/en/

Fisher, R.A., 1929. Tests of Significance in Harmonic Analysis. Proc. R. Soc. Lond. Ser. A 125, 54–59. doi:10.1098/rspa.1929.0151

Flint, L.E., Flint, A.L., 2002. The Solid Phase - Porosity., in: Dane, J.H., Topp, G.C. (Eds.), Methods of Soil Analysis Part - 4 Physical Methods: SSSA Book Series - 5. Soil Science Society of America, Madison, WI., pp. 241–254.

Fox, J., Weisberg, S., Adler, D., Bates, D., Baud-Bovy, G., Ellison, S., Firth, D., Friendly, M., Gorjanc, G., Graves, S., Heiberger, R., Laboissiere, R., Monette, G., Murdoch, D., Nilsson, H., Ogle, D., Ripley, B., Venables, W., Zeileis, A., R-Core, 2013. car: Companion to Applied Regression. Sage, Thousand Oaks, CA.

Friis, I., 1992. Forests and forest trees of northeast tropical Africa: their natural habitats and distribution patterns in Ethiopia, Djibouti and Somalia. H.M.S.O.

GARC, 2010. Socio-economic survey of Gumara-maksegnit watershed (Report). Gonder Agricultural Research Center, Gonder.

Gardner, W.R., 1958. Some steady-state solutions of the unsaturated moisture flow equation with application to evaporation from a water table. Soil Sci. 85, 228–232. doi:10.1097/00010694-195804000-00006

Gaskin, G.J., Miller, J.D., 1996. Measurement of Soil Water Content Using a Simplified Impedance Measuring Technique. J. Agric. Eng. Res. 63, 153–159. doi:10.1006/jaer.1996.0017

Gastwirth, J.L., Gel, Y.R., Miao, W., 2009. The Impact of Levene's Test of Equality of Variances on Statistical Theory and Practice. Stat. Sci. 24, 343–360. doi:10.1214/09-STS301

Gebremichael, D., Nyssen, J., Poesen, J., Deckers, J., Haile, M., Govers, G., Moeyersons, J., 2005. Effectiveness of stone bunds in controlling soil erosion on cropland in the Tigray Highlands, northern Ethiopia. Soil Use Manag. 21, 287–297.

Glendon, G.W., Or, D., 2002. The Solid Phase - Particle-Size Analysis., in: Dane, J.H., Topp, G.C. (Eds.), Methods of Soil Analysis Part - 4 Physical Methods: SSSA Book Series - 5. Soil Science Society of America, Madison, WI., pp. 255–293.

Goebel, W., Odenyo, V.A.O., 1984. Agroclimatic Resource Inventory for Land-Use Planning. Ethiopia, AG: DP/ ETH/ 78/ 003 Technical Report 2 (Report). FAO, Rome.

Grossman, R.B., Reinsch, T.G., 2002. The Solid Phase - Bulk Density and Linear Extensibility., in: Dane, J.H., Topp, G.C. (Eds.), Methods of Soil Analysis Part - 4 Physical Methods: SSSA Book Series - 5. Soil Science Society of America, Madison, WI., pp. 201–228.

Hengsdijk, H., Meijerink, G., Mosugu, M., 2005. Modeling the effect of three soil and water conservation practices in Tigray, Ethiopia. Agric. Ecosyst. Environ. 105, 29–40. doi:10.1016/j,agee.2004.06.002

Herweg, K., Ludi, E., 1999. The performance of selected soil and water conservation measures—case studies from Ethiopia and Eritrea. Catena 36, 99–114. doi:10.1016/S0341-8162(99)00004-1

Hopmans, J.W., Šimůnek, J., Romano, N., Durner, W., 2002. The Soil Solution Phase - Simultaneous Determination of Water Transmission and Retention Properties - Inverse Methods, in: Dane, J.H., Topp, G.C. (Eds.), Methods of Soil Analysis Part - 4 Physical Methods: SSSA Book Series - 5. Soil Science Society of America, Madison, WI., pp. 963–1008.

Hudson, N.W., 1987. Soil and water conservation in semi-arid areas, FAO Soils Bulletin. FAO, Rome.

Hurni, H., 1988. Degradation and Conservation of the Resources in the Ethiopian Highlands. Mt. Res. Dev. 8, 123. doi:10.2307/3673438

Hurni, H., 1998. Agroecological Belts of Ethiopia, Explanatory notes on three maps at a scale of 1:1,000,000 (Report). Bern, Switzerland.

Isaaks, E.H., Srivastava, R.M., 1989. Applied geostatistics. Oxford Univ. Press, New York, NY.

Jones, A., Breuning-Madsen, H., Brossard, M., Dampha, A., Deckers, J., Dewitte, O., Gallali, T., Hallett, S., Jones, R., Kilasara, M., Le Roux, P., Micheli, E., Montanarella, L., Spaargaren, O., Thiombiano, L., Van Ranst, E., Yamefack, M., Zougmoré, R., (eds.), 2013. Soil Atlas of Africa. European Commission. Publications Office of the European Union, Luxembourg.

Jones, A., Panagos, S., Barcelo, F., Bouraoui, F., Bosco, C., Dewitte, O., Gardi, C., Erhard, M., Hervás, J., Hiederer, R., Jeffrey, S., Lükewille, A., Marmo, L., Montanarella, L., Olazábal, C., Peterson, J.-E., Penizek, V., Strassburger, T., Tóth, G., Van Den Eeckhaut, M., Van Liederke, M., Verheijen, F., Viestova, E., Yigini, Y., 2012. The State of Soil in Europe (Report No. EUR 25186 EN). European Commission, Joint Research Centre.

Kreba, S.A., Coyne, M.S., McCulley, R.L., Wendroth, O.O., 2013. Spatial and Temporal Patterns of Carbon Dioxide Flux in Crop and Grass Land-Use Systems. Vadose Zone J. 12, 0. doi:10.2136/vzj2013.01.0005

Levene, H., 1960. Robust tests for equality of variances. 278 -292, in: Olkin, I., Ghurye, S.G., Hoeffding, W., Madow, W.G., Mann, H.B. (Eds.), Contributions to Probability and Statistics: Essays in Honor of Harold Hotelling. Stanford University Press, Palo Alto, CA.

Marsaglia, G., Tsang, W.W., Wang, J., 2003. Evaluating Kolmogorov`s Distribution. J. Stat. Softw. 8.

Mengistu, A., 2006. Ethiopia: Country Pasture/Forage Resource Profiles. FAO, Rome.

Meschede, D., 2006. Gerthsen Physik [die ganze Physik zum 21. Jahrhundert]. Springer, Berlin [u.a.].

Morgan, R.P.C., 2005. Soil erosion and conservation. Blackwell Publ, Malden, MA.

Mualem, Y., 1976. A new model for predicting the hydraulic conductivity of unsaturated porous media. Water Resour. Res. 12, 513–522.

Nielsen, D.R., Wendroth, O., 2003. Spatial and temporal statistics: sampling field soils and their vegetation. Catena Verlag.

Nyssen, J., Poesen, J., Gebremichael, D., Vancampenhout, K., D'aes, M., Yihdego, G., Govers, G., Leirs, H., Moeyersons, J., Naudts, J., Haregeweyn, N., Haile, M., Deckers, J., 2007. Interdisciplinary on-site evaluation of stone bunds to control soil erosion on cropland in Northern Ethiopia. Soil Tillage Res. 94, 151–163. doi:10.1016/j.still.2006.07.011

Nyssen, J., Poesen, J., Haile, M., Moeyersons, J., Deckers, J., 2000. Tillage erosion on slopes with soil conservation structures in the Ethiopian highlands. Soil Tillage Res. 57, 115–127. doi:10.1016/S0167-1987(00)00138-0

Oldeman, L.R., 1992. Global Extent of Soil Degradation, ISRIC Bi-Annual Report. ISRIC - World Soil Information, Wageningen.

Pachepsky, Y.A., Timlin, D.J., Rawls, W.J., 2001. Soil Water Retention as Related to Topographic Variables. Soil Sci. Soc. Am. J. 65, 1787. doi:10.2136/sssaj2001.1787

Page-Dumroese, D.S., Brown, R.E., Jurgensen, M.F., Mroz, G.D., 1999. Comparison of Methods for Determining Bulk Densities of Rocky Forest Soils. Soil Sci. Soc. Am. J. 63, 379. doi:10.2136/sssaj1999.03615995006300020016x

Pebesma, E., Graeler, B., 2013. gstat: spatial and spatio-temporal geostatistical modelling, prediction and simulation.

Philip, J.R., 1985. Reply To “Comments on Steady Infiltration from Spherical Cavities”. Soil Sci. Soc. Am. J. 49, 788–789. doi:10.2136/sssaj1985.03615995004900030055x

R Core Team, 2013. R: A Language and Environment for Statistical Computing. R Foundation for Statistical Computing, Vienna, Austria.

Reynolds, W.D., Elrick, D.E., 1991. Determination of Hydraulic Conductivity Using a Tension Infiltrometer. Soil Sci. Soc. Am. J. 55, 633. doi:10.2136/sssaj1991.03615995005500030001x

Ribeiro, P.J.Jr , Diggle, P.J., 2012. geoR: Analysis of geostatistical data.

Roose, E., 1996. Land husbandry. Components and strategy, 70 FAO Soils Bulletin. FAO, Rome.

Sachs, L., 1974. Angewandte Statistik - Planung und Auswertung, Methoden und Modelle, 4th ed. Springer-Verlag, Berlin Heidelberg.

Schaap, M.G., Leij, F.J., van Genuchten, M.T., 2001. ROSETTA: A computer program for estimating soil hydraulic parameters with hierarchical pedotransfer functions. J. Hydrol. 251, 163–176. doi:10.1016/S0022-1694(01)00466-8

Scherr, S.J., Yadav, S., 1996. Land Degradation in the Developing World: Implications for Food, Agriculture, and the Environment to the Year 2020. Intl Food Policy Res Inst, Washington, D.C.

Schwen, A., Yang, Y., Walton, R.J., Wendroth, O., 2012. A New Experimental Design Reveals the Impacts of Land Use and Irrigation Characteristics on Bromide Leaching. Vadose Zone J. 11, 0. doi:10.2136/vzj2012.0077

Seleshi, Y., Zanke, U., 2004. Recent changes in rainfall and rainy days in Ethiopia. Int. J. Climatol. 24, 973–983. doi:10.1002/joc.1052

Šimůnek, J., Angulo-Jaramillo, R., Schaap, M.G., Vandervaere, J.-P., van Genuchten, M.T., 1998. Using an inverse method to estimate the hydraulic properties of crusted soils from tension-disc infiltrometer data. Geoderma 86, 61–81. doi:10.1016/S0016-7061(98)00035-4

Šimůnek, J., van Genuchten, M.T., 1996. Estimating unsaturated soil hydraulic properties from tension disc infiltrometer data by numerical inversion. Water Resour. Res. 32, 2683–2696.

Šimůnek, J., van Genuchten, M.T., 1997. Estimating unsaturated soil hydraulic properties from multiple tension disc infiltrometer data. SOIL Sci. 162, 383–398. doi:10.1097/00010694-199706000-00001

Šimůnek, J., van Genuchten, M.T., 2000. The DISC Computer Software for Analyzing Tension Disc Infiltrometer Data by Parameter Estimation (No. 145). U.S. Salinity Laboratory, Riverside, CA.

Soil Measurement Systems Inc., 2013. Infiltrometers [WWW Document]. Soil Meas. Syst. Infiltrometers. URL http://www.soilmeasurement.com/tension_infil.html

Stevens Water, 2007. Comprehensive Stevens Hydra Probe User Manual.

Taddese, G., 2001. Land Degradation: A Challenge to Ethiopia. Environ. Manage. 27, 815–824. doi:10.1007/s002670010190

Topp, G.C., Ferré, P.A., 2002. The Soil Solution Phase - Methods for Measurement of Soil Water Content - Thermogravimetric Using Convective Oven-Drying., in: Dane, J.H., Topp, C.G. (Eds.), Methods of Soil Analysis Part - 4 Physical Methods: SSSA Book Series - 5. Soil Science Society of America, Madison, WI., pp. 422–424.

Topp, G.C., Galganov, Y.T., Ball, B.C., Carter, M.R., 1993. Soil water desorption curves. p. 569-579., in: Carter, M.R. (Ed.), Soil Sampling and Methods of Analysis. Lewis Publ, Boca Raton [u.a.].

Van-Camp, L., Bujarrabal, B., Gentile, A.-R., Jones, R.J.A., Montanarella, L., Olazábal, C., Selvaradjou, S.-K., 2004. Reports of the Technical Working Groups Established under the Thematic Strategy for Soil Protection. (Report No. EUR 21319 EN/2). Office for Official Publications of the European Communities, Luxembourg.

Van Genuchten, M., 1980. A Closed-Form Equation for Predicting the Hydraulic Conductivity of Unsaturated Soils. Soil Sci. Soc. Am. J. Vol 44 No 5 P 892-898 Sept. 1980 9 Fig 1 Tab 21 Ref.

Van Lynden, G., Lininger, H., Schwilch, G., 2002. The WOCAT Map Methodology, a Standardized Tool for Mapping Degradation and Conservation, in: Proceedings of the 12th ISCO Conference, Beijing 2002. Beijing.

Vancampenhout, K., Nyssen, J., Gebremichael, D., Deckers, J., Poesen, J., Haile, M., Moeyersons, J., 2006. Stone bunds for soil conservation in the northern Ethiopian highlands: Impacts on soil fertility and crop yield. Soil Tillage Res. 90, 1–15. doi:10.1016/j.still.2005.08.004

Warrick, A., 1992. Models for Disc Infiltrometers. Water Resour. Res. 28, 1319–1327.

Wendroth, O., Nielson, D.R., 2002. Soil Sampling and Statistical Procedure - Time and Space Series, in: Dane, J.H., Topp, G.C. (Eds.), Methods of Soil Analysis Part - 4 Physical Methods: SSSA Book Series - 5. Soil Science Society of America, Madison, WI., pp. 119–137.

Wooding, R.A., 1968. Steady infiltration from a shallow circular pond. Water Resour. Res. 4, 1259–1273.

Xu, J., Ma, X., Logsdon, S.D., Horton, R., 2012. Short, Multineedle Frequency Domain Reflectometry Sensor Suitable for Measuring Soil Water Content. Soil Sci. Soc. Am. J. 76, 1929. doi:10.2136/sssaj2011.0361

Yates, S.R., Warrick, A.W., 2002. Soil Sampling and Statistical Procedure - Geostatistics, in: Dane, J.H., Topp, G.C. (Eds.), Methods of Soil Analysis Part - 4 Physical Methods: SSSA Book Series - 5. Soil Science Society of America, Madison, WI., pp. 81–118.

Zachar, D., 1982. Soil Erosion (Developments in Soil Science 10). Elsevier, Bratislava.

Ziadat, F., Taimeh, A., Hattar, B., 2010. Variation of Soil Physical Properties and Moisture Content Along Toposequences in the Arid to Semiarid Area. ARID LAND Res. Manag. 24, 81–97. doi:10.1080/15324981003635396

Appendix

A.1 Topography of the hill slopes

Table A.1: Measurements of the elevation along both transects

Transect with SWC		Transect without SWC	
Distance (m)	Elevation (m a.s.l)	Distance (m)	Elevation (m a.s.l)
0.00	2028.74	0.00	2028.75
1.10	2028.73	1.06	2028.70
2.10	2028.60	1.97	2028.66
3.10	2028.53	3.18	2028.61
4.15	2028.46	4.35	2028.53
5.10	2028.40	5.19	2028.47
6.23	2028.30	5.83	2028.40
7.40	2028.28	7.04	2028.32
8.45	2028.17	8.07	2028.25
9.10	2028.13	9.27	2028.18
10.17	2028.09	10.14	2028.01
11.10	2028.01	11.19	2027.91
12.22	2027.94	12.00	2027.72
13.10	2027.82	12.94	2027.59
14.24	2027.78	13.80	2027.47
15.40	2027.68	14.74	2027.38
16.73	2027.60	15.73	2027.28
16.73	2027.60	16.42	2027.21
17.98	2027.43	17.71	2027.05
19.12	2027.26	18.14	2026.91
20.26	2027.13	18.84	2026.85
21.26	2027.05	19.87	2026.72
22.29	2027.02	20.98	2026.63
22.99	2026.98	22.05	2026.51
23.97	2026.97	22.88	2026.43
24.50	2026.96	23.86	2026.33
25.30	2026.55	24.83	2026.15
26.41	2026.36	25.71	2026.04
27.38	2026.24	26.66	2025.92
28.43	2026.17	27.68	2025.79
29.34	2026.10	28.56	2025.71
30.30	2025.95	29.75	2025.59
32.51	2025.81	30.92	2025.48
34.43	2025.61	32.01	2025.39
35.42	2025.51	33.03	2025.27
36.34	2025.38	34.16	2025.17
37.39	2025.29	35.32	2025.04
38.47	2025.23	36.43	2024.99
40.19	2025.06	37.39	2024.92

41.21	2024.96	38.76	2024.79
42.27	2024.81	40.08	2024.65
43.36	2024.77	40.65	2024.59
44.42	2024.71	41.41	2024.53
46.43	2024.56	41.86	2024.48
47.33	2024.46	42.22	2024.44
48.34	2024.33	42.93	2024.38
49.25	2024.29	43.82	2024.30
50.25	2024.22	44.98	2024.18
51.20	2024.20	45.67	2024.12
52.24	2024.15	46.58	2024.06
53.05	2023.81	47.41	2023.99
54.10	2023.76	48.52	2023.87
55.30	2023.67	49.37	2023.81
56.30	2023.58	50.78	2023.67
57.43	2023.49	51.45	2023.62
58.48	2023.46	52.32	2023.57
59.64	2023.35	53.57	2023.45
60.87	2023.27	54.25	2023.42
62.29	2023.17	55.11	2023.40
63.70	2023.12	-	-
65.10	2023.03	-	-
66.45	2022.90	-	-
67.75	2022.81	-	-
68.58	2022.80	-	-
69.73	2022.77	-	-
70.33	2022.73	-	-
70.61	2022.75	-	-
70.91	2022.80	-	-

Table A.2: Calculated values of inclination for the sampling points of both transects

Transect with SWC		Transect without SWC	
Distance (m)	Inclination ($m\ m^{-1}$)	Distance (m)	Inclination ($m\ m^{-1}$)
0.0	-0.049	0.0	-0.0105
1.0	-0.065	2.5	-0.0475
2.0	-0.073	5.0	-0.0773
6.1	-0.068	7.5	-0.1000
10.2	-0.061	10.0	-0.1159
14.3	-0.086	12.5	-0.1257
18.4	-0.111	15.0	-0.1302
22.5	-0.05	17.5	-0.1303
23.5	-0.007	20.0	-0.1270

24.5	0.01	22.5	-0.1215
25.5	-0.179	25.0	-0.1147
26.5	-0.131	27.5	-0.1076
27.5	-0.103	30.0	-0.1011
32.0	-0.092	32.5	-0.0959
36.5	-0.102	35.0	-0.0923
41.0	-0.085	37.5	-0.0904
45.5	-0.082	40.0	-0.0901
50.0	-0.067	42.5	-0.0907
51.0	-0.043	45.0	-0.0911
52.0	-0.003	47.5	-0.0897
52.5	-0.079	50.0	-0.0844
53.5	-0.074	52.5	-0.0723
54.5	-0.073	55.0	-0.0501
57.4	-0.072	-	-
60.3	-0.064	-	-
63.2	-0.061	-	-
66.1	-0.07	-	-
69.0	-0.038	-	-
70.0	0.009	-	-
71.0	0.089	-	-

A.2 Near surface volumetric water content

A.2.1 Calibration of the FDR sensor

Table A.3: Data set for the calibration of the FDR probe

$\sqrt{\varepsilon_r}$ (-)	θ (m^3 m^{-3})
6.910	0.382
5.939	0.350
6.619	0.343
6.289	0.330
6.593	0.382
5.889	0.274
6.496	0.370
6.792	0.394
6.671	0.396
6.932	0.419
6.743	0.334
6.782	0.383
7.668	0.454
7.912	0.450

7.544	0.466
7.809	0.421
8.035	0.433
7.928	0.436
7.945	0.473
8.088	0.464
8.241	0.459
8.066	0.453
7.666	0.453
7.667	0.472
7.858	0.439
8.056	0.451
7.610	0.457
7.935	0.418
8.142	0.468
8.180	0.472
8.355	0.513
7.811	0.465
7.579	0.440
7.921	0.424
7.451	0.449
7.360	0.453
7.042	0.413
7.272	0.422
7.502	0.445
7.459	0.433
7.427	0.457
7.334	0.436
6.889	0.385
8.274	0.487
6.914	0.344
8.073	0.494
6.125	0.374
8.056	0.500
6.759	0.434
8.218	0.477
8.294	0.509
6.672	0.392
6.679	0.413

A.2.2 Near surface volumetric water content data for the transects

Table A.4: Results for the measurements of the volumetric water content applying the FDR calibration to the measurements for the transect with SWC

Distance	Volumetric water content θ ($m^3\ m^{-3}$)								
	Date								
(m)	2012-06-22	2012-07-11	2012-08-20	2012-08-21	2012-08-23	2012-08-26	2012-08-28	2012-08-29	2012-08-30
0.0	0.347	0.456	0.415	0.426	0.411	0.436	0.379	0.445	0.390
1.0	0.272	0.447	0.375	0.399	0.468	0.396	0.416	0.460	0.414
2.0	0.254	0.346	0.293	0.340	0.430	0.376	0.353	0.437	0.403
6.1	0.327	0.327	0.291	0.323	0.389	0.416	0.387	0.454	0.401
10.2	0.175	0.354	0.312	0.323	0.416	0.368	0.380	0.468	0.449
14.3	0.310	0.297	0.335	0.403	0.441	0.445	0.437	0.461	0.455
18.4	0.325	0.373	0.388	0.348	0.462	0.439	0.430	0.462	0.425
22.5	0.298	0.355	0.344	0.402	0.470	0.462	0.434	0.472	0.459
23.5	0.304	0.429	0.417	0.408	0.471	0.467	0.469	0.482	0.475
24.5	0.326	0.441	0.428	0.424	0.457	0.446	0.473	0.470	0.459
25.5	0.317	0.441	0.394	0.430	0.452	0.472	0.418	0.444	0.409
26.5	0.336	0.441	0.415	0.418	0.421	0.405	0.449	0.444	0.398
27.5	0.334	0.310	0.339	0.389	0.418	0.412	0.421	0.457	0.432
32.0	0.233	0.310	0.380	0.348	0.418	0.402	0.372	0.470	0.448
36.5	0.283	0.306	0.351	0.387	0.421	0.414	0.386	0.441	0.443
41.0	0.291	0.423	0.315	0.358	0.422	0.441	0.369	0.462	0.436
45.5	0.291	0.388	0.378	0.342	0.389	0.456	0.391	0.475	0.425
50.0	0.299	0.408	0.407	0.394	0.432	0.456	0.415	0.478	0.450
51.0	0.313	0.398	0.432	0.397	0.452	0.470	0.436	0.489	0.466
52.0	0.313	0.398	0.414	0.420	0.442	0.469	0.480	0.454	0.474

52.5	0.302	0.427	0.320	0.411	0.426	0.449	0.432	0.439	0.422
53.5	0.305	0.364	0.324	0.349	0.417	0.410	0.371	0.461	0.419
54.5	0.290	0.347	0.360	0.395	0.420	0.420	0.381	0.431	0.424
57.4	0.297	0.403	0.336	0.355	0.440	0.424	0.345	0.425	0.427
60.3	0.273	0.294	0.377	0.395	0.406	0.422	0.400	0.404	0.407
63.2	0.282	0.302	0.307	0.387	0.416	0.425	0.332	0.419	0.434
66.1	0.323	0.310	0.399	0.332	0.415	0.409	0.407	0.434	0.424
69.0	0.258	0.310	0.419	0.384	0.438	0.416	0.408	0.431	0.424
70.0	0.315	0.334	0.411	0.397	0.436	0.407	0.408	0.429	0.419
71.0	0.351	0.370	0.421	0.423	0.427	0.433	0.434	0.423	0.442

Table A.5: Results for the measurements of the volumetric water content applying the FDR calibration to the measurements for the transect without SWC

Distance (m)	Volumetric water content θ (m^3 m^{-3}) Date						
	2012-07-11	2012-08-20	2012-08-21	2012-08-23	2012-08-26	2012-08-28	2012-08-30
0.0	0.387	0.396	0.421	0.448	0.416	0.403	0.401
2.5	-	-	0.314	0.424	0.412	0.388	0.289
5.0	0.345	0.333	0.371	0.429	0.439	0.322	0.325
7.5	-	-	0.222	0.387	0.360	0.363	0.412
10.0	0.305	0.377	0.289	0.416	0.409	0.406	0.405
12.5	-	-	0.398	0.455	0.334	0.375	0.428
15.0	0.378	0.355	0.270	0.382	0.421	0.390	0.366
17.5	-	-	0.379	0.377	0.371	0.360	0.398
20.0	0.330	0.375	0.379	0.426	0.331	0.407	0.432
22.5	-	-	0.353	0.397	0.303	0.386	0.314
25.0	0.333	0.330	0.337	0.348	0.416	0.425	0.447

27.5	-	-	0.351	0.408	0.416	0.397	0.397
30.0	0.335	0.369	0.394	0.381	0.414	0.409	0.373
32.5	-	-	0.338	0.428	0.405	0.377	0.431
35.0	0.340	0.388	0.366	0.420	0.427	0.417	0.415
37.5	-	-	0.362	0.413	0.388	0.376	0.419
40.0	0.345	0.380	0.396	0.424	0.425	0.402	0.437
42.5	-	-	0.353	0.370	0.414	0.402	0.433
45.0	0.335	0.397	0.389	0.407	0.391	0.404	0.411
47.5	-	-	0.369	0.402	0.403	0.384	0.426
50.0	0.313	0.385	0.368	0.413	0.406	0.398	0.422
52.5	-	-	0.382	0.412	-	0.398	0.438
55.0	0.271	0.387	-	-	-	-	0.334

A.3 Undisturbed soil samples

A.3.1 Transect with SWC

Table A.6: Results of the analysis of the undisturbed soil samples taken along the transect with SWC on June 22nd 2012.

Distance	Nr.	m_{wS+R}	m_{dS+SR}	m_W	V_W	m_{SR}	V_{SR}	m_{dS}	Θ	ρ_d	n
(m)	(-)	(g)	(g)	(g)	(cm^3)	(g)	(cm^3)	(g)	(m^3 m^{-3})	(g cm^{-3})	(m^3 m^{-3})
0.0	218	526.06	442.11	83.95	83.95	177.39	199.65	264.72	0.421	1.33	0.50
1.0	482	484.81	407.18	77.63	77.63	169.36	204.88	237.82	0.379	1.16	0.56
2.0	37	414.71	348.22	66.49	66.49	135.39	198.20	212.83	0.335	1.07	0.59
6.1	100	446.57	372.20	74.37	74.37	136.41	198.80	235.79	0.374	1.19	0.55
10.2	344	509.06	436.48	72.58	72.58	179.43	200.47	257.05	0.362	1.28	0.52
14.3	312	489.28	411.32	77.96	77.96	178.31	199.84	233.01	0.390	1.17	0.56
18.4	215	474.44	402.73	71.71	71.71	178.12	200.06	224.61	0.358	1.12	0.58
22.5	157	425.16	356.75	68.41	68.41	136.21	198.80	220.54	0.344	1.11	0.58
23.5	49	-	-	-	-	-	-	-	-	-	-
24.5	133	440.68	366.41	74.27	74.27	136.13	198.00	230.28	0.375	1.16	0.56
25.5	118	491.00	410.70	80.30	80.30	135.59	198.70	275.11	0.404	1.38	0.48
26.5	83	450.45	374.57	75.88	75.88	135.32	198.80	239.25	0.382	1.20	0.55
27.5	595	541.42	461.69	79.73	79.73	184.64	202.12	277.05	0.394	1.37	0.48
32.0	283	509.87	427.81	82.06	82.06	177.89	200.03	249.92	0.410	1.25	0.53
36.5	137	480.64	394.32	86.32	86.32	136.08	199.20	258.24	0.433	1.30	0.51
41.0	68	459.64	380.13	79.51	79.51	135.34	197.40	244.79	0.403	1.24	0.53
45.5	43	426.06	352.31	73.75	73.75	134.68	197.60	217.63	0.373	1.10	0.58
50.0	577	507.26	424.73	82.53	82.53	170.51	204.65	254.22	0.403	1.24	0.53
51.0	2	460.33	373.95	86.38	86.38	132.48	202.40	241.47	0.427	1.19	0.55
52.0	158	457.21	375.92	81.30	81.30	136.38	198.80	239.54	0.409	1.20	0.55
52.5	25	447.78	367.30	80.48	80.48	134.81	197.70	232.49	0.407	1.18	0.56

53.5	531	507.57	428.34	79.23	79.23	170.20	205.14	258.14	0.386	1.26	0.53
54.5	57	440.45	361.79	78.66	78.66	135.27	197.30	226.52	0.399	1.15	0.57
57.4	107	455.48	382.46	73.02	73.02	135.09	198.70	247.37	0.367	1.24	0.53
60.3	135	442.47	365.48	76.99	76.99	136.69	199.70	228.79	0.386	1.15	0.57
63.2	417	495.98	414.12	81.86	81.86	178.44	200.17	235.68	0.409	1.18	0.56
66.1	22	423.20	346.01	77.19	77.19	135.02	197.70	210.99	0.390	1.07	0.60
69.0	329	466.66	390.72	75.94	75.94	181.32	199.84	209.40	0.380	1.05	0.60
70.0	493	503.96	415.31	88.65	88.65	169.54	204.67	245.77	0.433	1.20	0.55
71.0	364	518.78	434.59	84.20	84.20	178.72	199.93	255.87	0.421	1.28	0.52

Table A.7: Results of the analysis of the undisturbed soil samples taken along the transect with SWC on July 11th 2012.

Distance (m)	Nr. (-)	m_{wS+R} (g)	m_{dS+SR} (g)	m_W (g)	V_W (cm^3)	m_{SR} (g)	V_{SR} (cm^3)	m_{dS} (g)	Θ ($m^3\ m^{-3}$)	ρ_d ($g\ cm^{-3}$)	n ($m^3\ m^{-3}$)
0.0	508	499.12	422.99	76.13	76.13	170.59	205.26	252.40	0.371	1.23	0.54
1.0	157	499.21	405.57	93.64	93.64	136.21	198.80	269.36	0.471	1.35	0.49
2.0	43	464.46	372.42	92.04	92.04	134.68	197.60	237.74	0.466	1.20	0.55
6.1	216	522.86	435.76	87.10	87.10	179.10	201.02	256.66	0.433	1.28	0.52
10.2	151	471.54	384.04	87.50	87.50	136.72	198.70	247.32	0.440	1.24	0.53
14.3	138	452.88	375.09	77.79	77.79	136.54	198.10	238.55	0.393	1.20	0.55
18.4	435	472.23	404.63	67.60	67.60	178.22	199.54	226.41	0.339	1.13	0.57
22.5	346	486.75	414.09	72.66	72.66	177.88	199.98	236.21	0.363	1.18	0.55
23.5	118	470.98	384.06	86.92	86.92	135.59	198.70	248.47	0.437	1.25	0.53
24.5	59	488.50	401.83	86.67	86.67	136.17	198.20	265.66	0.437	1.34	0.49
25.5	595	513.70	434.17	79.54	79.54	184.64	202.12	249.53	0.394	1.23	0.53
26.5	88	490.24	402.33	87.91	87.91	135.02	197.40	267.31	0.445	1.35	0.49
27.5	283	493.80	418.05	75.75	75.75	177.89	200.03	240.16	0.379	1.20	0.55

32.0	417	543.99	456.94	87.05	87.05	178.44	200.17	278.50	0.435	1.39	0.47
36.5	57	449.20	369.98	79.22	79.22	135.27	197.30	234.71	0.402	1.19	0.55
41.0	11	456.61	375.90	80.71	80.71	132.44	197.80	243.46	0.408	1.23	0.54
45.5	37	451.51	368.91	82.60	82.60	135.39	198.20	233.52	0.417	1.18	0.56
50.0	137	421.88	347.72	74.16	74.16	136.08	199.20	211.64	0.372	1.06	0.60
51.0	68	485.93	400.29	85.64	85.64	135.34	197.40	264.95	0.434	1.34	0.49
52.0	133	502.84	416.88	85.96	85.96	136.13	198.00	280.75	0.434	1.42	0.46
52.5	531	539.10	443.79	95.31	95.31	170.20	205.14	273.59	0.465	1.33	0.50
53.5	100	475.52	389.18	86.34	86.34	136.41	198.80	252.77	0.434	1.27	0.52
54.5	553	523.82	434.54	89.28	89.28	169.47	204.47	265.07	0.437	1.30	0.51
57.4	66	442.35	363.31	79.04	79.04	134.82	197.70	228.49	0.400	1.16	0.56
60.3	218	468.69	392.88	75.81	75.81	177.39	199.65	215.49	0.380	1.08	0.59
63.2	493	480.31	398.84	81.47	81.47	169.54	204.67	229.30	0.398	1.12	0.58
66.1	344	469.51	392.80	76.71	76.71	179.43	200.47	213.37	0.383	1.06	0.60
69.0	83	450.85	364.15	86.71	86.71	135.32	198.80	228.83	0.436	1.15	0.57
70.0	364	490.66	408.99	81.67	81.67	178.72	199.93	230.27	0.408	1.15	0.57
71.0	551	506.52	418.66	87.86	87.86	170.30	204.32	248.36	0.430	1.22	0.54

Table A.8: Results of the analysis of the undisturbed soil samples taken along the transect with SWC on August 29th 2012.

Distance (m)	Nr. (-)	m_{wS+R} (g)	m_{dS+SR} (g)	m_W (g)	V_W (cm^3)	m_{SR} (g)	V_{SR} (cm^3)	m_{dS} (g)	Θ ($m^3\ m^{-3}$)	ρ_d ($g\ cm^{-3}$)	n ($m^3\ m^{-3}$)
0.0	351	537.65	446.55	91.10	91.10	179.72	200.73	266.83	0.454	1.33	0.50
1.0	135	508.19	418.27	89.92	89.92	136.69	199.70	281.58	0.450	1.41	0.47
2.0	508	533.30	437.70	95.60	95.60	170.59	205.26	267.11	0.466	1.30	0.51
6.1	493	501.85	415.62	86.23	86.23	169.54	204.67	246.08	0.421	1.20	0.55
10.2	86	484.30	398.28	86.02	86.02	134.88	198.80	263.40	0.433	1.32	0.50
14.3	410	549.23	462.22	87.01	87.01	182.00	199.57	280.22	0.436	1.40	0.47

18.4	216	532.79	437.74	95.05	95.05	179.10	201.02	258.64	0.473	1.29	0.51
22.5	3	473.84	381.05	92.80	92.80	132.10	200.10	248.95	0.464	1.24	0.53
23.5	59	475.45	384.40	91.05	91.05	136.17	198.20	248.23	0.459	1.25	0.53
24.5	49	462.88	373.76	89.12	89.12	135.04	196.90	238.72	0.453	1.21	0.54
25.5	151	502.66	412.59	90.07	90.07	136.72	198.70	275.87	0.453	1.39	0.48
26.5	366	535.70	441.09	94.61	94.61	178.72	200.32	262.37	0.472	1.31	0.51
27.5	137	462.60	375.20	87.40	87.40	136.08	199.20	239.12	0.439	1.20	0.55
32.0	551	505.98	413.77	92.22	92.22	170.30	204.32	243.47	0.451	1.19	0.55
36.5	595	524.24	431.85	92.39	92.39	184.64	202.12	247.21	0.457	1.22	0.54
41.0	100	442.86	359.81	83.05	83.05	136.41	198.80	223.40	0.418	1.12	0.58
45.5	157	460.29	367.20	93.09	93.09	136.21	198.80	230.99	0.468	1.16	0.56
50.0	577	506.70	410.04	96.66	96.66	170.51	204.65	239.53	0.472	1.17	0.56
51.0	22	507.24	405.86	101.38	101.38	135.02	197.70	270.84	0.513	1.37	0.48
52.0	531	507.03	411.69	95.34	95.34	170.20	205.14	241.49	0.465	1.18	0.56
52.5	218	531.71	443.93	87.78	87.78	177.39	199.65	266.54	0.440	1.34	0.50
53.5	550	497.88	412.03	85.86	85.86	184.87	202.46	227.16	0.424	1.12	0.58
54.5	283	502.33	412.46	89.87	89.87	177.89	200.03	234.57	0.449	1.17	0.56
57.4	138	455.02	365.31	89.71	89.71	136.54	198.10	228.77	0.453	1.15	0.56
60.3	276	478.95	396.75	82.20	82.20	179.08	199.10	217.67	0.413	1.09	0.59
63.2	149	441.40	357.65	83.75	83.75	135.86	198.30	221.79	0.422	1.12	0.58
66.1	43	452.76	364.83	87.93	87.93	134.68	197.60	230.15	0.445	1.16	0.56
69.0	527	491.48	403.95	87.53	87.53	184.38	202.03	219.57	0.433	1.09	0.59
70.0	57	452.20	362.01	90.20	90.20	135.27	197.30	226.74	0.457	1.15	0.57
71.0	344	483.15	395.68	87.47	87.47	179.43	200.47	216.25	0.436	1.08	0.59

A.3.2 Transect without SWC

Table A.9: Results of the analysis of the undisturbed soil samples taken along the transect without SWC on July 24th 2012.

Distance (m)	Nr. (-)	m_{wS+R} (g)	m_{dS+SR} (g)	m_W (g)	V_W (cm^3)	m_{SR} (g)	V_{SR} (cm^3)	m_{dS} (g)	Θ ($m^3\ m^{-3}$)	ρ_d ($g\ cm^{-3}$)	n ($m^3\ m^{-3}$)
0.0	118	474.36	390.03	84.33	84.33	135.59	198.7	254.44	0.424	1.28	0.52
5.0	551	492.92	411.82	81.10	81.10	170.30	204.3	241.52	0.397	1.18	0.55
10.0	404	546.86	454.18	92.68	92.68	178.47	200.2	275.71	0.463	1.38	0.48
15.0	133	493.32	404.68	88.64	88.64	136.13	198.0	268.55	0.448	1.36	0.49
20.0	157	489.93	399.41	90.52	90.52	136.21	198.8	263.20	0.455	1.32	0.50
25.0	138	473.62	395.46	78.16	78.16	136.54	198.1	258.92	0.395	1.31	0.51
30.0	151	514.49	418.17	96.32	96.32	136.72	198.7	281.45	0.485	1.42	0.47
35.0	344	528.76	439.39	89.37	89.37	179.43	200.5	259.96	0.446	1.30	0.51
40.0	86	497.67	401.32	96.36	96.36	134.88	198.8	266.44	0.485	1.34	0.49
45.0	531	555.19	452.36	102.84	102.84	170.20	205.1	282.16	0.501	1.38	0.48
50.0	83	500.16	398.53	101.63	101.63	135.32	198.8	263.21	0.511	1.32	0.50
55.0	508	521.50	428.34	93.16	93.16	170.59	205.3	257.75	0.454	1.26	0.53

Table A.10: Results of the analysis of the undisturbed soil samples taken along the transect without SWC on August 20th 2012.

Distance (m)	Nr. (-)	m_{wS+R} (g)	m_{dS+SR} (g)	m_W (g)	V_W (cm^3)	m_{SR} (g)	V_{SR} (cm^3)	m_{dS} (g)	Θ ($m^3\ m^{-3}$)	ρ_d ($g\ cm^{-3}$)	n ($m^3\ m^{-3}$)
0.0	100	461.43	385.47	75.97	75.97	136.41	198.80	249.06	0.382	1.46	0.45
5.0	22	442.29	373.09	69.20	69.20	135.02	197.70	238.07	0.350	1.46	0.45
10.0	312	506.05	437.53	68.52	68.52	178.31	199.84	259.22	0.343	1.12	0.58
15.0	43	427.17	361.91	65.26	65.26	134.68	197.60	227.23	0.330	1.47	0.45
20.0	86	462.31	386.30	76.02	76.02	134.88	198.80	251.42	0.382	1.47	0.44
25.0	366	462.24	407.28	54.96	54.96	178.72	200.32	228.56	0.274	1.12	0.58
30.0	595	509.62	434.82	74.80	74.80	184.64	202.12	250.18	0.370	1.09	0.59
35.0	137	468.62	390.17	78.45	78.45	136.08	199.20	254.09	0.394	1.46	0.45
40.0	59	477.33	398.80	78.53	78.53	136.17	198.20	262.63	0.396	1.46	0.45
45.0	49	480.79	398.28	82.51	82.51	135.04	196.90	263.24	0.419	1.46	0.45
50.0	435	478.31	411.77	66.54	66.54	178.22	199.54	233.55	0.333	1.12	0.58
55.0	218	497.90	421.46	76.44	76.44	177.39	199.65	244.07	0.383	1.13	0.58